University of Nottingham

Doctoral Thesis

Dynamics of non-equilibrium ^{6}Li Feshbach molecules via magnetic field ramp

by Vineetha Naniyil

A thesis presented in the fulfilment of the requirements for the degree of Doctor of Philosophy

Cold Atom Research Group
Department of Physics and Astronomy
University of Nottingham
2021

Head of School
Prof. Mark Fromhold

Supervisors
Dr. Lucia Hackermueller

Dr. Weibin Li

Examiners

Dr. Stephen Powell

Dr. Marzena Szymanska

To my father

This thesis is the result of the author's original research. It has been composed by the author and has not been previously submitted for examination which has led to the award of a degree.

Signed: Vineetha Naniyil

Date: 30-06-2021

Abstract

In this thesis, the dynamics of Feshbach molecule formation via magnetic field ramp is investigated. The work presented in this thesis dealt with production and study of bosonic Feshbach molecule from fermionic ^{6}Li atoms by quenching the magnetic field across the broad Feshbach resonance at 834.1 G. The fraction of atoms converted to Feshbach molecules is measured experimentally and the dependence of temperature and the rate at which the magnetic field is ramped during the process has been presented. The formation of Feshbach molecule via magnetoassociation of ultracold ^{6}Li atoms close to quantum degeneracy is also explored in this thesis.

A new development in theoretical simulation of the dynamics of Feshbach molecules creation and extraction of the atom-molecule coupling coefficient is also detailed in this work. The first experimental measurement of the atom-molecule coupling coefficient at different temperatures of atomic cloud varies from 3.2 μK to 130 nK has been presented here. An enhancement of the atom-molecule coupling strength is observed as the atoms close to degeneracy and we find that a qualitative agreement between the experimental result and theoretically calculated value. The Landau-Zener transition describes the dynamics of Feshbach molecule formation at higher temperature. The enhancement of the atom-molecule coupling coefficient at lower temperature reveals the many-body coherence in the system, which is not captured by the conventional Landau-Zener model.

The dependence of molecule conversion as a function of mean density and the final magnetic field are also studied in this thesis. The dependence of magnetic field on the creation of Feshbach molecule shows a shift in the centroid of the error function, which is used to fit with the experimental data. The theoretical explanation of the shift from the Feshbach resonance has yet to be studied.

Acknowledgements

I owe my deepest gratitude to my thesis supervisor Dr. Lucia Hackermueller for her patience, encouragement, extensive knowledge and the continuous support during my study and research. Her guidance was of immense help in all aspects of my research and writing of this thesis. I could not have imagined having a better supervisor and mentor for my PhD study.

I am also extremely grateful to my second supervisor Dr. Weibin Li for his unconditional help for theoretical simulations for my experimental studies and many helpful discussions.

I also owe a debt of gratitude to Dr. Nathan Cooper, who helped whenever I was facing a problem in the laboratory. His inputs to the experimental setup has really helped me during the time of setting up my experiment. He was extremely helpful to reach solutions for the various issues I have had during my experimental work.

Besides my advisers, I would like to give a very special thanks to the rest of my colleagues Elisa, Somaya, Guy, Craig and Yijia for their unparalleled support and insightful comments during my PhD study. They have also helped me to provide a friendly and exceptionally good atmosphere in the University. I would also like to thank the rest of the cold atom group for the valuable discussions and support during my PhD study.

I would also like to thank warmly the workshop staff, electronic technicians, and engineers, who helped in one way or the other during my study.

My PhD study was funded by Vice chancellor's scholarship from University of Nottingham, I am extremely grateful to get this scholarship. I could not have imagined doing my PhD and thesis work without this scholarship.

Finally I would like to acknowledge my wonderful family members who were with me all the time, especially my husband Shijin and my brother Sajeesh for their unconditional support and encouragement.

Contents

List of Figures

Chapter 1

Introduction

I was really fascinated about the technique of laser cooling and trapping of atoms during my postgraduate study. It inspired me to learn more about the cooling and trapping of atomic systems. Atoms can be divided into two categories, which are Bosons and Fermions. Particles which do not obey the Pauli exclusion principle are called Bosons and those ones which obey the Pauli exclusion principle are known as Fermions. The Pauli exclusion principle states that no two particles can have the same quantum numbers. For bosons, many particles can have the same quantum numbers. At temperature $T = 0$, bosons quickly condense into the ground state and form a Bose-Einstein Condensate (BEC), while fermions slowly start filling up the lowest lying energy state with unity occupation and form a Fermi sea. The study of Fermi gases is one of the leading edge of quantum matter research field. The enormous growth in the study of fermionic system gives a platform for understanding and accessing fundamental physical phenomena. Recently, the Fermi gases are used as central to many advanced research field like new fundamental physics [1], controlled chemistry [2] and the quantum simulation of complex many-body systems [3].

The introduction of laser and laser cooling techniques has led to a breakthrough

in cooling and trapping of atoms, which allows a reduction in the temperature of the atomic systems to microkelvin. The research field of laser cooling and trapping has been developed at a high pace in the last ten years. There are many elegant techniques that have been implemented in ultracold atoms studies [4, 5]. The study of ultracold atoms has numerous applications in spectroscopy, ultracold chemistry, simulation of condensed matter systems, nuclear physics and metrology. Laser cooling has paved the way to observe Bose-Einstein condensation (BEC), which started a completely new interesting research field and it took 60 years from the theoretical prediction to the final experimental implementation.

A Feshbach resonance gives a platform to study conversion of fermionic atoms to bosonic molecules in cold and ultracold atomic systems. The molecules produced from fermionic atoms are remarkably stable against inelastic decay. Tunability of the atomic interactions given by Feshbach resonance allow us to experimentally produce and to study Feshbach molecules [6], mBEC [7], equation of state of strongly interacting Fermi gases [8], fermionic polaron behaviour [9], spin-orbit coupling effect [10] and anisotropic character of p-wave or higher partial wave interactions [11]. Cold and ultracold molecules have the potential to dramatically influence precision tests of fundamental physics [1, 12–15], physical chemistry [16–20] and few body physics [21–24]. Experiments with ultracold Fermi gases can explore the crossover from a BEC type system to a fermionic superfluid with Bardeen-Cooper-Shrieffer (BCS) type pairing [25–27].

In a gaseous medium, Bose-Einstein Condensation (BEC) can be achieved via evaporative cooling methods together with thermalisation of the ensemble. The scattering length can be tuned through resonance by applying a magnetic field and ultimately tuning the energy of the channel potential carried by the atoms through their magnetic moment. A Feshbach resonance can also be used to asso-

ciate atoms into ultracold molecules. B. DeMarco and D. Jin at JILA have created the first degenerate Fermi gas of atoms in ^{40}K. In 2005, Feshbach molecules via magnetic field ramp were created [28].

The physics of creation of cold molecules from ultracold atoms is an interesting area since it has been an important challenge in the experimental and theoretical ultracold physics. Feshbach molecules have numerous applications in precision measurements [29], high resolution spectroscopy [30], ultracold chemistry [31] and quantum information processing [32]. Feshbach molecules can be created by photo-association [33–35], three-body recombination near Feshbach resonance and magneto-association [36, 37]. Molecules can be produced by an external adiabatic magnetic field sweep across a Feshbach resonance in ultracold systems. The magnetic field ramp method was proposed by Van Abeelen and Verhaar in 1999 [38], Timmermans in 1999 [36] and Mies in 2000 [37]. By sweeping the magnetic field adiabatically, molecules are created on the repulsive side of the resonance. Molecule creation is a reversible process therefore one can convert molecules back to atoms by reversing the magnetic field ramp. Feshbach molecules creation via magnetoassociation can also be used to study unitary dynamics [39], collective dynamics [40] and many-body effects [41]. The experimental and theoretical study on magnetoassociation of fermionic (^{6}Li) atoms to bosonic molecules have been explored in this thesis.

Here we are investigating a non-equilibrium phenomena of molecular creation in strongly interacting fermionic gases. A broad Feshbach resonance in a fermionic mixture of Lithium-6 allows tuning the interaction strength in the lowest energy states through s-wave scattering. This setting allows the study of strongly interacting degenerate Fermi gases, molecular BEC, superfluidity, and pairing in fermionic many-body systems. Creation of ultracold [1, 42] and condensed [7]

molecules via magnetoassociation have been studied in Fermi gases of atoms and these systems have created a lot of interest in the research field. This thesis presents the creation of bosonic molecules from a two components Fermi gas of atoms via magnetic field ramp across the broad Feshbach resonance in ^{6}Li. Theoretical studies on the dynamics of Fermi gases of atoms into molecules are also presented in this thesis. The dynamics of molecules creation via magnetoassociation can be controlled by the ramp time and initial atomic cloud temperature. The dynamics of Feshbach molecules can be explained by Landau-Zener transition and many-body process. The atom-molecule coupling coefficient, which is the key parameter of the creation of Feshbach molecules is obtained from the experimental data and it is compared with the theoretically calculated value. The quest to develop new and efficient experimental scheme to produce large molecules with highly stable is therefore still a crucial challenge. The experimental results achieved during my PhD period is presented in a research paper under review, which is given in Appendix H.

This thesis is structured in the following way.

Chapter 2 : Theoretical background

Summarises the basic concept/theory behind laser cooling and trapping, scattering process involved in quantum gases and Feshbach resonance.

Chapter 3: Experimental setup

Describes the experimental system capable of cooling and trapping of ^{6}Li atoms to ultracold temperatures. The presentation of technical aspects of the experimental apparatus is given in this chapter.

Chapter 4 : Experimental methods

Presents the experimental approach to produce cold atomic samples, optimisation of magneto optical trap and the methods to prepare ultracold atoms in the lowest energy level. The Feshbach molecules creation via magnetic field ramp is also described in this chapter.

Chapter 5 : The $^6Li_2$ Feshbach molecules formation

Major achievement of my thesis work is presented in this chapter. This chapter begins with some theoretical and experimental studies on Feshbach molecule creation. This is followed by discussion of comparison of Landau-Zener model and Power law approach. This chapter will be devoted to the presentation and characterisation of the dependence of ramp speed, atomic could temperature, mean density and final magnetic field to the Feshbach molecule creation from fermionic ^{6}Li atoms.

Chapter 6 : Theoretical model

The dynamics of Feshbach molecule creation is formulated and explained in this chapter. The measurements of coupling constant from experiment and comparison with theoretical calculation is presented in this section. The dependence of temperature on molecular conversion is described here.

Chapter 7 : Conclusion and Future work

I summarise major achievements of my experimental and theoretical studies on Feshbach molecules creation in ^{6}Li atoms. Finally, I conclude with a brief discussion of future research directions and some exciting ideas to be realised in the near future with the same experimental apparatus.

1.1 Publications

During my PhD I have co-authored the following articles:

- Vineetha Naniyil, Yijia Zhou, Guy Simmonds, Nathan Cooper, Weibin Li, and Lucia Hackermuller. "Observation of collectivity-enhanced magnetoassociation of 6Li in the quantum degenerate regime" (2021). Submitted to Physical Review Research. Updated in arXiv (Reference number : arXiv:2102.01805)

- N. Cooper, E. Da Ros, C. Briddon, V. Naniyil, M. T. Greenaway, and L. Hackermüller. "Prospects for strongly coupled atom-photon quantum nodes". Scientific Reports 9.1 (2019), p.7798 [43].

Chapter 2

Theoretical background

This thesis is based on the dynamics of Feshbach molecule creation from fermionic Lithium atoms. This chapter presents the basic concepts of interaction of atoms with light and magnetic field. The theoretical concept of laser cooling, atom trapping and atom-atom scattering are also described in the following section. An important property of alkali atoms, the so-called Feshbach resonance, is presented in order to understand the physics of Feshbach molecules, creation via a magnetic field ramp.

2.1 Interaction of atoms with light

Absorption and emission of light are the result of atom light interaction in which an atom gets excited from its ground state to an excited state and spontaneously emits the light and reaches its stable ground state. The atom light interaction can be simply explained by semi-classical theory, considering a classical electric field interacting with atoms, which are treated quantum mechanically. Consider the situation of a two-level atomic system, in which an atom having a ground state 'g' and excited state 'e' are coupled by monochromatic light. The interaction of

an atom with a plane wave having an electric field $\hat{E} = \hat{\epsilon}E_0 cos(kr - \omega t)$ with an amplitude E_0 which is directed along the unit vector $\hat{\epsilon}$ and a frequency ω can be expressed by a time-dependent Schrödinger equation given by,

$$i\hbar\frac{\partial\Psi(r,t)}{\partial t} = \hat{H}\Psi(r,t). \tag{2.1}$$

Here $\hat{H} = \hat{H}_0 + \hat{V}$, where $\hat{H}_0$ represents the unperturbed Hamiltonian and $\hat{V} = \hat{d}\cdot\hat{E}$, where $\hat{d}$ is electric dipole moment and $\hat{E}$ is the electric field. From the solution of time-dependent Schrödinger equation one can obtain the Rabi frequency $\Omega = \frac{E_0}{\hbar}\langle e|\hat{d}\cdot\hat{\epsilon}|g\rangle$, which represents atom field coupling. The interaction of atoms with monochromatic light causes the atoms to undergo Rabi-oscillation, in which population oscillates between the two levels. Then the atom settle down to its steady state followed by these oscillations, where the excitation rate equals the decay rate. Since the atomic excited state decays by spontaneous emission, one has to consider the time evolution of the density matrix governed by Liouville's equation, which allows us to include the effect of spontaneous emission,

$$\frac{d\rho}{dt} = \frac{i}{\hbar}[\hat{\rho},\hat{H}] - \begin{pmatrix} -\Gamma\rho_{ee} & \frac{\Gamma}{2}\rho_{ge} \\ \frac{\Gamma}{2}\rho_{eg} & \Gamma\rho_{ee} \end{pmatrix} \tag{2.2}$$

where $\hat{H} = \frac{\hbar}{2}\begin{bmatrix} 0 & \Omega \\ \Omega & -2\Delta \end{bmatrix}$ with detuning Δ and Γ is the decay rate of the excited state. The elements of the density matrix obey the constraints, which are $\tilde{\rho}_{gg} + \tilde{\rho}_{ee} = 1$ and $\tilde{\rho}_{ge} = \tilde{\rho}^*_{eg}$. One can expand the equation 2.2 and obtain the optical Bloch equations [44], from which we can obtain the steady-state solution of the equations by setting the time derivative to zero. For strong field, $\Omega \to \infty$ tends to equalize the population so that the excited level population can be expressed as,

$$\tilde{\rho}_{ee} = \frac{1}{2}\frac{s}{1 + s + \frac{4\Delta^2}{\Gamma^2}} \tag{2.3}$$

where s is the on-resonant saturation parameter, $s = \frac{I}{I_{\text{sat}}} = \frac{2\Omega^2}{\Gamma^2}$. The saturation intensity represents the strength of the transition, which can be written as,

$$I_{\text{sat}} = \frac{2\pi^2\hbar\Gamma c}{3\lambda^3} \tag{2.4}$$

where $\frac{1}{\Gamma}$ is the atomic excited state lifetime and λ is the wavelength. We can obtain the scattering rate R_{sc} by multiplying the steady state population of the excited state with decay rate Γ,

$$R_{\text{sc}}(I, \Delta) = \Gamma\tilde{\rho}_{ee}. \tag{2.5}$$

Since the maximum population of the excited state is $\tilde{\rho}_{ee} = \frac{1}{2}$, we can also express the scattering rate as, $R_{\text{sc}} = \frac{\Gamma}{2}$. The scattering rate has a Lorentzian lineshape and at low intensity the width of the lineshape is the natural linewidth Γ, whereas at high intensity the width increases and it becomes power broadened.

2.2 Interaction of atoms with magnetic field

The separation between atomic energy levels can be tuned by an external magnetic field, which is known as the Zeeman effect. The interaction of atoms with an external magnetic field $\hat{B}$, can be considered as a perturbation to the atomic system, so that Hamiltonian is given by,

$$\hat{H}_{ZE} = -\mu \cdot \hat{B} \tag{2.6}$$

where $\mu = -\mu_B L - g_s\mu_B S$ is the magnetic moment of the atom, which is a combination of orbital and spin magnetic moments. Here L and S are the orbital angular momentum and spin operators, respectively. So the Hamiltonian can also be expressed as [44],

$$\hat{H}_{ZE} = \frac{\langle L \cdot J\rangle + g_s\langle S \cdot J\rangle}{J(J+1)}\mu_B\hat{B}J_z, \tag{2.7}$$

since we project the magnetic moment onto J in the vector model. Here J represents the total electronic angular momentum. When the atomic interaction with an external magnetic field is stronger than the spin-orbit interaction, one has to consider the magnetic moment of the nucleus, $\mu_I = g_I\mu_N I$. So the perturbation to the atomic system (Hyperfine interaction) can be expressed as,

$$\hat{H}_{HFS} = -\mu_I \cdot \hat{B} = AI \cdot J. \tag{2.8}$$

where A is the magnetic dipole hyperfine constant. When the magnetic energy becomes significant compared to the hyperfine energy, F is not a good quantum number anymore and J precesses about $\hat{B}$. So that the Hamiltonian for the interaction with an external magnetic field $\hat{B}$ is given by,

$$\hat{H}_B = \frac{-\mu_B}{\hbar}(g_S\hat{S} + g_L\hat{L} + g_I\hat{I}), \tag{2.9}$$

where g is the Landé g-factor for the corresponding quantum numbers. Therefore the combined interaction Hamiltonian is,

$$\hat{H}_{\text{int}} = \hat{H}_B + \hat{H}_{HFS}. \tag{2.10}$$

Since we are interested in D_2 line transition in Lithium (^{6}Li), the magnetic field dependence on its ground state and excited state are important in this context and they are shown in the figures 2.1 and 2.2.

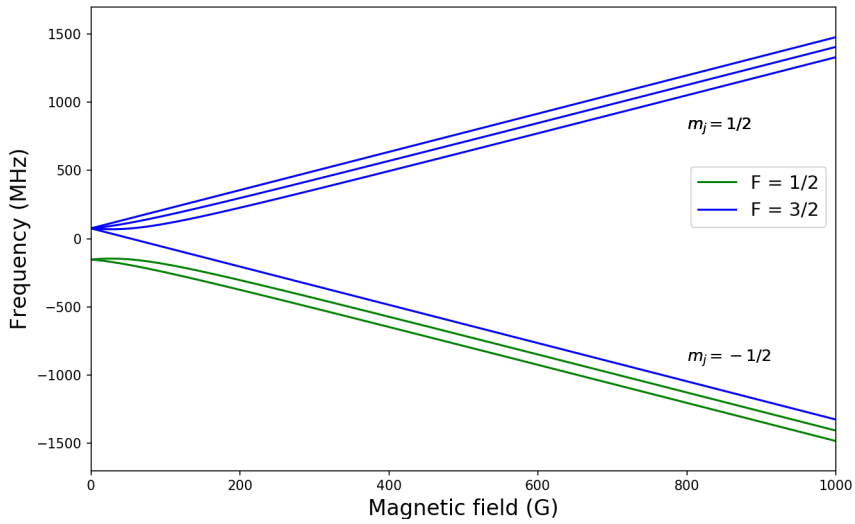

Figure 2.1: Breit-Rabi diagram for the $2^2S_{1/2}$ ground state of ^{6}Li.

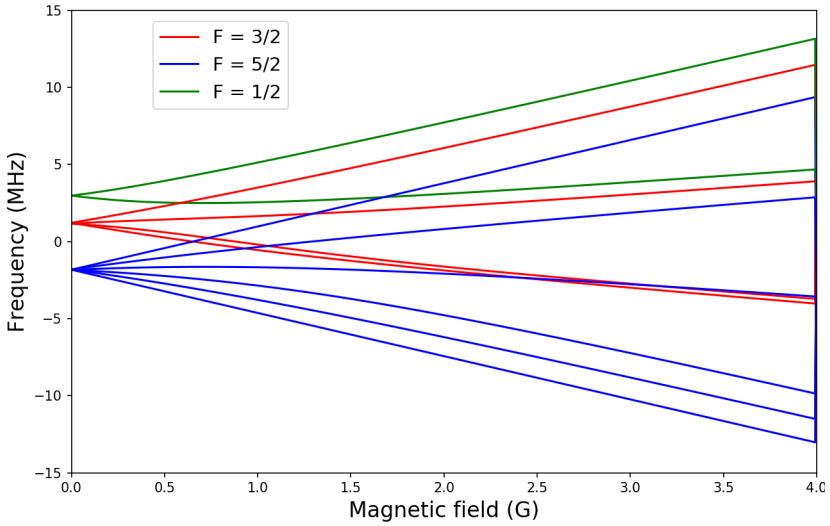

Figure 2.2: Breit-Rabi diagram for the $2^2P_{1/2}$ excited state of ^{6}Li.

When the atoms are in the high magnetic field regime, the nuclear spin essentially decouples from the electron spin. This is known as the Paschen-Back effect of the hyperfine structure. In the high field region the states depends on the orientation of the electron spin.

2.3 Atomic structure of ^{6}Li

The most prominent isotopes of Lithium (Li) found in nature are ^{7}Li and ^{6}Li. The solid form of Li presents a silvery grey color. The abundance of ^{7}Li is 92.4% and that of ^{6}Li is 7.6%. The existence of ^{7}Li is a composite boson while ^{6}Li is a composite fermion. Like all alkali ^{6}Li has a single valence electron and electronic configuration of the ground state is $1S^2 2S^1$. Lithium-6 has three electrons and three neutrons with total nuclear spin of 1 and total electron spin $\frac{1}{2}$. The interaction between orbital angular momentum and electron spin can be expressed by total electronic angular momentum given by,

$$\hat{J} = \hat{L} + \hat{S}, \tag{2.11}$$

and therefore the quantum number $\hat{J}$ can take half-integer values between $|L - S| \leqslant J \leqslant (L + S)$. Two prominent spectroscopic features D1 and D2 result from the interaction between the intrinsic angular momentum of the valence electron and angular momentum of its orbit. Transitions between $2^2S_{\frac{1}{2}} \rightarrow 2^2P_{\frac{1}{2}}$ and $2^2S_{\frac{1}{2}} \rightarrow 2^2P_{\frac{3}{2}}$ are called D1 transition and D2 transition respectively, shown in figure 2.3. The D2 line has been widely used for cooling of atoms in ultracold systems. The key feature of ^{6}Li is its wide range Feshbach resonance ($\sim 300\,\mathrm{G}$) and it also has large photon-recoil energy compared to other alkalis, since it has a small mass. To explain the gross structure of atomic energy levels, one has to incorporate the nuclear spin of the atom, since electrons create a magnetic field that interacts with the nuclear spin $\hat{I}$. Therefore the total angular momentum of the system given by the operator $\hat{F}$,

$$\hat{F} = \hat{J} + \hat{I}, \tag{2.12}$$

where $\hat{I}$ is the total nuclear angular momentum operator. The values for quantum number $\hat{F}$ ranges all half integer values between $|J - I| \leqslant F \leqslant (J + I)$. Therefore the F values for $2^2S_{\frac{1}{2}}$ and $2^2P_{\frac{1}{2}}$ are $\frac{1}{2}$ and $\frac{3}{2}$, while that for $2^2P_{\frac{3}{2}}$ are $\frac{1}{2}$, $\frac{3}{2}$ and $\frac{5}{2}$. Other optical properties of ^{6}Li are given in the table 2.1.

Table 2.1: Optical properties of the D2 line of ^{6}Li, data is taken from [45].

Property	Value
Wavelength (vacuum), λ	670.977338 nm
Wavenumber (vacuum), $\frac{k}{2\pi}$	14903.633 cm^{-1}
Frequency,ν	446.799677 THz
Lifetime, τ	27.102 ns
Natural Linewidth, Γ	36.898 $\times 10^6 s^{-1}$(5.8724 MHz)
Atomic Recoil velocity,υ_{rec}	9.886776 cm.sec^{-1}
Recoil Temperature, T_{rec}	3.535811 μK

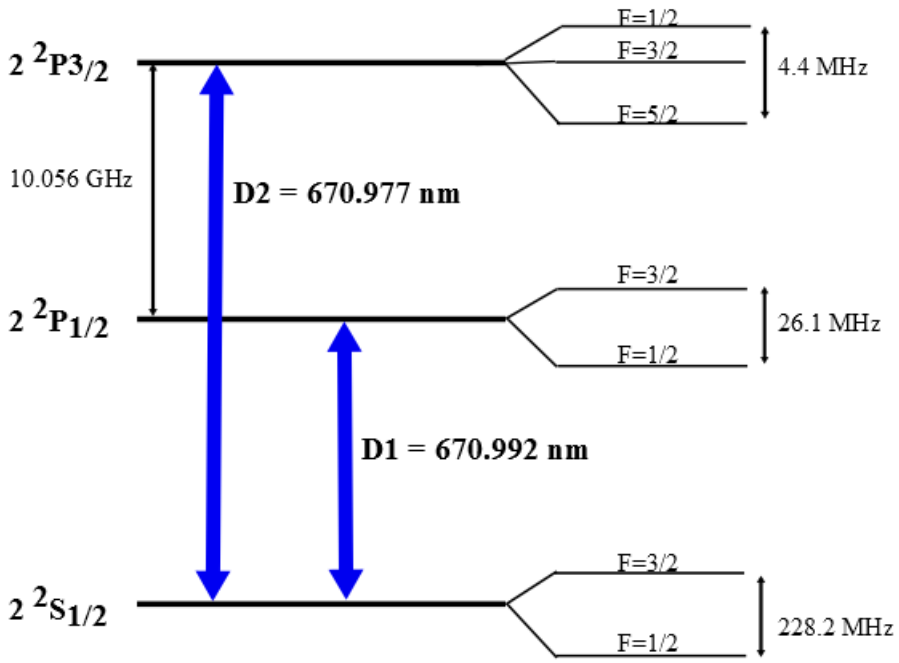

Figure 2.3: Energy level diagram of ^{6}Li. Energy splittings are not to scale. This figure is adapted from [45].

2.4 Theory of laser cooling and trapping

Laser cooling and trapping of atoms based on radiation pressure force was proposed in the late 70s by Ashkin [46]. The radiation pressure force arises from the momentum exchange of photons onto the atoms resulting in a cooling effect on atoms when they interact with photons. Laser cooling allows the atoms to cool down to the limit of the Doppler temperature [47], $T_D = \frac{\hbar\Gamma}{2k_B}$, where Γ is the linewidth of the transition and k_B is the Boltzmann constant. The interaction between magnetic moments and the light fields in an inhomogeneous magnetic field confines the atoms in the centre of the vacuum chamber, where the magnetic field is nearly zero, the so called Magneto-Optical Trap (MOT). Laser cooling and trapping pave the way for ultracold atomic physics including Bose-Einstein Condensates, Fermionic quantum degeneracy and precision measurements of fun-

damental physics.

2.4.1 Doppler cooling

Interaction of light with atoms results in the absorption and emission of photons. In this process the incident electric field will induce a dipole moment in the atom. The transfer of momentum from a photon to the atom occurs such that the atom experiences a kick opposite to the direction of motion of the atom. This momentum transfer results in a force, which is referred to as radiation pressure force. Scattering of many photons leads to an average force, which results in slowing of atoms. The scattering force F_{sc}, is the product of photon momentum, $\hbar k$ and the rate at which the light scattered R_{sc} [44], which is given by,

$$R_{\text{sc}} = \frac{\Gamma}{2} \frac{\frac{\Omega^2}{2}}{\delta^2 + \frac{\Omega^2}{2} + \frac{\Gamma^2}{4}}, \tag{2.13}$$

where $\delta = \omega - \omega_0 + kv$. Here ω and ω_0 give the laser frequency and atomic resonance frequency respectively. The Doppler shift and Rabi frequency are represented by kv and Ω respectively. The rate of scattered intensity to the saturation intensity can be expressed as,

$$\frac{I}{I_{sat}} = \frac{2\Omega^2}{\Gamma^2}. \tag{2.14}$$

Therefore the scattering force can be written as [44],

$$F_{\text{sc}} = \hbar k \frac{\Gamma}{2} \frac{\frac{I}{I_{sat}}}{1 + \frac{I}{I_{sat}} + \frac{4\delta^2}{\Gamma^2}}. \tag{2.15}$$

Photon scattering is an essential feature of laser cooling and trapping of atoms. For a moving atom in the presence of two or more counter-propagating laser beams, the Doppler effect leads to an imbalance in the direction of force due to the difference in Doppler shifts.

Consider a two level atom in a pair of counter propagating beams from a laser with frequency below the atomic resonance frequency. For atoms moving in the opposite direction to the laser beam propagation, the Doppler shift will make the frequency appear higher, thus red-detuning the laser will shift the frequency back towards the resonance, counteracting the Doppler shift. Therefore high levels of scattering would occur when the red-detuned light interacts with an atom moving against the direction of light propagation, whereas less scattering occurs when the light interacts with an atom moving in the same direction of the beam. Atoms moving parallel to the beam will experience a considerably smaller force. Although these atoms will be accelerated by this smaller force, a comparatively larger damping force acting on the atoms moving opposite to the direction of beam propagation will decrease their velocity, and consequently their kinetic energy, thus resulting in an overall cooling effect. Cooling of atoms occurs if the laser frequency is smaller than the resonance frequency of the atom. The net force is therefore given by [44],

$$F_{\text{molasses}} = F_{\text{sc}}(\omega - \omega_0 - k\upsilon) - F_{\text{sc}}(\omega - \omega_0 + k\upsilon), \tag{2.16}$$

$$\cong F_{\text{sc}}(\omega - \omega_0) - k\upsilon\frac{\delta F}{\delta\omega} - [F_{\text{sc}}(\omega - \omega_0) + k\upsilon\frac{\delta F}{\delta\omega}], \tag{2.17}$$

$$\cong -2\frac{\delta F}{\delta\omega}k\upsilon, \tag{2.18}$$

for low velocity ($k\upsilon \ll \Gamma$) has been assumed. The molasses force can also be expressed as,

$$F_{\text{molasses}} = -\alpha\upsilon, \tag{2.19}$$

where $\alpha = -2\frac{\delta F}{\delta\omega}k$, is the damping coefficient.

2.4.2 Doppler cooling limit

In the optical molasses stage, atoms undergo absorption and emission events which leads to the heating effect from the photon recoil. For an atom interacting with two counter propagating beams the radiation forces tend to cancel each other, however the fluctuations from these are cumulative. It is due to the fact that the root mean square velocity of the atoms are increased during the absorption and spontaneous emission processes. Due to both events the kinetic energy of the atom increases by $2E_r$ and the rate at which atom get heated up can be expressed as,

$$\frac{dE_{\text{heat}}}{dt} = (2R_{\text{sc}})(2E_r). \tag{2.20}$$

The rate at which the kinetic energy changes as a result of an applied cooling beam can be expressed as,

$$\frac{dE_{\text{cool}}}{dt} = -\alpha v^2. \tag{2.21}$$

A steady state can be achieved when the heating and cooling compensate each other, therefore one can determine the equilibrium velocity by the equation,

$$\frac{dE_{\text{total}}}{dt} = \frac{dE_{\text{heat}}}{dt} + \frac{dE_{\text{cool}}}{dt} = 0, \Longrightarrow v_{\text{eq}}^2 = 4E_r R_{\text{sc}}/\alpha. \tag{2.22}$$

Then the temperature limit due to the fluctuation can be obtained from the equation which relates the kinetic energy and temperature, which is given as,

$$\frac{1}{2}mv_{\text{eq}}^2 = \frac{1}{2}k_B T. \tag{2.23}$$

By substituting $\alpha = 2\hbar k^2 \frac{-2\delta}{\delta^2 + \frac{\Gamma^2}{4}} R_{\text{sc}}$, the expression for the temperature takes the form [44, 48],

$$k_B T = \frac{\hbar\Gamma}{4} \frac{(1 + 2\delta/\Gamma)^2}{-2\delta/\Gamma}. \tag{2.24}$$

The minimum temperature can be obtained when $\delta = \omega - \omega_0 = -\Gamma/2$, and is called Doppler temperature. It is the minimum temperature achievable by Doppler cooling method. The Doppler temperature T_D is given by,

$$T_D = \frac{\hbar\Gamma}{2k_B}. \tag{2.25}$$

The Doppler cooling limit for the ^{6}Li is 140 μK, however the minimum temperature obtained from the experiment is 500 μK, since lithium-6 has the unresolved excited state hyperfine levels.

2.4.3 Magneto-Optical Trap

Laser cooled atoms can be trapped in a spatial confinement generated by an inhomogeneous magnetic field along with the appropriate arrangement of circularly polarised beams, called Magneto-Optical Trap (MOT). This is a standard technique used in many cold atom experiments. In the Magneto-optical trap, the imbalance in the scattering forces of the laser beams due to the quadrupole magnetic field produced by the coils strongly confines the atoms in the centre of the magnetic field gradient where the magnetic field is nearly zero.

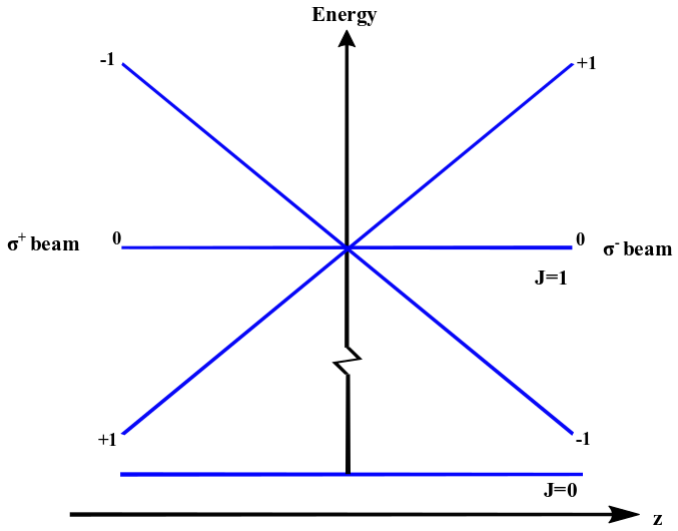

Figure 2.4: Trapping of atoms in the MOT. The figure illustrates the trapping of atoms in the MOT using circularly polarised beams and the quadrupole magnetic field. The splitting of energy level J=1 to the three sublevels is also shown here.

The quadrupole magnetic field in the MOT set up produces a uniform magnetic

field gradient close to the zero of the field and it perturbs the energy levels due to the Zeeman effect. This splits the hyperfine level $J = 1$ level to three sublevels with m_J=0,±1 as can be seen in the figure 2.4. Consider two counter propagating circularly polarised ($\sigma\pm$) beams along the z-direction, which are red detuned from the resonance frequency. When the atoms are in the region $z > 0$, they experience a stronger scattering from the $\sigma-$ beam, since m_J=-1 transition moves closer to the resonance and it pushes the atoms back towards the centre of the trap where the magnetic field is nearly zero. Similarly for atoms in the region where $z < 0$, the m_J=+1 transition moves closer to the resonance and atoms experience a stronger scattering from $\sigma+$ beam and atoms are pushed towards the trap centre. The net force experienced by the atoms depends on the frequency detuning $\delta = \omega - \omega_0$ and it can be expressed as [44],

$$F_{\mathrm{MOT}} = F_{\mathrm{sc}}^{\sigma+}\left(\omega - kv - (\omega_0 + \beta z)\right) - F_{\mathrm{sc}}^{\sigma-}\left(\omega + kv - (\omega_0 - \beta z)\right) \tag{2.26}$$

$$F_{MOT} = -2\frac{\partial F}{\partial \omega}(kv + \beta z) \tag{2.27}$$

$$= -\alpha v - \frac{\alpha\beta}{k} z. \tag{2.28}$$

where βz is the Zeeman shift at a displacement z. In the case of 3D MOT, the atoms are trapped in the centre where three sets of orthogonally polarised beams intersect each other.

2.4.4 Dipole trapping

Along with the scattering force an atom also experiences another force called the dipole force when it interacts with light. This has been widely used in many experiments with ultracold atoms. A conservative force that attracts the atoms in the high intensity region when red-detuned light interacts with atoms. The dipole force can be expressed as [44],

$$F_{\mathrm{dipole}} = \frac{-\hbar\delta}{2} \frac{\Omega}{\delta^2 + \frac{\Omega^2}{2} + \frac{\Gamma^2}{4}} \frac{\delta\Omega}{\delta z}. \tag{2.29}$$

The dipole force vanishes when the light is on resonance, i.e.$\delta = 0$. This dipole force can be used to manipulate or confine atoms at the focus of a laser beam, this technique has been used widely in optical dipole trapping, optical tweezers and in optical lattices. In this work, the evaporative cooling is performed in the optical dipole trap created by 1070 nm laser which is red-detuned from the lithium-6 transition. The optical dipole trap is created by focussing a Gaussian laser beam in the MOT chamber.

2.5 Scattering theory

Elastic and inelastic collisions play an important role in achieving quantum degeneracy of bosons and fermions. Elastic (coherent) scattering describes a process during which particle energy is unchanged whereas particle energy changes during inelastic (incoherent) scattering processes. Thermalisation in trapped atomic samples occurs by collisions, which ensures evaporative cooling of atoms. We consider here two particles of the same mass M, interacting through the potential $V(r_1 - r_2)$, as can be seen in the figure 2.5. The Hamiltonian of the system can be expressed as,

$$\hat{H} = \frac{\hat{p_1}^2}{2M} + \frac{\hat{p_2}^2}{2M} + V(r_1 - r_2). \tag{2.30}$$

In this case, the center of mass moves as a free particle with a mass $2M$ and the relative mass of the system can be represented as, $m_r = \frac{M}{2}$. So the Schrödinger equation of scattering of two particles with an energy, $E_k = \frac{\hbar^2 k^2}{2m_r}$ in a potential V(r) is given by [44],

$$\left(\frac{p^2}{2m_r} + V(r)\right) \Psi_k(r) = E_k \Psi_k(r), \tag{2.31}$$

where we assume that V(r) goes to zero when $|r|$ goes to infinity. For $|r| \gg b$ (where b is the range of action of the potential V(r)), the solution of equation 2.31 has the following form:

$$\Psi_k(r) \sim e^{ik.r} + f(k, \mathbf{n}, \mathbf{n'})\frac{e^{ik.r}}{r} \tag{2.32}$$

where $\mathbf{n} = \frac{\mathbf{k}}{k}$ and $\mathbf{n'} = \frac{\mathbf{r}}{r}$. For the lower energy limit, scattering amplitude is independent of the directions of **n** and **n'**. It depends only on the angle Θ between the two unit vectors **n** and **n'**. In the quantum mechanical description of low energy scattering, the solution of the Schrödinger equation can be written as the sum of the incident wave plus the wave scattered by the potential that expands outward from $r = 0$, which is given in 1D by [44],

$$\Psi_k(r) \sim e^{ik.r} + f(k, \theta)\frac{e^{ik.r}}{r}, \tag{2.33}$$

where $f(k, \theta)$ is the scattering amplitude from which we can obtain the total scattering cross section by integration. The scattering cross section is given by the equation,

$$\sigma(k) = \int_{\Omega} |f(k, \theta)|^2 d\Omega. \tag{2.34}$$

One can expand the incident and scattered wave functions on a basis set of eigenfunctions of $\hat{L^2}$ and $\hat{L_z}$, where $\hat{L}$ is the relative angular momentum and z denotes the direction of the incident wave function. Therefore the scattering amplitude takes the form,

$$f(k, \theta) = \frac{1}{2ik}\sum_{l=0}^{\infty}(2l + 1)(e^{2i\delta_l} - 1)P_l \cos\theta, \tag{2.35}$$

and the scattering cross-section,

$$\sigma(k) = \sum_{l=0}^{\infty}\sigma_l(k), \tag{2.36}$$

where $\sigma_l(k) = \frac{4\pi}{k^2}(2l + 1)\sin^2\delta_l(k)$. For identical particles we have to take into account the symmetrisation principle, which states that,

$$\Psi(r_1, r_2) = \epsilon\Psi(r_2, r_1), \tag{2.37}$$

where $\epsilon = +1$ for polarised bosons and -1 for polarised fermions. So the partial waves that contribute to the scattering cross-section for bosons correspond to even values of l only, whereas odd values of l contribute for fermions. As a consequence we can write as follows:

$$\sigma(k) = \frac{8\pi}{k^2} \sum_{\text{l even}} (2l+1)\sin^2\delta_l(k); \qquad \text{for bosons} \tag{2.38}$$

$$\sigma(k) = \frac{8\pi}{k^2} \sum_{\text{l odd}} (2l+1)\sin^2\delta_l(k); \qquad \text{for fermions} \tag{2.39}$$

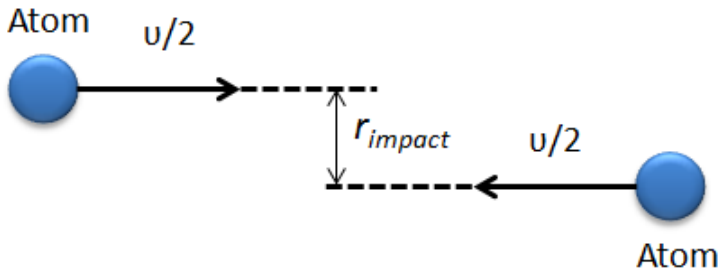

Figure 2.5: A pair of colliding atoms. Two colliding particles having equal mass and velocity separated by a distance r_{impact} take part in a scattering process. This figure is adapted from [44].

Consider the situation of a pair of colliding atoms that have relative angular momentum $\hbar l \simeq m_r \upsilon r_{\text{impact}}$, where υ is the relative velocity and r_{impact} is the impact parameter. For a collision to happen r_{impact} must be less than the range of interaction, i.e., $\hbar l \lesssim m_r \upsilon r_{\text{int}} = h r_{\text{int}}/\lambda_{\text{dB}}$. This implies that $l \lesssim 2\pi r_{\text{int}}/\lambda_{\text{dB}}$. When the energy is sufficiently low so that $\lambda_{\text{dB}}/2\pi \gg r_{\text{int}}$ and $l = 0$, the atoms have no relative angular momentum. This regime in which the scattered wave function is a spherical wave proportional to $Y_{l=0,m=0}$, is known as s-wave scattering regime. The total s-wave scattering cross section for distinguishable particles can be expressed as [49],

$$\sigma = \frac{\mathrm{d}\sigma}{\mathrm{d}\Omega}\mathrm{d}\Omega = \frac{4\pi a^2}{1 + a^2 k^2}, \tag{2.40}$$

where a is the scattering length. The cross section for low energy s-wave elastic scattering of non-identical particles is given by,

$$\sigma_{\text{fermions}} = 4\pi a^2 \tag{2.41}$$

and

$$\sigma_{\text{bosons}} = 8\pi a^2. \tag{2.42}$$

Note that the elastic scattering cross section of two identical fermions becomes zero due to anti-symmetrisation of the wave function. For bosons, the elastic scattering cross section is twice that of fermions due to symmetrisation of the wave function.

2.6 Feshbach resonance

A Feshbach resonance is an extraordinary property of ultracold atoms through which one can tune the interaction between atoms by an external magnetic field. It occurs when the energy of the colliding atoms is nearly degenerate with the energy of a bound molecular state. Thus it is an emergent tool to study both strongly and weakly interacting gases through the BEC-BCS crossover. For a collision process, atoms can be specified by two different quantum numbers separated by a small distance with an internal energy E_α. The atoms are prepared in a channel with relative kinetic energy hence the total energy of the system in the channel can be referred as,

$$E_{\text{total}} = E_\alpha + E_{K.E}. \tag{2.43}$$

Any channel with an energy $E_{\text{channel}} \leq E_{\text{total}}$ is called as an open channel where atoms are still separate atoms after the collision. A channel with energy $E_{\text{channel}} > E_{\text{total}}$ is called a closed channel where it can support two or more atoms in a bound molecular state. The open and closed channel potential of colliding particles is shown in the figure 2.6.

The open and closed channel potentials of colliding particles move with respect to each other under the influence of an altering external magnetic field. Therefore the energy difference can be expressed as [50],

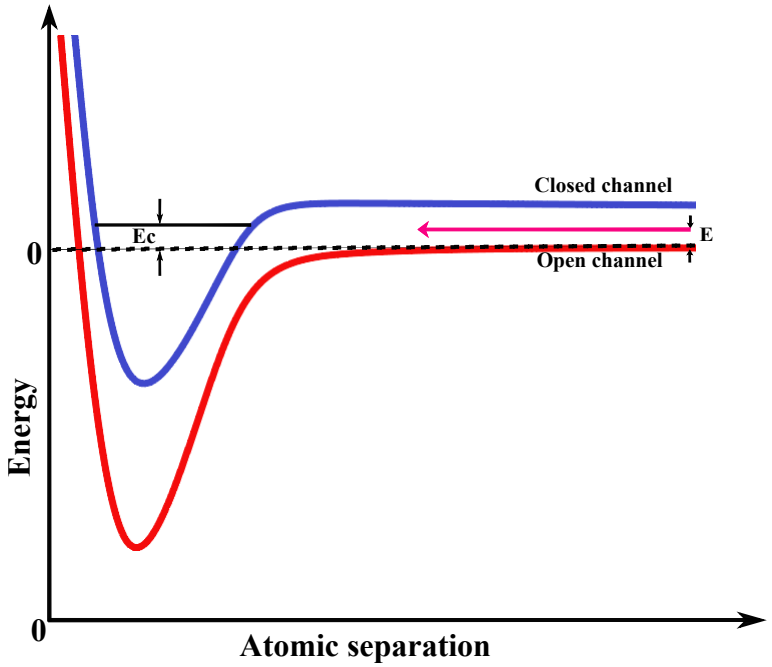

Figure 2.6: Open and closed channel potential of colliding particles. This figure illustrates the two channel model for a Feshbach resonance.

$$E_{\mathrm{C}} - E =\triangle\ \mu(B - B_0), \tag{2.44}$$

where E_{C} and E are the energy of closed and open channel respectively. Here B is the external magnetic field and B_0 is the magnetic field at resonance position exists, where the scattering length goes to $\pm\infty$. The difference between the open and closed channel magnetic moments is given by $\Delta\mu$. When the energy of a closed channel bound state is resonant with the energy of the colliding particle ($E_{\mathrm{C}} - E = 0$), the scattering length goes to infinity. This is called a Feshbach resonance. The scattering length can be expressed as a function of magnetic field, which is given by [51],

$$a(B) = a_{\mathrm{BG}}\left(1 - \frac{\Delta}{B - B_0}\right), \tag{2.45}$$

where a_{BG} is known as the background scattering length and Δ is width of the resonance with B_0 indicates the magnetic field at which the centre of the Feshbach resonance occurs.

2.6.1 Feshbach resonance in ^{6}Li

Spin mixtures of lower energy states in ^{6}Li exhibits two Feshbach resonances. For the spin mixture used, a Fehsbach resonance occurs at $B_0 = 834\,\mathrm{G}$ with width of $\Delta B = 262.3\,\mathrm{G}$ and a far narrower $\Delta B = 0.23\,\mathrm{G}$, resonance has been predicted and observed at $B_0 = 543.8\,\mathrm{G}$. By measuring the binding energy close to the resonance, a precise measurement of the wider Feshbach resonance in ^{6}Li is calculated as $B_0 = 832.18\,\mathrm{G}$ [52]. The Feshbach resonance in ^{6}Li is shown in the figure 2.7.

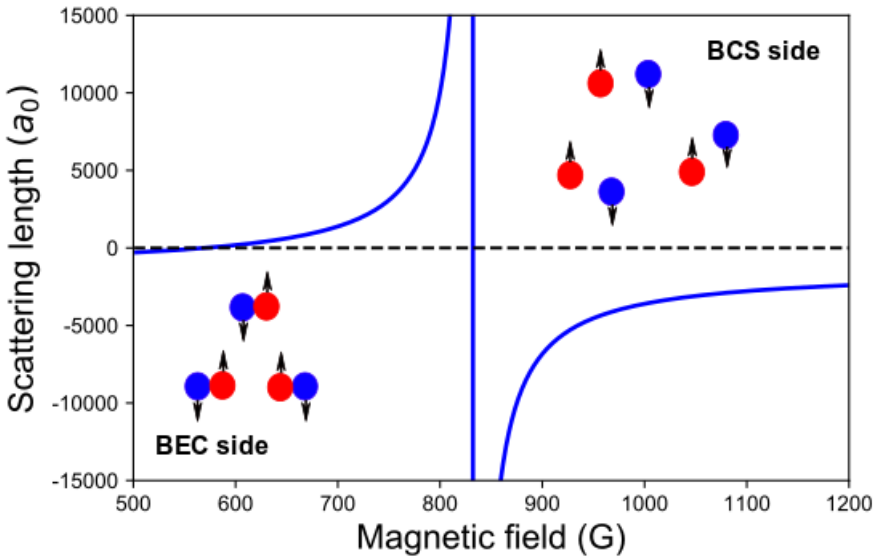

Figure 2.7: Feshbach resonance in ^{6}Li. The figure shows the tunability of the s-wave interactions in a spin mixture of ^{6}Li atoms in the two lowest spin states ($m_F = \pm 1/2$). The vertical line indicates the Feshbach resonance position at 834 G. On the y-axis, the scattering length is shown in units of the Bohr radius, $\mathrm{a_0} = 5.27 \times 10^{-11}\,\mathrm{m}$.

There are three different regimes in a Feshbach resonance for fermionic mixtures.

- BCS-regime: $a < 0$, weakly attractive Fermi gas exists. At zero temperature, ground state of the system becomes a fermionic superfluid.
- BEC-regime: $a > 0$, repulsive potential. Atoms in the two spin states can

form molecules and at zero temperature these molecules can condense into BEC.

- BEC-BCS crossover: $a \to \infty$, Feshbach resonance. The effective range of interaction is negligible.

The existence of a Feshbach resonance opens the possibility to study the change from a repulsive gas to an attractive one and vice versa, and the association of atomic pairs into molecules and vice versa, which is the main content of this thesis.

2.7 Fermi gas

The advent of ultracold Fermi gases with tunable interactions provides great challenges for many-body quantum theories. The distribution function of average number of fermions with energy ϵ_r is,

$$n_{\text{r, Fermi}} = \frac{1}{\exp(\frac{\epsilon_r - \mu}{k_B T}) + 1}. \tag{2.46}$$

Non-identical particles are needed to exploit s-wave interactions at lower temperature. The Fermi energy of a trapped, non-interacting two component gas is given by,

$$E_F = \hbar\overline{\omega}\,(3N)^{1/3}\,, \tag{2.47}$$

where $\overline{\omega}$ is the geometrically averaged oscillation frequency in the harmonic trapping potential and N refers to the total number of atoms in both spin states. The energy of the highest filled state refers to the Fermi energy. The corresponding Fermi temperature can be obtained as,

$$T_F = \frac{E_F}{k_B}, \tag{2.48}$$

and the Fermi number k_F follows the relation, $\frac{\hbar^2 k_F^2}{2m} = E_F$. For non-interacting particles, k_F is related to the peak number density, $n_0 = \frac{k_F^3}{3\pi^2}$ in the trap centre and $\frac{1}{k_F a}$ refers to the interaction parameter. The BEC regime follows $\frac{1}{k_F a} \gg 1$ and BCS regime follows $\frac{1}{k_F a} \ll$ -1.

2.8 Bose-Einstein Condensation

Bose-Einstein Condensation is a macroscopic quantum phenomena which occurs at temperatures on the order of nanokelvin. Atoms achieve a new quantum state called Bose-Einstein Condensate (BEC) when the de-Broglie wavelength becomes comparable to the inter particle spacing. The Bose-Einstein Condensation was first theoretically predicted by Sathyandra Nath Bose for photons in 1924 and the theory was extended to include bosonic matter particles in 1924 by Albert Einstein. The first gaseous condensate was produced by Eric Cornell, Carl Wieman and colleagues in 1995. BEC occurs when the phase space density becomes $n\lambda_{dB}^3 \geq 1$ which can be expressed as,

$$n\lambda_{dB}^3 = n\left(\frac{h^2}{2\pi mk}\right)^{3/2} \geq 1, \tag{2.49}$$

where $\lambda_{dB} = \sqrt{\frac{2\pi\hbar^2}{mk_BT}}$. Therefore T can be expressed as $T \leq \frac{h^2}{2\pi mk} n^{2/3}$. The molecular BEC can be described by a wave function, which obeys the Gross-Pitaevskii equation [53] given by,

$$\left[-\frac{\hbar^2\nabla^2}{2M} + V_M(r) + g|\Psi(r,t)|^2\right]\Psi(r,t) = i\hbar\frac{\partial\Psi(r,t)}{\partial t} \tag{2.50}$$

where $g = \frac{4\pi\hbar^2 a_M}{M}$ which describes the intermolecular interactions and $V_M(r)$ is the trapping potential experienced by the molecules. The first BEC in fermions was created in 2003 with ^{40}K [7] and $^6Li_2$ [54].

2.9 Feshbach molecules

Feshbach resonances open a wide range of possibilities to tune interactions, which provides the experimental realisation of molecules creation from ultracold atoms. A few different methods have been demonstrated to create molecules from ultracold atoms. Those methods are photoassociation, three-body recombination near Feshbach resonance, coherent two-body transfer near Feshbach resonance via magnetic field sweep, RF association and magnetic field modulation. The most commonly used method is three body recombination near a Feshbach resonance. The molecules created by a three body recombination process are preferentially in a weakly bound molecular state. In a three-body recombination process, three atoms collide and two of the atoms form a bound state releasing enough energy to eject a third atom from the trap. Lower temperature molecules created by this method, can then evolve into a molecular Bose-Einstein condensates. This is one of the most efficient methods and it produces molecules having twice the atomic polarisability.

The dynamics of Feshbach molecule creation from ultracold ^{6}Li atoms by sweeping the magnetic field across the Feshbach resonance are studied in this thesis. Feshbach resonances provide the experimental key to couple pairs of colliding atoms into molecules and vice versa. Atoms above the Feshbach resonance (BCS side) can be converted adiabatically into molecules on the BEC side by applying a time dependent magnetic field and a reverse magnetic field ramp can be used to dissociate molecules into atoms again. Weakly bound, long lived molecules can be produced via this method. For high temperatures this process can be described by a Landau-Zener model, which predicts a conversion efficiency of 100% if the ramp rate is sufficiently slow. The transition probability is proportional to $1 - e^{-\alpha\dot{\beta}^{-1}}$ [55, 56], where α is a constant which can be thought of as atom-molecule coupling strength and $\dot{\beta}^{-1}$ is the inverse ramp rate. This process can

be approximated as an adiabatic passage through a two-level avoided crossing in which a pair of free atoms and a bound vibrational level of the diatomic molecules are considered the two states in the process. There are different theoretical approaches to describe the dynamics of molecule creation via this method, however a complete, detailed understanding of the process has never been achieved since the experimental parameters like temperature are difficult to include in the theoretical model. A new theoretical approach developed by theoretical group in the University of Nottingham to explain the dynamics of ^{6}Li molecular conversion via magnetic field ramp, which is given in the chapter 6. A comparison of our experimental results of ^{6}Li molecular conversion rate with different theoretical models is given in the chapter 5.

Chapter 3

Experimental setup

This chapter describes technical details of the experimental apparatus used to prepare a fermionic ^{6}Li atom cloud for creating Feshbach molecules via a magnetic field ramp. The details of cooling lasers, the dipole beam laser, vacuum system, Lithium oven, magnetic coils and control system are explained in this chapter. Conventional laser cooling and trapping methods are used to prepare a cold ^{6}Li atomic cloud. The experimental setup consists of lasers and optics to guide and shape the laser beams for the cooling, trapping and imaging of atoms. Other essential components are the atomic source, Zeeman slower, magnetic field coils and vacuum chambers with ion and sublimation pumping system. The schematic diagram of the experimental setup is shown in the figure 3.1 . Most of this particular experimental apparatus have been described in previous PhD theses [47, 49], so this chapter will focus on the new parts of the apparatus and the main points of experimental system.

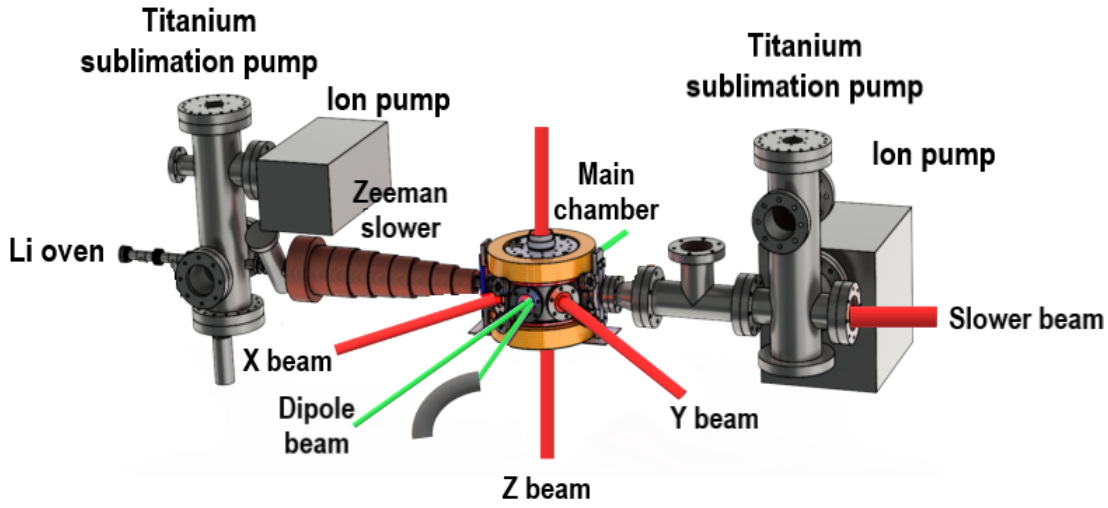

Figure 3.1: Experimental apparatus for cooling and trapping ^{6}Li atoms.

3.1 Laser system

There are two home built external cavity diode lasers (ECDL) used in the experimental setup. One of them is used as reference laser for saturation absorption spectroscopy and other one as imaging laser for absorption imaging of atoms. Home built diode lasers are easy to build by fixing a laser diode into a lens tube and a grating on a translation mount. A maximum power of 15 mW can be obtained from the laser at room temperature, which is more than sufficient to setup a saturated absorption spectroscopy system with offset locking and also for an imaging system. The grating (GH 13-18 V) mounted in front of the laser diode is used to tune the wavelength of the laser by changing the angle of the grating. A temperature controller is connected to the peltier element (CP 85438) and a thermocouple (TH 10 thermistor) is attached to the laser mount for maintaining the temperature of the laser, which yields the stability of the laser. A photograph of the home built external cavity diode laser is given in appendix A.

The main source of light for the experiment is derived from a tapered amplifier

laser (Toptica DLC TA Pro 670), which also includes a master diode laser. The master diode acts as a source of seed power to the TA chip, which amplifies the signal to give an output power of $\sim 300\,\mathrm{mW}$. Most of the output light from TA Pro is used as repumper light. Some of the remaining light is used to seed a home built tapered amplifier, which consists of TA chip attached to a home built mount. The home built TA consists of two lenses mounted before and after the TA chip and two peltier elements attached to mount. The output from the home built TA is used for cooling and slower light to produce a magneto-optical trap in the main chamber. The distributed beam powers in X, Y, and Z direction to produce a ^{6}Li MOT in our experimental system are given in the table 3.1.

Table 3.1: Beam power for ^{6}Li Magneto-optical trap

Beam	Cooler(mW)	Repumper(mW)
X	33	19
Y	29	16
Z	40	18
Slower	22	12

3.2 Vacuum system

Ultracold atom experiments can be performed in ultrahigh vacuum environments only. Our experimental setup is comprised of two vacuum chambers attached via Zeeman slower. Both vacuum chambers are pumped by an Agilent ion getter pump and an additional Titanium sublimation pump. The Lithium oven is attached to one of the chambers where an atomic beam block has been implemented to block the atoms moving from this chamber to the main chamber when it is not needed. In addition to the valve for separating the two chambers, a Zeeman slower is also attached between them, which helps to reduce the velocity of atoms reaching to the main chamber, ultimately improving atom loading in

the magneto-optical trap (MOT).

The cooling and trapping of ^{6}Li atoms are performed in the main chamber under a background pressure of $< 10^{-11}$ mbar, whereas the background pressure in the Lithium oven chamber is in the range of 10^{-8} mbar. The MOT coils attached to the main chamber produce quadrupole fields for the spatial confinement of atomic clouds inside the main chamber. In addition to the MOT coils, Feshbach coils are attached to the same chamber for producing high magnetic fields, which is a homogeneous field produced on one axis in the trap region. Cooling water is passing through these coils to transport heat due to high current away from the coils without affecting the optical bench.

3.3 Lithium oven

The lithium oven consists of a stainless steel tube into which a few grams of chunk ^{6}Li enriched to 95 %, were placed. Electric heating wire was wound around this tube 15 times to uniformly heat the tube to a temperature of 400° C. This setup can provide enough flux to load 2×10^8 ^{6}Li atoms into the MOT in 12-15 s. A thermocouple is attached to the oven to monitor its temperature and an insulation covering helps to maintain the temperature inside the oven. As can be seen in the Figure 3.2a, the oven is attached to the vacuum chamber. A sublimation pump and an ion pump are attached to the oven chamber to maintain the high level of vacuum, as well as a valve for attaching a roughing pump to recover this pressure if the chamber needs to be opened. We can estimate the pressure inside the chamber by a pressure gauge or by the current drawn from the ion pump. A motor controlled shutter is placed to block the atomic beam when it is not needed. A valve is attached to separate the Lithium oven from the main chamber

in case more lithium needs to be added to the oven. A strong fluorescence in the presence of resonant light can be observed when the oven operates at 400° C, shown in the Figure 3.2b.

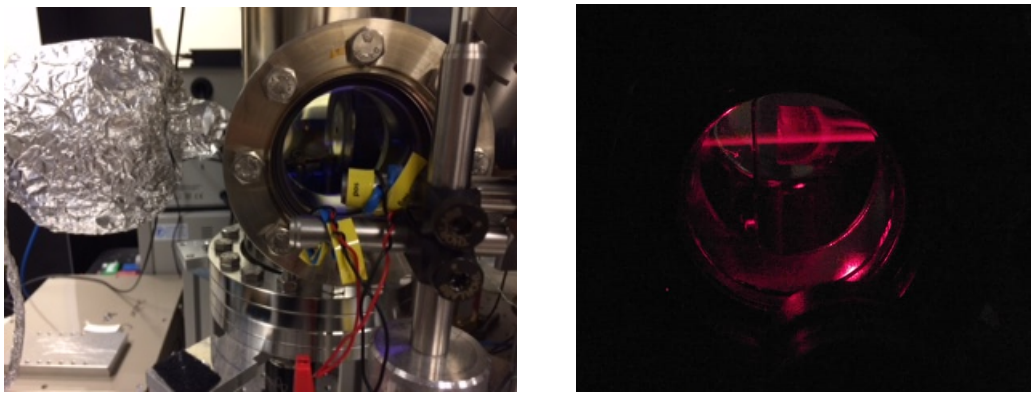

(a) **(b)**

Figure 3.2: Photographs of the lithium oven. (a) Li oven wrapped in aluminium foil (left) and a viewing window of the oven chamber (right), (b) fluorescence in the oven chamber due to resonant light.

At this temperature, the oven provides 3.7×10^{16} atoms per second which is calculated from [57, 58],

$$I_{\text{oven}} = \frac{1}{4} n A \bar{\nu}. \tag{3.1}$$

where I_{oven} gives the number of atoms per unit time passing through the area of the oven aperture (A) at a certain temperature (T). The atomic density inside the oven is given by n, and the mean velocity of the atoms by $\bar{\nu}$. Atomic density (n) and mean velocity ($\bar{\nu}$) of the atoms can be determined from

$$n = \frac{P}{k_B T}, \tag{3.2}$$

$$\bar{\nu} = \sqrt{\frac{8 k_B T}{M}}, \tag{3.3}$$

where P is the vapour pressure in Torr inside the oven and M represents the mass of lithium. The vapour pressure of a gas can be obtained by the Antoine equation [59],

$$\log_{10}(P) = A - \frac{B}{T + C}, \tag{3.4}$$

where A, B, and C are the Antoine coefficients (constants). The atomic flux provides an adequate loading of the MOT (2×10^8atoms in 15 s).

3.4 Zeeman Slower

The normal operating temperature of the Lithium oven is $400 - 420^\circ$ C, which produces ^{6}Li atoms with a most probable velocity of $\sim 1370 - 1390\,\mathrm{ms}^{-1}$, calculated from the expression $v_p = \sqrt{\frac{2k_BT}{m}}$. Zeeman slowers have been used in many laser cooling and trapping experiments since they reduce the velocity of the atoms using a spatially varying magnetic field. The atoms are captured and cooled in the MOT when they are slowed down to the capture velocity of $v_c \sim 230\,\mathrm{ms}^{-1}$, given by $v_c = \left(\frac{2F_{\max}D}{m}\right)^{1/2}$, where D is the MOT laser beam diameter and $F_{\max}$ is the maximum force that a beam of any intensity can impart upon an atom, which is given by $F_{\max} = \hbar k\frac{\Gamma}{2}$.

As described in the thesis by S.Warriar [47], the Zeeman slower is divided into nine sections of coil windings (along the axis of the slower), over a variable number of layers (radially outwards from the axis of the slower). The optimised parameters of Zeeman slower result in a mean atomic velocity of $\sim 158\,\mathrm{ms}^{-1}$, within the capture velocity calculated. The atoms that are captured by the Zeeman slower experience a counter propagating beam called slower beam that is red-detuned from resonance. The optimum current for the Zeeman slower is 8.1 A, which was characterised and studied in our experimental system [47].

3.5 Magnetic field coils

Magnetic field gradients generated by current carrying coils cause a splitting in the atomic energy levels which, when used in combination with Doppler cooling lasers, provides spatial confinement for atoms in the MOT. Five pairs of magnetic field coils are used in the experimental setup. One pair of magnetic field coils in anti-Helmholtz configuration produces the magnetic field gradient in the main chamber where laser cooled atoms are trapped. These MOT coils run a current of 40 A and produce a magnetic field gradient of $0.488\,\mathrm{G\ cm^{-1}A^{-1}}$ [47]. Other three pairs of magnetic field coils are called compensation coils, in which the current runs though these coils in a parallel formation creating a homogeneous magnetic field around the trap region so that one can change the position of the MOT in three axes by independently adjusting the current passing through these coils.

Another pair of magnetic field coils in Helmholtz configuration is used to produce an offset magnetic field to tune the interaction of atoms by changing the magnetic field in proximity to a Feshbach resonance. These coils are known as Feshbach coils, which create a field strength of $2.7\,\mathrm{GA^{-1}}$ at the centre of the main chamber with a magnetic field gradient of $2\,\mathrm{mGA^{-1}cm^{-1}}$. The experiments on strongly interacting Fermi gas need to be performed in a high magnetic fields, where the nuclear spin essentially decouples from the electron spin. The Feshbach coils in our system can be used to generate more than 1000 G, so that one can easily cover the full range of interest for the creation of $^6Li_2$ Feshbach molecules. The current required for these magnetic fields quickly heats up the coils, so water is circulated through them.

3.6 Dipole laser setup

An equal mixture of spin half ^{6}Li atoms ($F = 1/2, m_F = \pm 1$) are trapped using a dipole potential created by a far red-detuned laser beam, which is passed through the main chamber twice such that it crosses itself at an angle of 14°. This crossed dipole trap is formed using a 100 W, 1070 nm beam produced by an IPG Photonics YLP-100-LP-AC fibre laser, with each beam focused to a waist of 80 μm. The dipole trap setup consists of an acousto-optic modulator (AOM) for controlling the power in the beam by allowing the first order beam to pass through the system. The crossed beam trap depth is calculated for 100 W, is $\frac{U_0}{k_B} = 0.96$ mK [47].

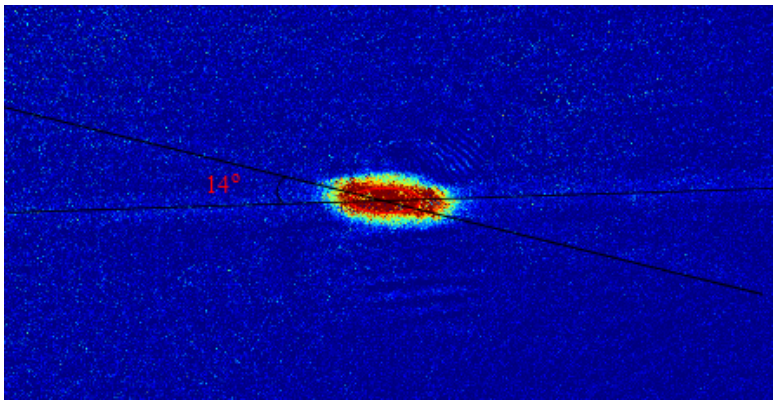

Figure 3.3: Dipole trap created in the experimental setup. The figure shows an absorption image of dipole trap on the vertical imaging screen taken by the Manta camera. The image is taken using a high field imaging technique at 860 G.

The dipole beam path has different electronic and optical components to shape and guide the beam into the main chamber. The output beam from the IPG laser source passes through an AOM, where the power of the beam is being controlled in the lower power regime (< 20 W) using a feedback circuit. The first order beam is directed to the main chamber and focused down in the middle of the magnetic trap position determined by a method explained in the chapter 4. Both ingoing and return beam are focused down by using a $f = 125$ mm gradient index lens (LightPath Technologies, GRADIUM) and they cross each other at the centre

of main chamber to form a much deeper dipole potential than one beam alone, where atoms can be trapped and studied (as seen in figure 4.9).

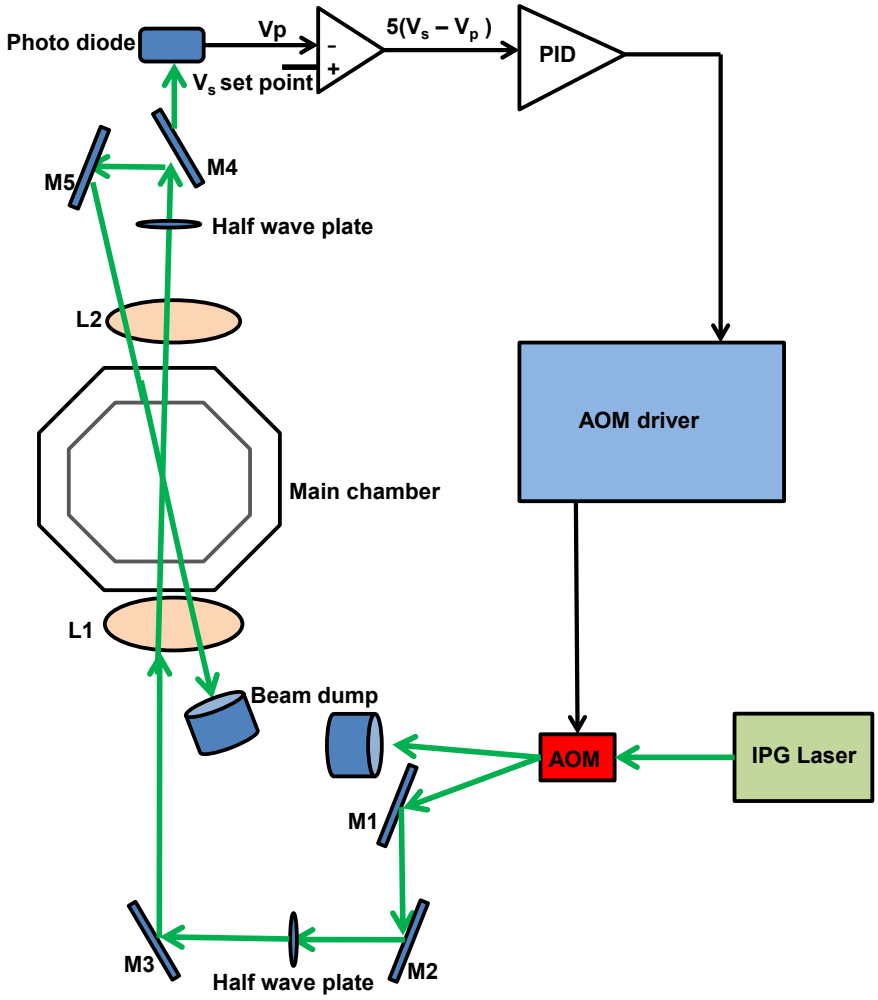

Figure 3.4: The schematic diagram of dipole trap setup.

The feedback mechanism is controlled by an electronic circuit which comprises of a photodiode, comparator circuit and a PID card (Proportional Integration Differential card) as seen in the schematic digram of the dipole trap setup in figure 3.4. A small part of the return beam is taken to a photodiode and the signal is then compared with a set point in the comparator circuit which is connected to a PID card. The output of the PID card is connected to the AOM driver box,

where the power of the beam is controlled. The AOM driver box consists of two AOM controllers which are called primary and secondary AOM controllers. The output of the AOM is adjusted accordingly. Half wave plates are used in the optics since orthogonally polarised light helps to prevent atom loss from the trap due to Raman scattering processes.

The IPG laser can be controlled by its software interface as well as by the experimental sequence in which the power of the beam can be controlled at different stages of the experiment. The calibration of the beam power is shown in figures 3.5 and 3.6.

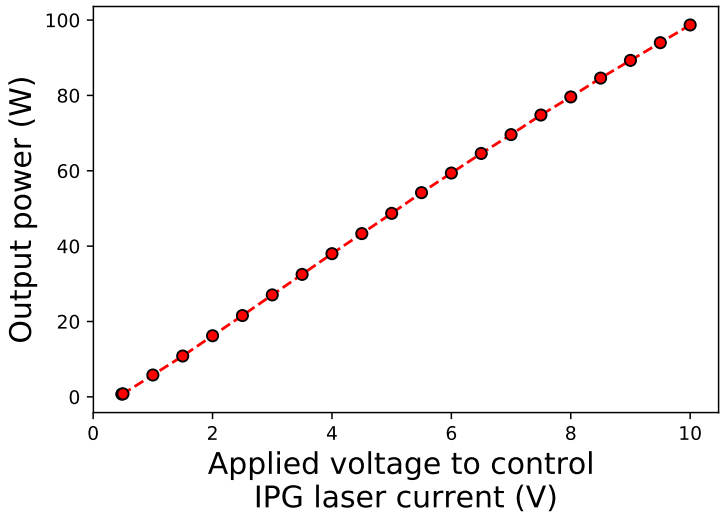

Figure 3.5: IPG output power calibration by changing the current passing through it.

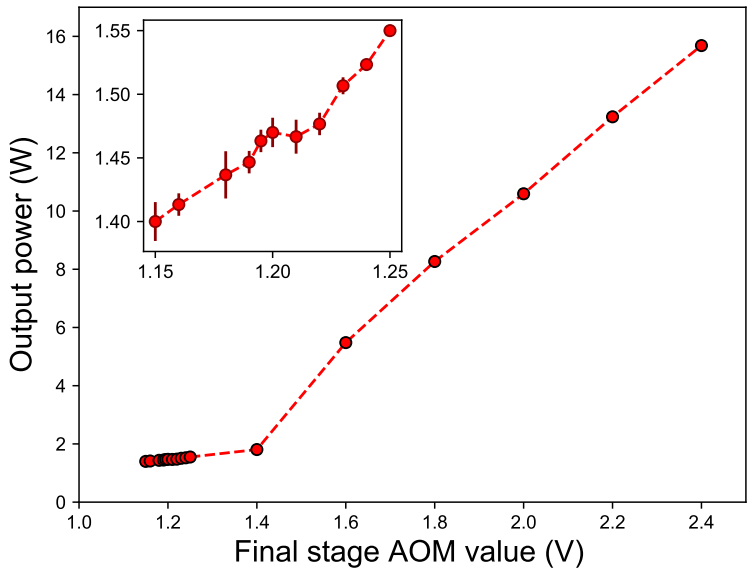

Figure 3.6: IPG power calibration by AOM control voltage. IPG power calibration by AOM control voltage in the lower power regime ($<$ 20 W). The primary AOM value is changed by fixing the secondary AOM value at 2.5 V. The error of each data point is calculated from three measurements and they are too small.

3.7 Control system

The experiment is controlled by a computer interface program called Pyplayer, which is programmed in C^{++} and Python. This program takes the control of the National Instruments PXIe-8130 controller, which communicates to the hardware through its add on digital and analogue output cards. This controls most of the electronic and optical components which are needed for the smooth operation of the experiment. The Pyplayer provides an output signal defined with a temporal resolution of 1 μs and a voltage regulation of 16 bits spanning from -10 V to 10 V. The controller and the program are easy to conceptualise and help to implement adding and removing different stages in the experiment through digital and analogue channels. The client program was developed by previous PhD students

who worked on this project. Further details of the program are given in M. D. Jones thesis [60]. A screen shot of experimental stages in Pyplayer is shown in the figure 3.7.

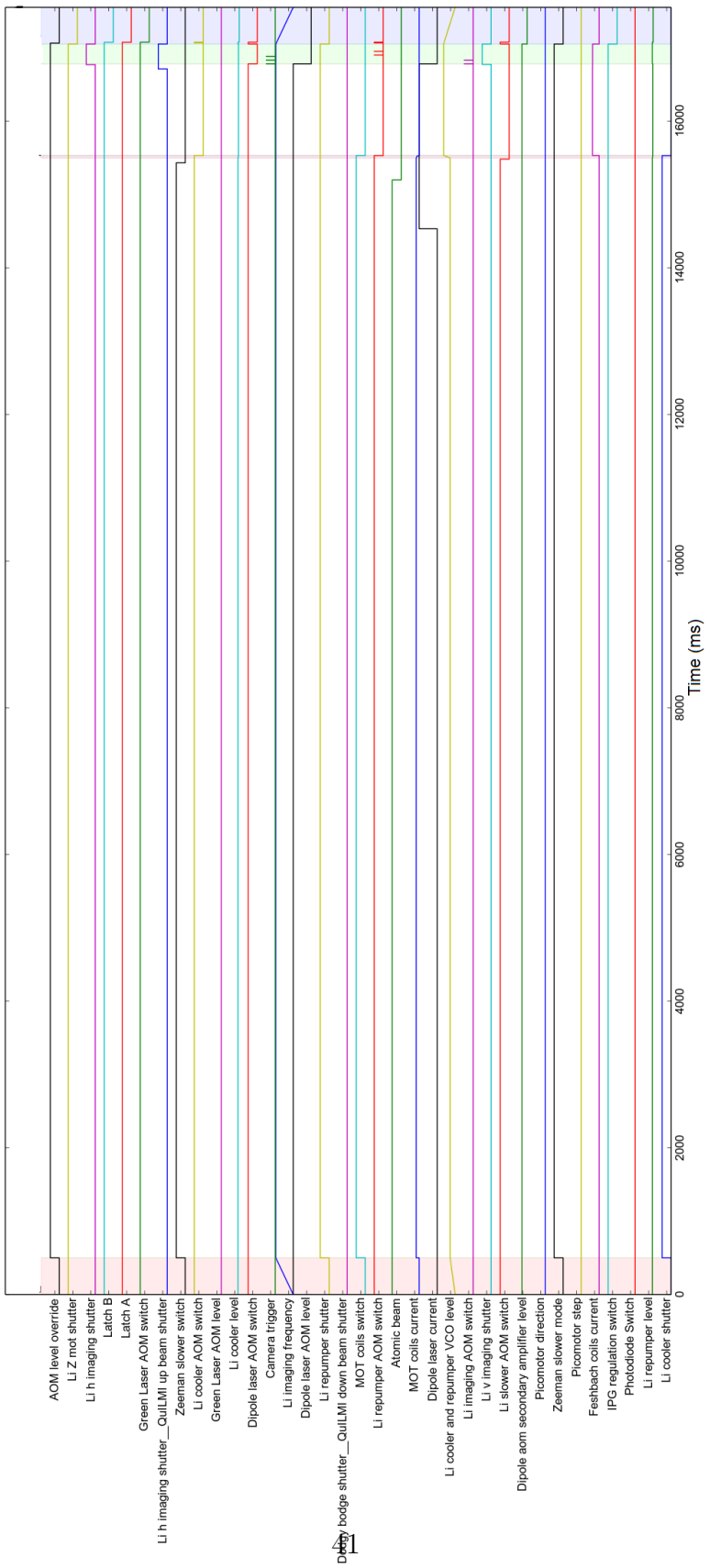

Figure 3.7: A Screen shot of experimental sequence. The figure shows the schematic of experimental steps in Pyplayer with desired outputs for each digital and analog channel against time from the start of the experimental sequence to the end of the sequence.

Chapter 4

Experimental methods

The aim of the experiment is to create bosonic Feshbach molecules from fermionic ^{6}Li atoms. This chapter focuses on experimental techniques of laser cooling, loading and trapping ^{6}Li atoms into the dipole trap, and details the further steps carried out to improve phase space density of the atomic cloud by evaporative cooling. Finally, the steps involved in the conversion of fermionic atoms into molecules by sweeping the magnetic field across a Feshbach resonance are also reviewed.

4.1 Laser cooling and trapping

Conventional laser cooling and trapping methods are used in our experimental setup. These methods include Zeeman slowing, an optical molasses stage, MOT compression, optical dipole trapping followed by evaporative cooling methods, and absorption imaging. The first step in the experiment involves cooling atoms down to temperatures ranging from milli kelvin to micro kelvin. Laser cooling of atoms is based on the Doppler effect. The oscillating electric field of the laser induces a dipole moment opposite to the direction of atoms, which results in de-

creasing velocity of atoms and cooling them at a position where the magnetic field gradient is nearly zero. The Spatial confinement of atoms introduced by the magnetic field and photon scattering via polarisation of the beams is used to create an atomic cloud, so called magneto-optical trap (MOT). A Toptica TA Pro laser is used to produce light that optically couples the cooling and re-pumper transition of ^{6}Li, as required for cooling and trapping of atoms in the MOT. The laser beam passes through acousto-optic modulators (AOMs), which detunes the light by -114 MHz and +114 MHz for the cooler and re-pumper beams respectively. An additional laser frequency shift has to be provided for the Zeeman slower from the cooler beam, which is then called the slower beam. This is done by applying a further AOM which shift the frequency by -80 MHz from the cooling light.

4.1.1 Optical molasses

Initially, 5 grams of solid (chunk) ^{6}Li were placed in the oven which is operated in the temperature range of 400-420 °C, produces atoms with velocity of 1300 ms^{-1}. The atoms are then slowed by the Zeeman slower consisting of coils of wire with a tapered density along the axis of the beam propagation (z-direction). This produces a B-field with a varying magnitude along the z-direction. The scattering of photon along the slower results in a reduction of the atomic velocity. The spatially varying Zeeman shift of the resonant frequency enables lower velocity classes of atoms to be resonant with the slower beam even when the velocity of the atoms changes. Cooling and trapping in the magneto-optical trap is performed in the main chamber where cooler and re-pumper beams intersect and interact with the atoms. Six counter propagating circularly polarised beams interact with the atoms and form a cold atomic cloud in the centre of the main chamber, this stage is called the optical molasses stage.

4.1.2 Magneto-optical trap (MOT)

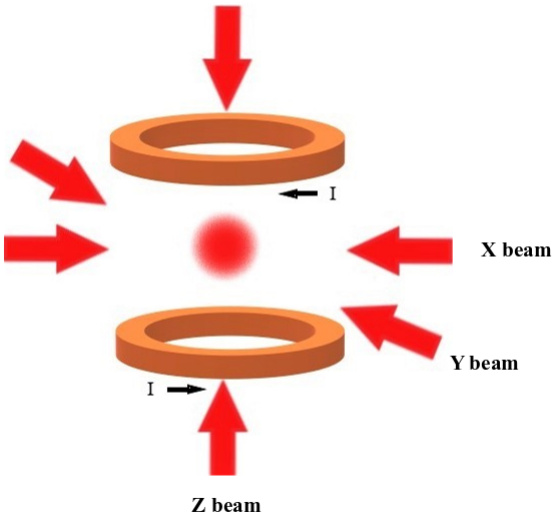

Figure 4.1: Schematic diagram of laser cooling and trapping. The current, which passes through the MOT coils provides a gradient in the magnetic field at the centre of the main chamber, where laser cooled atoms can be trapped and studied. Three counter propagating circularly polarised beams in three directions also help to confine the atoms in the region, where the magnetic field gradient is nearly zero.

The Magneto-optical trap (MOT) is a method to provide a spatial confinement for the atoms by inhomogeneous magnetic field to produce trapped atoms. A quadrupole magnetic field created by a pair of anti-Helmoltz coils can produce a gradient in magnetic field inside the vaccum chamber. Along with three counter propagating laser beams atoms will be trapped in the region of zero magnetic field. The trapped, cold ensemble of atoms can be produced and atoms can have the temperature below 1 milli kelvin to several hundred micro kelvin. The apparatus uses the magnetic field gradient produced by the magnetic coils called MOT coils in anti-Helmholtz configuration. The circularly polarised light provides a spatial dependence of the spontaneous force, which confines the atoms into the region where the gradient of magnetic field is nearly zero. The schematic diagram of MOT apparatus is illustrated in the figure 4.1. The figure 4.2 is a photograph of

the ^{6}Li MOT loading through one of the view ports of main chamber.

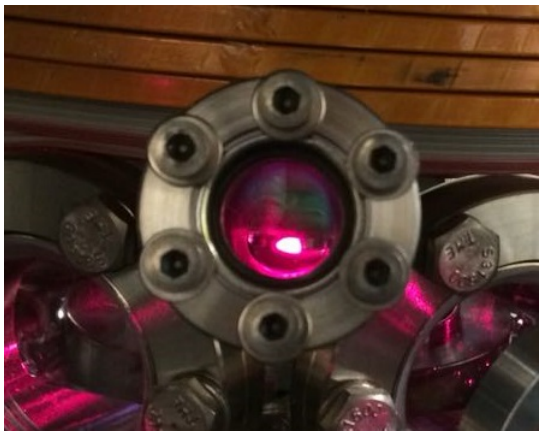

Figure 4.2: ^{6}Li MOT through a view port into the main chamber. The bright spot inside the chamber is the fluorescence of the atomic cloud during MOT loading.

4.1.3 ^{6}Li MOT compression

A high density, lower temperature atomic cloud is needed for an efficient transfer of atoms into the dipole trap. To increase the density of the atomic cloud, while cooling it further to $500\,\mu$K, a MOT compression process is implemented. Different methods can be used to reduce the atom cloud temperature. Since the excited state ($2^2P_{3/2}$) of ^{6}Li atom is unresolved, sympathetic cooling is not possible in the current experimental system. During the MOT loading stage the cooler and re-pumper beams are set to be resonant with the transitions $F = 3/2 \rightarrow F' = 5/2$ and $F = 1/2 \rightarrow F' = 3/2$ respectively. The MOT compression stage helps to reduce the cloud temperature from $2000\mu K$ to $500\mu K$ in the current experimental setup. This stage involves simultaneously ramping down the cooler and re-pumper beam powers using the AOMs and also ramping down the magnetic field gradient. During MOT compression process, the detuning of the MOT beam changes from -32.2 MHz (-5.48Γ) to -4 MHz (-0.6Γ), the density of the atoms increases and the cloud temperature decreases as the detuning is ramped close to $-\frac{\Gamma}{2}$, such

that it reaches the minimum temperature and also increases phase space density of atoms. The minimum temperature limit is called Doppler temperature, which is 140 μK for ^{6}Li. In the final stage of the MOT compression, the re-pumper beam power is set to be ramping down slower than the cooler beam power in order to make sure that most of the atoms are prepared in the lower hyperfine manifold $F = \frac{1}{2}, m_F = \pm\frac{1}{2}$. Therefore both $m_F = \pm\frac{1}{2}$ are populated equally at the end of MOT compression process. In order to exploit s-wave interactions at ultralow temperature, non-identical particles need to be created. The dipole beam is turned on one second before the final stage of the MOT compression when the MOT beams turn off, providing an efficient transfer of atoms into the dipole trap. The optimisation of MOT loading and compression parameters has to be carefully performed in order to increase the density and lowering the temperature, while retaining a large amount of atoms collected before the MOT. The optimisation of the MOT loading time and the MOT loading detuning for the current experimental setup is shown in the figure 4.3. The optimum loading time for ^{6}Li MOT is chosen to be 15 s and the MOT loading detuning value is chosen where more number of atoms are loaded in the MOT. For the compression phase, The final detuning value is chosen by scanning the detuning values and set to be -4 MHz, where the maximum atom number is obtained in the MOT compression stage as shown in the figure 4.4(a). The absorption image of a compressed ^{6}Li MOT is shown in the figure 4.4.

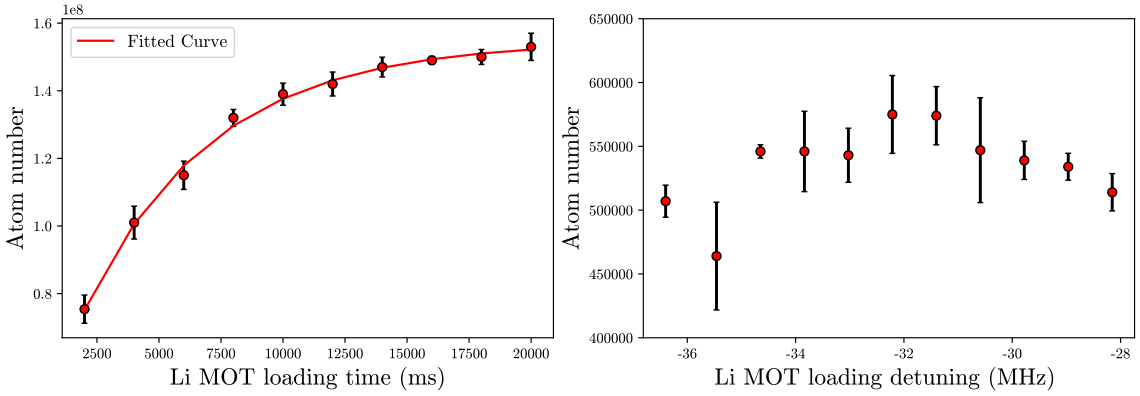

(a) **(b)**

Figure 4.3: Optimisation of ^{6}Li MOT. The ^{6}Li MOT loading time (a) and ^{6}Li MOT loading detuning (b). In both cases, the error bars are the standard error of three measurements.

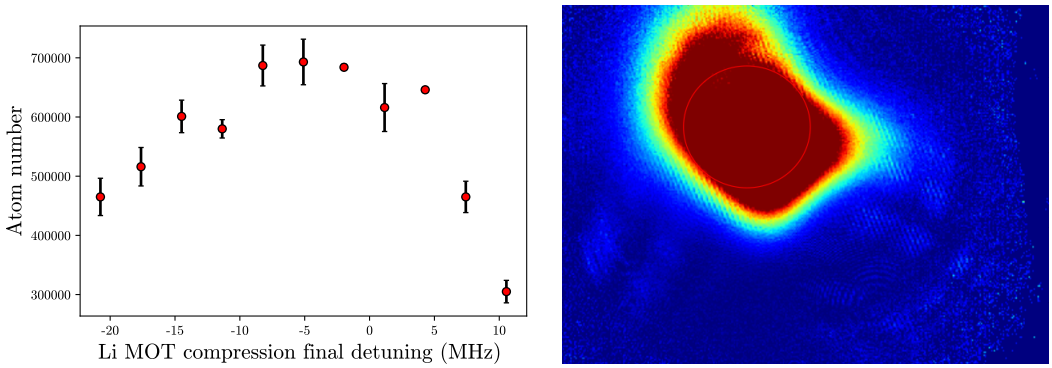

(a) **(b)**

Figure 4.4: The ^{6}Li MOT compression final detuning and an absorption image of compressed ^{6}Li MOT. The graph shows the optimisation of ^{6}Li MOT compression final detuning (a). The error bars are the standard error of three measurements. The second figure is an absorption image of a compressed MOT containing 2×10^8 ^{6}Li atoms (b) on the horizontal imaging screen taken by CCD camera.

4.2 Evaporative cooling methods

Evaporative cooling methods are used to increase the phase space density in a conservative potential by further reducing the temperature of the cold atomic sample. The first method is plain evaporation, in which the system allows high

energy particles to escape by holding the atoms in the highly focused beam without changing the trapping potential. The dipole beam provided by the IPG laser, which is switched on at the end of the MOT compression stage and an optical power of 100 W is held atoms for 1.2 s to allow for plain evaporation to occur, resulting in a temperature of $200\,\mu$K in the cloud. The atom number and temperature of the cold sample by varying the duration of the plain evaporative cooling phase at 100 W of optical dipole trap power is shown in the figure 4.5.

The second method is forced evaporation, by reducing the trap depth by decreasing the power in the dipole beam. Forced evaporation has to be performed slow enough such that the atomic cloud can rethermalise. This includes current evaporation followed by AOM (Acousto optic modulator) evaporation. The current evaporation method involves lowering the dipole laser current directly whereas during the AOM evaporation, we lower down the output power of the dipole beams by reducing the diffracted power through the AOM. During the current evaporation stage, the dipole beam power is ramped down from 100 W to 34 W in 1000 ms by reducing the current of the IPG laser linearly. This process helps to decrease the temperature of the cloud to $63\,\mu$K. The third method used in the experiment is called AOM evaporative cooling. This involves exponentially lowering the trap depth step by step and then holding the atoms in the final trap depth ($\sim 12.1\,\mu\mathrm{KW}^{-1}$) for 200 ms. During the evaporative cooling process, the temperature of the cloud can be varied from $200\,\mu$K to 100 nK depending on the final AOM value. Primary and secondary AOM controllers are used to control the beam power in the lower power range (< 34 W). The feedback circuit used in the dipole trap setup controls and improves the stability of the output beam in the lower range of power. All three methods of evaporative cooling are shown in the figure 4.6(a). After evaporation cooling, we prepare about $\sim 2 \times 10^5$ atoms at temperatures of 100 nK. The atom number and cloud temperature can be varied

according to the desired final power in the dipole trap. The absorption image of atomic cloud after evaporative cooling is shown in the figure 4.6(b).

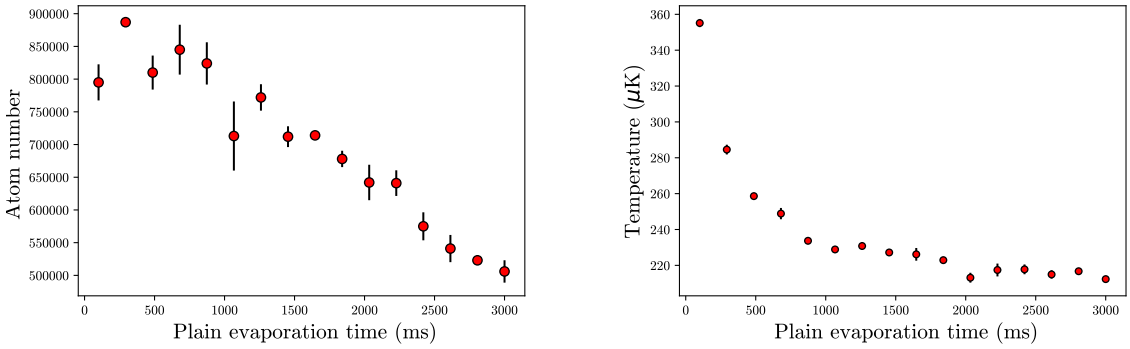

(a) **(b)**

Figure 4.5: Atom number and temperature of atomic cloud at different plain evaporation time. Atom number at different plain evaporation time (a) and temperature of atom cloud for varying duration of plain evaporative cooling at 100 W of optical power (b).

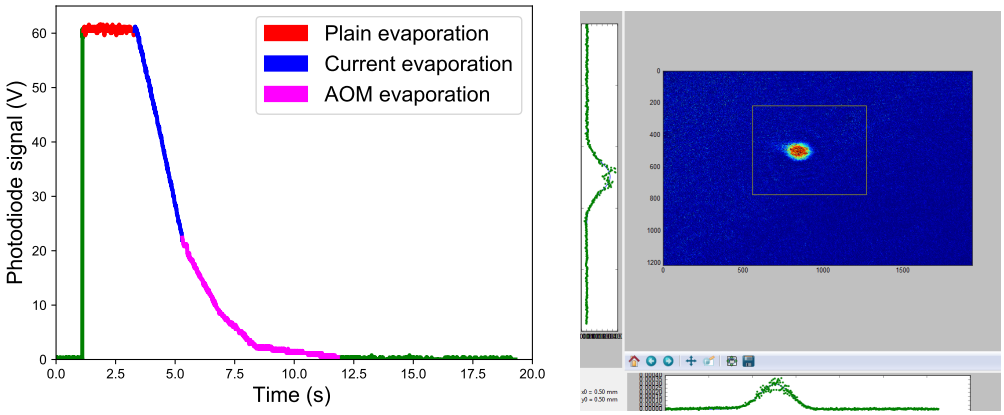

(a) **(b)**

Figure 4.6: Dipole beam power during evaporative cooling methods (a) and absorption image of atoms after AOM evaporative cooling (b). The figure (a) shows the change in dipole beam power during evaporative cooling process captured by a photodiode. The absorption image of the cloud taken after a fall time of 1.5 ms and the temperature of the atomic cloud is determined to be 517 nK.

4.3 Absorption imaging

Fluorescence imaging and absorption imaging techniques are suitable for MOT imaging. The former method can be considered non-destructive since it uses light scattered from the MOT, whereas the latter one is a destructive method, since it destroys the cloud through absorption of photons by atoms. The implementation of absorption imaging is relatively straight forward and it allows one to measure atom number, size, density distribution and temperature of the cloud. One of the home-built ECDL lasers is used for absorption imaging, detuned -110 MHz from the transition where the the frequency of the imaging laser is set to be resonant with a cyclic atomic transition, $F = \frac{3}{2} \rightarrow F' = \frac{5}{2}$. The resonant laser beam is impinged onto the atomic cloud and the transmitted light through the atomic cloud is detected for the imaging process. There are two CCD (charge-coupled device) based cameras to take images of the atomic cloud, one in horizontal and another in the vertical direction. The camera Guppy F-038-B is used for the horizontal imaging set up, which has a magnification of 0.48 whereas a magnification of 3.333 is used by the vertical imaging system, in which a Manta-G235B is used for taking images of the atomic cloud in high fields.

Three images are taken during the absorption imaging process, the first image is with atoms, blasting them away, the second image is taken with just the light after the atoms have dissipated, and the third one is the background image, with no light and no atoms. Consider a situation with an on-resonance imaging beam interacting with a cloud of atoms. The probability of a photon is absorbed within an infinitesimal distance can be determined by the expression,

$$\frac{\partial I(x,y,z)}{\partial x} = -\sigma n(x,y,z), \tag{4.1}$$

where σ and $n(x,y,z)$ are the absorption cross section and the spatial density of the atoms in three dimensions respectively. When the imaging beam passes

through the cloud, the light intensity is damped exponentially, which can be calculated by the equation given below,

$$I(x,y,z) = I_0 \exp\left(-\sigma \int_0^x n(x^{'},y,z)dx^{'}\right) = I_0 e^{-OD_{(y,z)}}. \tag{4.2}$$

The optical density $OD_{(y,z)}$ is given by,

$$OD_{(y,z)} = \sigma \int_0^x n(x^{'},y,z)dx^{'}. \tag{4.3}$$

From these equations, one can determine the total number of atoms, which is given by,

$$N = \iiint n(x,y,z)dx\,dy\,dz = \frac{1}{\sigma}\iint OD_{(y,z)}dy\,dz. \tag{4.4}$$

Two methods have been used to calculate the last double integral in the equation. One method is Gaussian fitting on the image profile and the second one uses imaging from a sum of pixel values. Our CCD cameras are set to take three images in consecutive intervals such that they take an image with atoms referred to as $I(y,z)$(RAW), the image taken after all the atoms have dissipated is referred to as $I_0(y,z)$(REF) and third one is a background image (BCKGRD). The figures in 4.7 show examples of three consecutive images taken during absorption imaging of ^{6}Li MOT. The optical density obtained from these images is given by,

$$OD(y,z) = -ln\frac{I(y,z)}{I_0(y,z)} = -ln\frac{\text{RAW-BCKGRD}}{\text{REF-BCKGRD}}. \tag{4.5}$$

The absorption image of a compressed ^{6}Li MOT is shown in the figure 4.8.

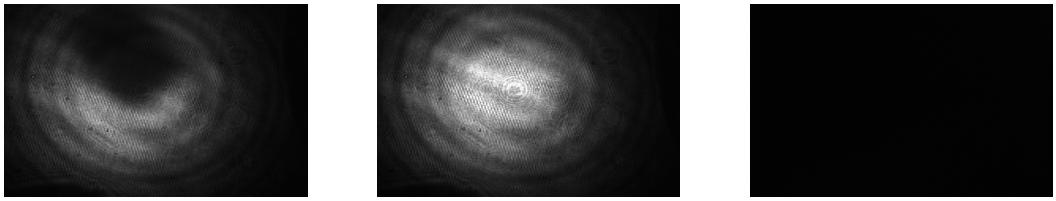

(a) (b) (c)

Figure 4.7: Three consecutive images taken by CCD camera during absorption imaging of compressed MOT.

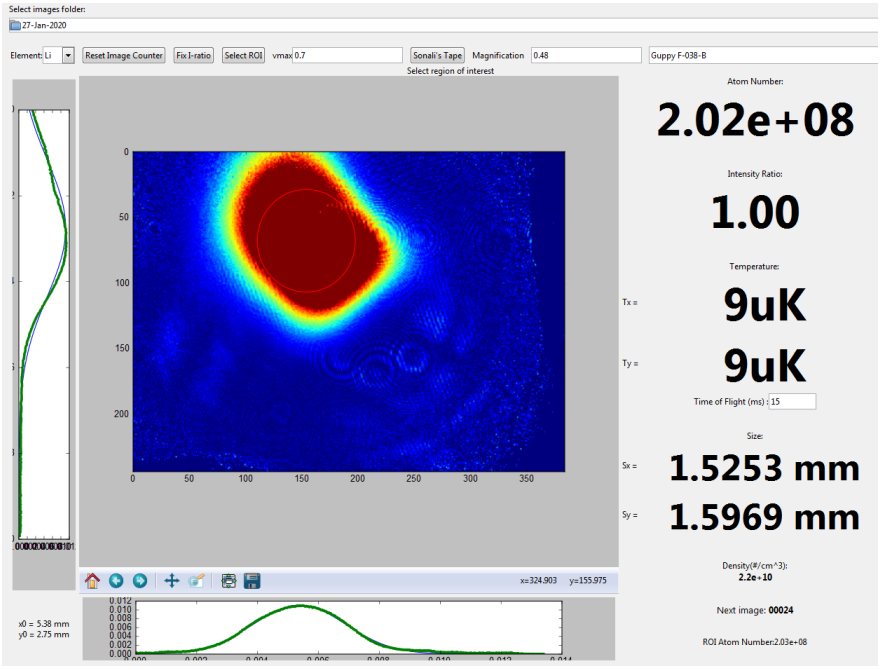

Figure 4.8: Absorption image of ^{6}Li MOT on the horizontal imaging screen.

4.3.1 High magnetic field imaging

The interaction of atoms with a magnetic field turns over into the high-field regime even at quite moderate magnetic field. In this case the Zeeman energy becomes larger than the hyperfine interaction energy and the nuclear spin essentially decouples from the electron spin. The imaging transitions will shift in frequency when the energy of the atomic states is shifted due to an external magnetic field. One of the imaging systems in our experimental set up is used to take images of

atomic clouds at high magnetic field produced by Feshbach coils. In the low field regime, re-pumper light is needed to keep the atoms in the desired cyclic transition. However the transition becomes closed above 200 G and absorption imaging can be performed without the need of re-pumper light. An offset circuit consisting of two voltage controlled oscillators (VCOs) allows the imaging system to perform both low-field and high-field imaging. The high-field VCO gives a detuning ranging from -600 MHz to -1230 MHz, which covers the imaging of atoms interacting with magnetic fields varying from 450 G to 950 G. The absorption images of dipole trapped atoms in the low-field and high-field are shown in the figure 4.9.

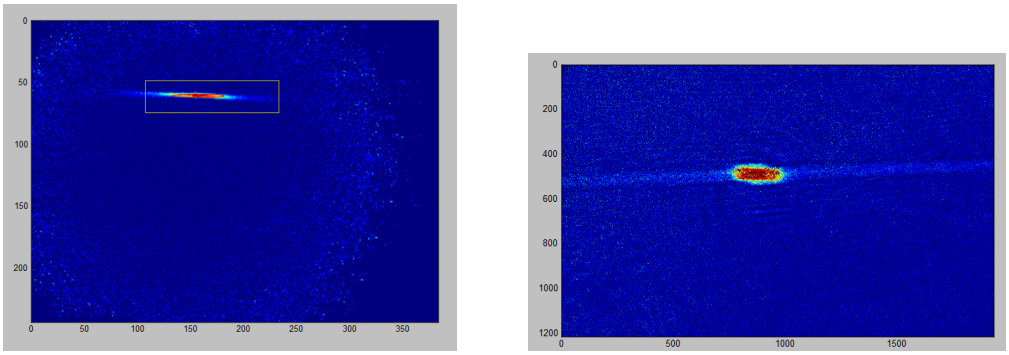

(a) **(b)**

Figure 4.9: Absorption images of atoms held in the optical dipole trap after plain evaporative cooling from (a) the horizontal camera in the low-field regime and (b) the vertical camera in the high-field regime. The image shows 10^6 atoms trapped in the dipole trap. The X and Y scales are in mm.

4.4 Temperature measurements

Time of flight (TOF) imaging is the standard technique to measure the temperature of an atomic cloud. This method involves thermal expansion of the cloud by releasing the atoms from the trap and imaging after different fall times. By assuming the atomic cloud is spherically symmetric, the Gaussian radius of the ballistically expanded cloud can be estimated by [61]

$$\sigma_t = \sqrt{\sigma_0^2 + \sigma_v^2 t^2}, \tag{4.6}$$

where σ_v stands for Gaussian radius of the velocity distribution associated with the temperature. The initial cloud radius and the radius after a fall time of t are represented by σ_0 and σ_t respectively. The plot of σ_t^2 versus t^2 will be a straight line for sufficiently long time of flights and the slope of the straight line gives the temperature of the atomic cloud which can be obtained from the equation,

$$T = \frac{M}{k_B}\sigma_v^2. \tag{4.7}$$

where M is the mass of the lithium atoms and k_B is the Boltzmann constant. The temperature measurement of ^{6}Li MOT is shown in figures 4.10 and 4.11.

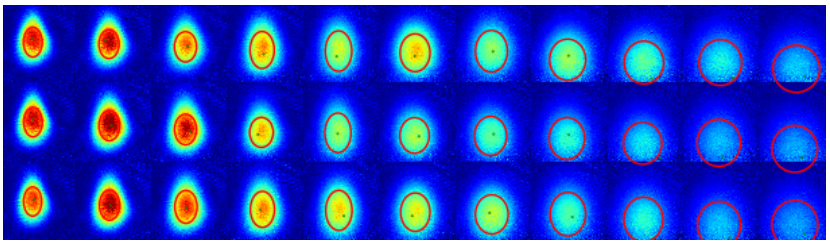

Figure 4.10: Time of flight images of the ^{6}Li MOT.

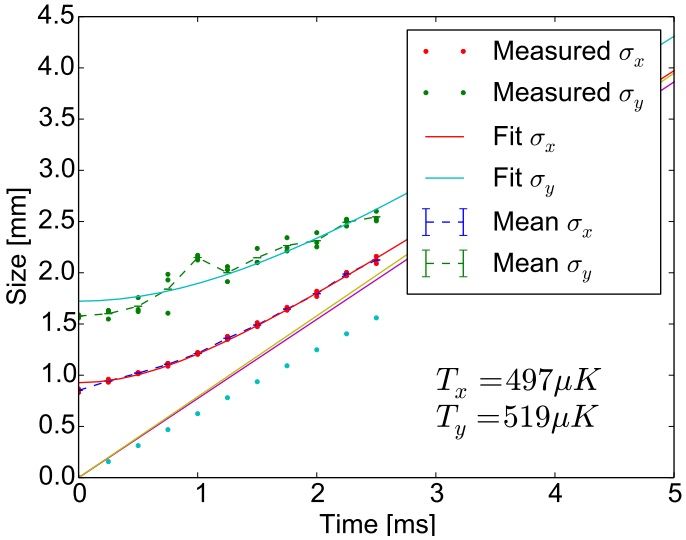

Figure 4.11: A plot of size vs time graph to calculate the temperature of the MOT by TOF method.

4.5 Zero-crossing measurements

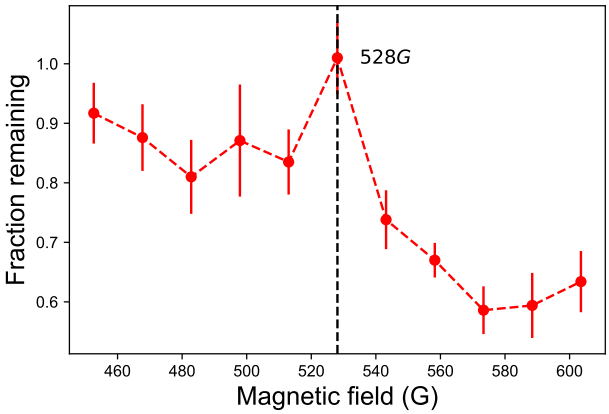

Figure 4.12: Zero-crossing measurement in ^{6}Li. The fraction of atoms surviving after 5 seconds of hold duration is plotted against magnetic field.

In order to use a Feshbach resonance for our experiments, we need to calibrate the coils that we are using to generate the Bfield. The magnetic field at which a Feshbach resonance occurs is difficult to determine due to the infinite scattering length, whereas the magnetic field at which the scattering length crosses zero can be accurately determined. Scattering length zero-crossings can be used to calibrate the high magnetic field generated by varying currents passing through the Feshbach coils. A scattering length zero-crossing in ^{6}Li was determined at a value close to 528 G [62]. For this measurements, plain evaporation takes place when the atoms are transferred into the dipole trap and held over long time scale $\sim$5 s. However, at zero scattering length thermalisation is suppressed leading to a reduction in plain evaporation, and a large number of atoms remain in the dipole trap. The magnetic field at which more atoms are trapped after long hold durations in the dipole trap gives the value of zero scattering length, which corresponds to 528 G in ^{6}Li. The figure 4.12 shows a plot of the fraction of atoms that were present in the dipole trap after 1 second hold duration, that survived until 5 seconds of hold time, vs magnetic field maintained throughout the hold duration.

An increase of the surviving fraction can be seen from the peak detected at 528 G. The conversion factor from magnetic field to the current in the coil controlled by sequence (which corresponds to the voltage value in the sequence) is found to be 226.31 G/V.

4.6 Magnetic trap

Magnetic trap provides a force that moves the atomic cloud to where the magnetic field gradient is nearly zero. Determining the position of the magnetic trap is an important step in this experiment. This can be measured by creating a magnetic trap by connecting the Feshbach coils in anti-Helmholtz configuration. Magnetic trap is used to confine low temperature atomic cloud produced by laser cooling technique. The aim of the experiment is to study the dynamics of Feshbach molecules creation from fermionic atoms via magnetic field ramp across the Feshbach resonance. Generating homogeneous magnetic field in the same position as that of magnetic trap centre is needed to create bosonic ^{6}Li molecules from fermionic atoms via magnetic field ramp. The homogeneous magnetic field can be produced by connecting Feshbach coils in Helmholtz configuration. Absorption images of magnetic trap in both horizontal and vertical imaging give the position of the magnetic trap. The dipole beams are then aligned such that they cross each other at the centre of the magnetic trap. The absorption image of magnetic trap on horizontal imaging screen is shown in the figure 4.13.

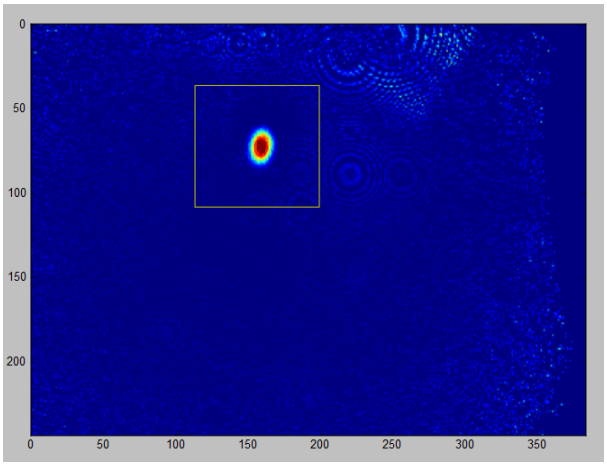

Figure 4.13: Absorption image of a magnetic trap in the horizontal imaging screen. The x and y scale are in millimetre. The loading time for magnetic trap is chosen to be 100 ms for precise measurement of the magnetic trap centre.

4.7 Lifetime measurements of atoms in the dipole trap

The lifetime of atoms in the dipole trap is limited by collisional losses. One-body loss dominates for lower density and the lifetime of atoms in the trap relies on collisions with background gases. In the case of higher atom densities, two-body losses and three-body losses limit the lifetime of atoms in the trap. Two-body losses involve radiative escape, fine structure and hyperfine structure changing collisions, whereas three-body losses occur when the gas is close to degeneracy. The life time of atoms in the dipole trap can be determined by the loss of atoms after holding the atoms for long duration, then the life time can be measured from the exponential decay of the number of trapped atoms. The exponential decay can be expressed by the equation,

$$\frac{dN(t)}{dt} = -\alpha N. \tag{4.8}$$

The solution to the equation 4.8 is,

$$N(t) = N_0 e^{-\alpha t} + \text{offset}. \tag{4.9}$$

Here $N(t)$ is the trapped atom number at a time t and N_0 is the initial number of atoms in the trap. The lifetime of trapped atoms (τ) relates to the decay rate α which is given by the expression, $\tau = \frac{1}{\alpha}$. Then the equation 4.9 can be rewritten as,

$$N(t) = N_0 e^{-t/\tau} + \text{offset}. \tag{4.10}$$

The experimental data can be fitted with the exponential decay function and one can determine the lifetime of trapped atoms by calculating $\frac{1}{e}$ of initial atom number in the trap. The lifetime of atoms after AOM evaporative cooling is found to be 19.082±5.158 s, which is determined by fitting the number of atoms reduced after holding them in a dipole trap, which is plotted and shown in the figure 4.14.

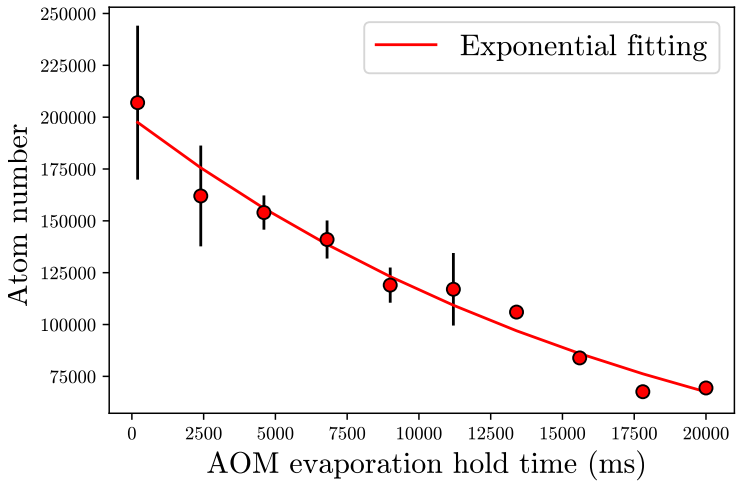

Figure 4.14: Lifetime measurement of atoms in the dipole trap after AOM evaporative cooling. The temperature of the cloud is 1.5 μK and the measurement was taken at 773.5 G.

4.8 Trapping frequency measurement

Elastic and inelastic collisions play a major role in thermalisation of atoms in the dipole trap. S-wave collisions are forbidden for fermions which decreases the

scattering rate at lower temperature. But fermions in different internal states interact with each other and the interactions reach their maximum at a unitary limit. The collisional parameter Φ can be defined as $\Phi = \frac{\Gamma}{\omega}$, where Γ is the scattering rate, and ω is the trapping frequency. The scattering rate Γ can be calculated from the equation $\Gamma = n\sigma\nu$, where n, σ and ν are density of scatterers, scattering cross-section and average velocity of atoms respectively. The harmonic potential of an ideal Fermi gas is given by,

$$V_{ho} = \frac{1}{2}m\omega_x x^2 + \frac{1}{2}m\omega_y y^2 + \frac{1}{2}m\omega_z z^2. \tag{4.11}$$

Here, ω_x, ω_y and ω_z are the trapping frequencies in x, y, and z directions respectively. The geometrical average of the three trapping frequencies can be expressed as, $\omega_{ho} = (\omega_x\omega_y\omega_z)^{1/3}$. Two different methods have been used to measure trapping frequencies in a cold ensemble. The breathing mode oscillations is used to calculate the radial trap frequency whereas the longitudinal trap frequency measurements are performed by centre of mass oscillations. In order to calculate the radial frequency, the atomic cloud is disturbed by a sudden change in the trapping potential, which provides breathing mode oscillation in the system. The size of the cloud oscillates at twice the trapping frequency. The cloud size measurements are taken at different hold times after the trapping potential change. This method gives a size vs time graph with a damping sine function, the frequency of this oscillation in the size of the atomic cloud gives twice the trapping frequency at provided trap depth. In the centre of mass oscillation method, trap depth is increased very briefly results in centre of mass oscillations and then position vs time graph can be obtained by changing the hold time after the kick in the trap depth. The graph is fitted with a sine function (as can be seen in the figure 4.16) and the trapping frequency is calculated from it. The plots to describe the two methods used for trapping frequency measurements are given in the figure 4.15.

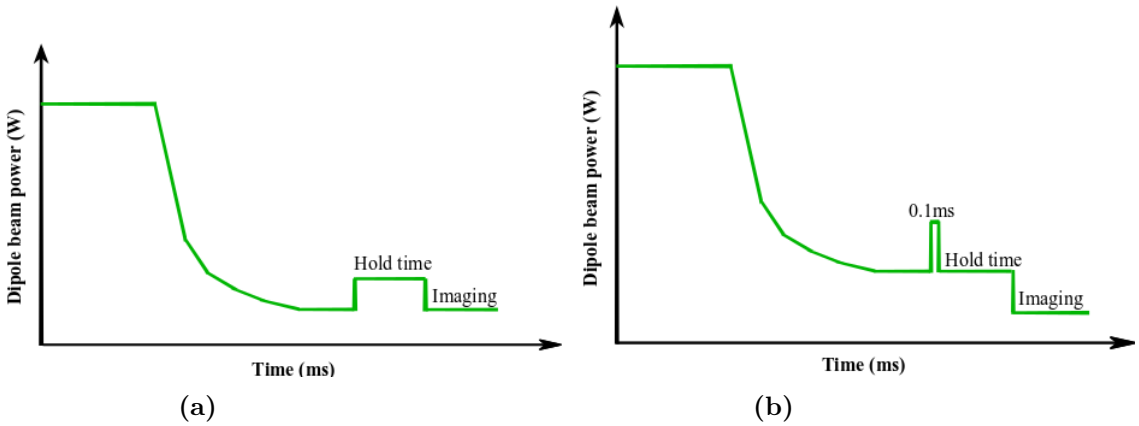

Figure 4.15: Breathing mode oscillation method (a) and Centre of mass oscillation method (b).

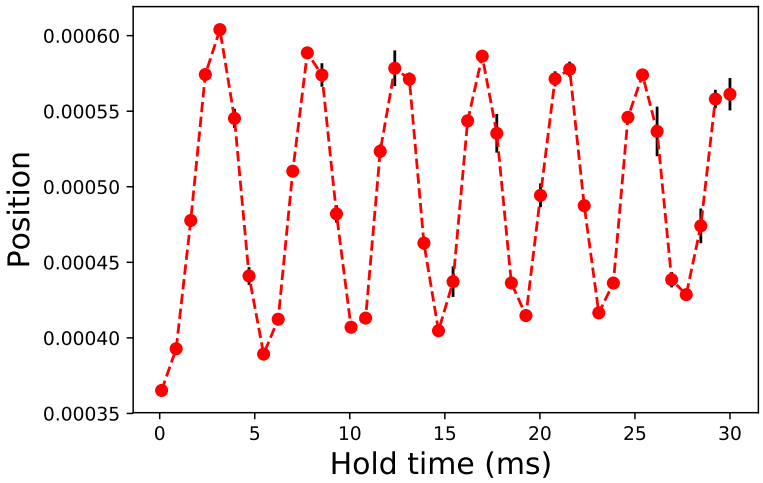

Figure 4.16: Position vs time graph obtained from centre of mass oscillation method.

4.9 In-situ Imaging and cloud size measurements

In-situ images have been used to obtain spatial density profiles of the atomic cloud from which one can determine condensate fraction of a molecular BEC, temperature and chemical potential of the cloud. The $^6Li_2$ molecular BEC (mBEC) can be produced in our experimental setup and images of the same are taken by in-situ imaging technique in which images are taken without fall time. In-situ images of

the mBEC are characterised by a bimodal spatial distribution that represents a narrow condensed fraction and a broader thermal distribution, which have studied in details in P. Jouve's thesis [63]. In this experiment, in-situ imaging is performed over time of flight imaging to determine the cloud size and mean density of the atomic cloud in its initial state before performing magnetic field ramp for creation of Feshbach molecules. The cloud size is determined by fitting the spatial profile of the atomic cloud with a Gaussian function, $f(x) = A\exp\left(-(x-\mu)^2/2\sigma^2\right)$ in x direction. The fitting parameter σ (standard deviation) can be obtained from the curve fitting, which gives the RMS width of the cloud. The half width half maximum (HWHM) can be calculated by multiplying σ with a factor of 1.1775. The spatial distribution obtained from an in-situ image of atomic cloud at 860 G is shown in the figure 4.17.

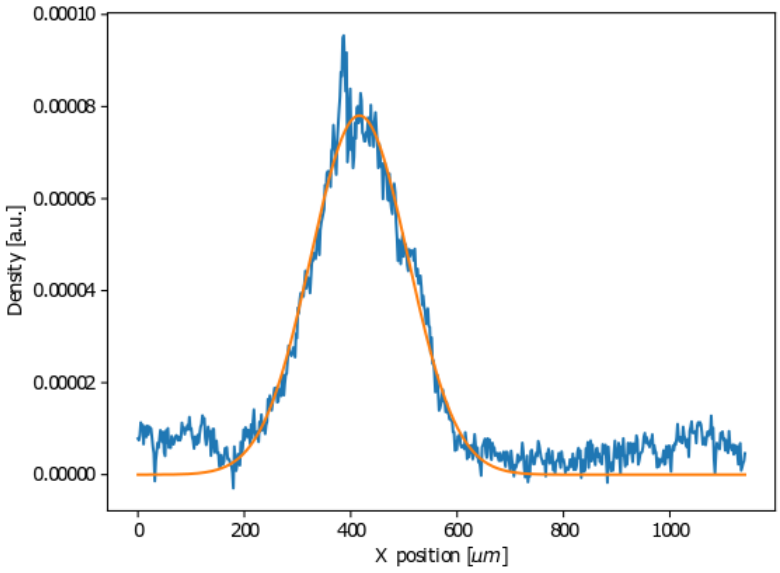

Figure 4.17: Spatial distribution obtained from an In-situ image of the atomic cloud at 860 G. The temperature of the cloud is 600 nK and the calculated HWHM is 9.49 $\times 10^{-5}$ mm.

4.10 Creation of Feshbach molecule

There are different methods to produce Feshbach molecules from fermionic ^{6}Li atoms. Two methods that are possible in our current experimental setup are the creation of mBEC via three-body collisions in the BEC side of the Feshbach resonance [64,65], and creation of ^{6}Li molecules via magnetoassociation [36–38]. The first method involves loading the ^{6}Li mixture of two spin states in the elliptical shaped dipole trap created by IPG laser and holding the atoms to the BEC limit of the Feshabch resonance during the evaporative cooling process. The molecules are formed by three-body recombination when the temperature of the cloud becomes comparable to the molecular binding energy ($E_b = \frac{\hbar^2}{ma^2}$). More detailed studies on $^6Li_2$ mBEC and in-situ imaging of mBEC are given in P. Jouve's thesis [63].

This thesis work focuses on the creation of ultracold $^6Li_2$ molecules from fermionic atoms by sweeping the magnetic field across a Feshbach resonance. The Feshbach resonance can be used as a tool for controlling interactions in ultracold bosonic and fermionic gases. The experiments are performed on mixture of two different spin states. It is possible to transfer mixture of lower energy states $|1/2, -1/2\rangle$ and $|1/2, 1/2\rangle$ into weakly bound Li_2 molecules by scanning over a Feshbach resonance from the region of attractive interaction to a repulsive regime. Using our current experimental setup we can prepare an equal mixture of $|1/2, -1/2\rangle$ and $|1/2, 1/2\rangle$ atoms in the dipole trap at 860.6 G, thus placing the atoms on the BCS side of the Feshbach resonance. The magnetic field is then ramped linearly from 860.6 G to the BEC side of the Feshbach resonance (707 G). The linear magnetic field ramp from 860.6 G to 707 G, which is represented by the current passes through Feshbach coils collected through current transducer attached to the coils is shown in the figure 4.18. During the magnetic field sweep, some fermionic atoms associate into Feshbach molecules, which can be determined by the ab-

sorption imaging of remaining atoms at 707 G. This gives the unassociated atoms from which one can calculate fraction of atoms that are converted into Feshbach molecules. Detailed experimental studies on the creation of $^6Li_2$ molecules from fermionic atoms via magnetic field ramp method is given in chapter 5.

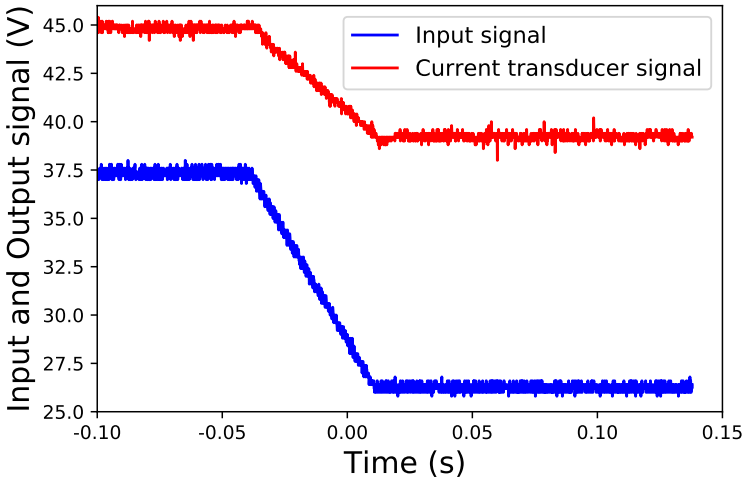

Figure 4.18: Feshbach coil ramping. Oscilloscope signals represents the magnetic field ramping from 860.6 G to 707 G. The blue line represents the input signal given to the Fshbach coil power supply whereas the red line is the output signal from current transducer, which is attached to the Feshbach coils.

Chapter 5

Feshbach molecule formation in Lithium-6

This chapter provides the experimental realisation of Feshbach molecules creation from fermionic ^{6}Li spin mixtures by sweeping the magnetic field through a Feshbach resonance. The dependence of the creation of ^{6}Li Feshbach molecule as a function of the initial cloud temperature, mean density, ramp rate and final magnetic field are given in this chapter. The theoretical approaches to describe the dynamics of the molecule formation from fermionic atoms via a magnetic field ramp are also outlined here. The comparison of existing theoretical models to the experimental data is studied and the experimental method to determine the lifetime of Feshbach molecules is presented in the last section.

5.1 Feshbach molecule formation via magnetic field ramp

Fermionic atoms can be transferred into bosonic molecules by a sweep of magnetic field across a Feshbach resonance in cold and ultracold atomic systems [66]. Long

lived, energetically stable and vibrationally excited molecules can be prepared by this method. The process is based on magneto-association and is reversible, therefore one can transform molecules back into atoms by reversing the magnetic field ramp [67]. Theoretical and experimental studies on these systems provide new insights due to their exotic properties such as unitary dynamics and strong interactions.

The detailed study on dynamics of molecular production via linear downward sweep of magnetic field through a Feshbach resonance is interesting. The processes are not yet fully understood theoretically, a detailed experimental study is needed especially in the low-temperature regime where the existing overlap of atomic and molecular wave functions have the potential to enable additional, coherent coupling processes. The study on this topic is demanding since the complexity to incorporate all experimental parameters in the theoretical studies. There are several theoretical approaches to predict the conversion efficiency of molecules in cold and ultracold atomic systems [68–70]. The Landau-Zener model gives an explanation for this process at high temperatures, where a pair of atoms is converted into exactly one molecule [71]. The Landau-Zener model can be applied to isolated pairs of atoms. In the research work [70], it is predicted that for a large particle number, the power law can be used to describe the process. The existing experimental data is not precise enough to distinguish between the two models.

5.1.1 Theoretical and experimental studies on Feshbach molecules

Theoretical and experimental studies on Feshabch molecules created via magneto-association have opened up an exciting regime of BEC-BCS crossover and strong

interactions. The formation process is however not fully clear and there are different theoretical models available. A theoretical study predicts that the molecule formation is based on two-body interaction and the conversion efficiency is depending on the phase space density [72]. On the other hand, a theoretical model has been introduced [68], that treats the bosonic molecules as a classical field and seeding the pairing amplitudes with random phases. It has been predicted and observed that the atom-molecule conversion efficiency is limited by the initial temperature of the Fermi gas. Lifetime of $\sim 1\,\mathrm{s}$ has been reported in an experimental system, which was studied on ^{6}Li narrow Feshbach resonance at $\sim 543\,\mathrm{G}$ [73]. A theoretical explanation for the molecular creation process is given by considering multiple collisions per atom during the magnetic ramp [69]. One of the key points in this paper is, that the effective adiabatic rate constant is proportional to the initial phase space density. It also states that, when the ramp time (t_{ramp})$\gg$ average time between collisions (τ_{col}), multiple collisions occur on an atom during the magnetic field ramp, so the LZ model cannot be applicable in this case. But in the case of $t_{\mathrm{ramp}} \ll \tau_{\mathrm{col}}$, an individual atom will undergo at most a single collision with its nearest neighbour atom such that the LZ model can be applied to the isolated pairs of atoms in ultracold mixtures. The expression for τ_{col} is $\tau_{\mathrm{col}} \approx \frac{\hbar}{k_B T_F}$, the derivation is given in Appendix B.

5.2 Theoretical approach on Feshbach molecule creation via magnetic field ramp

5.2.1 Landau-Zener model

A Landau-Zener model can be used to predict the efficiency of the association of atoms into ultracold molecules when a linear magnetic field sweeps across a

Feshbach resonance. During the ramping of the magnetic field strength B(t), the energy of the resonance state changes linearly in time. According to a many-body configuration interaction approach, the energy of a system that changes with time can be expressed as [74],

$$E_{\mathrm{res}}\left(B(t)\right) = E_0 + \left[\frac{dE_{\mathrm{res}}}{dB}\left(B_{\mathrm{res}}\right)\right]\left[\frac{dB}{dt}\left(t_{\mathrm{res}}\right)\right]\left(t - t_{\mathrm{res}}\right) \tag{5.1}$$

where t_{res} refers to the time at which the energy of the resonance state reaches the dissociation threshold energy of the open channel, i.e. when $B(t_{\mathrm{res}}) = B_{\mathrm{res}}$ and $E_{\mathrm{res}}(B_{\mathrm{res}}) = \mathrm{E}_0$. The final populations can be determined by the Landau-Zener formula assuming a linear crossing of the Feshbach resonance with the initial populations, $|C_0(t_i)|^2 = 1$ and $|C_{\mathrm{res}}(t_i)|^2 = 0$. The final populations are represented as $|C_0(t_f)|^2$ and $|C_{\mathrm{res}}(t_f)|^2$, which are given by the equations,

$$|C_0(t_f)|^2 = e^{-2\pi\delta_{LZ}} \tag{5.2}$$

$$|C_{\mathrm{res}}(t_f)|^2 = 1 - e^{-2\pi\delta_{LZ}} \tag{5.3}$$

in the limits $t_{\mathrm{i}} \to -\infty$ and $t_{\mathrm{f}} \to \infty$. Here δ_{LZ} represents the Landau-Zener parameter, which is the main parameter that controls the molecular efficiency. This was determined by F.H. Mies.et al. in 2000 [37]. The Landau-Zener parameter can be expressed as,

$$\delta_{\mathrm{LZ}} = \frac{(N-1)4\pi\hbar|\mathrm{a_{bg}}||\Delta B|}{Vm|\frac{\mathrm{dB}}{\mathrm{dt}}(t_{\mathrm{res}})|}. \tag{5.4}$$

Here N refers to the number of atoms in sample volume V. The Landau-Zener parameter depends on the background scattering length a_{bg}, the resonance width ΔB and the ramp speed $|\frac{\mathrm{dB}}{\mathrm{dt}}(t_{\mathrm{res}})|$. In the adiabatic limit, the LZ model predicts that the probability of finding the atom pair in a bound molecular state is unity.

5.2.2 Power-law approach

A theoretical model was developed for the nonlinear adiabatic conversion of fermionic atoms to bosonic molecules [70]. This model predicts a linear dependence of the remaining atomic fraction Γ_A on the sweep rate $\dot{B}$ during the molecule conversion process via magnetic field ramp method explained in section 5.1. This theoretical model is based on a collisionless, single bosonic mode Hamiltonian in the interaction representation, given by [70]:

$$H = \sum_{k,\sigma} \epsilon_k \mathrm{c}^\dagger_{k,\sigma}\mathrm{c}_{k,\sigma} + \varepsilon(t)\mathrm{b}^\dagger_0\mathrm{b}_0 + \mathrm{g}\left(\sum_k \mathrm{c}_{k,\uparrow}\mathrm{c}_{-k,\downarrow}\mathrm{b}^\dagger_0 + H.c.\right). \tag{5.5}$$

Here the kinetic energy of an atom with mass m is given by $\epsilon_k{=}\hbar^2k^2/2m$. In the case of ^{6}Li, the annihilation operators for atoms $\mathrm{c}_{k,\sigma}$ obey fermionic anti-commutation relations, and the annihilation operators for molecules b_0 obey bosonic commutation relations. The molecule energy varies with time during the magnetic field sweep and it is represented by $\varepsilon(t)$, g is the atom molecule coupling strength. The Hamiltonian of the system can also be represented in terms of the operators J_x, J_y and J_z, which is given by,

$$H = \frac{N}{2}\left(\Delta(t)J_z + g\sqrt{\frac{N}{2}}J_x\right), \tag{5.6}$$

where $\Delta(t) = 2\epsilon - \varepsilon(t)$, by the assumption made that a degenerative model can be used, as the exact values of ϵ_k do not effect the molecule conversion efficiency, i.e. $\epsilon_k = \epsilon$ for all values of k. The operators are defined as $J_x = J_+ + J_-$, $J_y = -i(J_+ - J_-)$ and $[J_+, J_-]$ is a quadratic polynomial in J_z, which is represented as,

$$J_z = \frac{\sum_{k,\sigma} \mathrm{c}^\dagger_{k,\sigma}\mathrm{c}_{k,\sigma} - 2\mathrm{b}^\dagger_0\mathrm{b}_0}{N}. \tag{5.7}$$

The total number of particles N is conserved and it is given by,
$N = 2\mathrm{b}^\dagger_0\mathrm{b}_0 + \sum_{k,\sigma} \mathrm{c}^\dagger_{k,\sigma}\mathrm{c}_{k,\sigma}$. The operators J_+ and J_- are defined as:

$$J_+ = \frac{\sum_k \mathrm{c}^\dagger_{-k,\downarrow}\mathrm{c}^\dagger_{k,\uparrow}\mathrm{b}_0}{(N/2)^{3/2}}, \tag{5.8}$$

$$J_- = \frac{\mathrm{b}^\dagger_0 \sum_k \mathrm{c}_{k,\uparrow}\mathrm{c}_{-k,\downarrow}}{(N/2)^{3/2}}. \tag{5.9}$$

The equations of motion for the association of fermionic atoms to bosonic molecules in Heisenberg picture can be obtained and represented by the operators J_x, J_y, J_z. In the mean field limit, these operators are replaced by their expectation values and the equations of motion are analogues to the Bloch vector on a two dimensional surface. The detailed of the derivation of these equations are given in the research paper [70]. A linear dependence of the fraction of remnant atoms on the sweep rate is explained by the mean-field calculation, which shows that the power law dependence remnant fraction of atoms becomes linear for $\frac{g^2}{\dot{B}N} > 1$, that means $\Gamma_A \propto \dot{B}$. The theoretical calculations explain that the transformation of the exponential Landau-Zener model for a single pair of particles to the power law behaviour for large particle number results from taking into account many-body effects. The results of the power law dependence of the atom-molecule conversion process is given as, $\Gamma_A \propto \dot{B}$ for the initial molecular population, which is smaller than the $1/N$ quantum fluctuations, where as $\Gamma \propto \dot{B}^{1/3}$, when it is larger. The power law model is studied by fitting the experimental data with the equation given by,

$$\Gamma_A = C\dot{B}^b. \tag{5.10}$$

where C is a proportionality constant and b is the power law index. The fitted curves with the experimental data are shown in 5.5.

5.3 Creation and detection of ^{6}Li Feshbach molecules

Atoms with unlike spins are prepared in the lowest energy state by using laser cooling and trapping methods, which are explained in chapter 4. These include Zeeman slowing, optical molasses stage, MOT compression and dipole trapping of atoms. Our experimental system is capable of preparing 2×10^8 ^{6}Li atoms at a temperature of $\sim$500 μK in the MOT. An equal mixture of spin half atoms ($F = 1/2, m_F = \pm1/2$) are trapped in a dipole trap potential created by a 100 W, 1070 nm IPG laser. The experimental system is capable of loading 2 $\times10^6$ atoms into the dipole trap and 3×10^5 atoms in each spin state at a temperature of $\sim$1 μK with a peak density of $\sim6\times10^{12}$ cm^{-3} can be prepared. During the final stage of the evaporative cooling process, the magnetic filed is ramped linearly from above the Feshbach resonance (860.6 G) to below the Feshbach resonance (707 G) in order to create Feshbach molecule via magneto-association. The magnetic field ramping points are shown in the figure 5.1.

A schematic diagram of the experimental methods for creation of ^{6}Li molecules via magnetic field ramp is illustrated in figure 5.2. The fraction of molecules created via magnetic filed ramp is measured by absorption images of unassociated atoms remaining at 707 G. The fraction of atoms which are converted into molecules is determined by measuring the decrease in atom number of the cloud after the magnetic field sweep. An absorption image of the initial atomic cloud and the atoms remaining after the magnetic field ramp taken after a fall time of 1.5 ms are depicted in figure 5.3. The molecular conversion is studied by varying the inverse ramp rate $\dot{B}^{-1}$. In accordance with the adiabaticity criterion, we found that a higher number of atoms are converted into molecules during a slow ramp (see figure5.4). The inverse ramp rate is calculated as follows, $\dot{B}^{-1} = \frac{t_{\mathrm{ramp}}}{B_i - B_f}$,

where t_{ramp} is the ramp time of the magnetic field from the initial magnetic field B_i to the final magnetic field B_f.

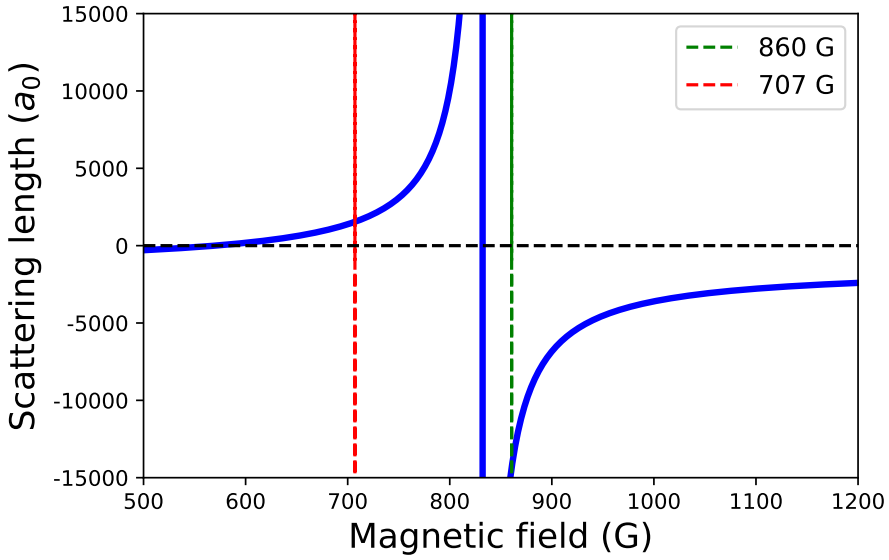

Figure 5.1: Magnetic field ramping points. The green and red dotted lines represents the points where magnetic field ramp starts (860.6 G) and ends (707 G) during the process.

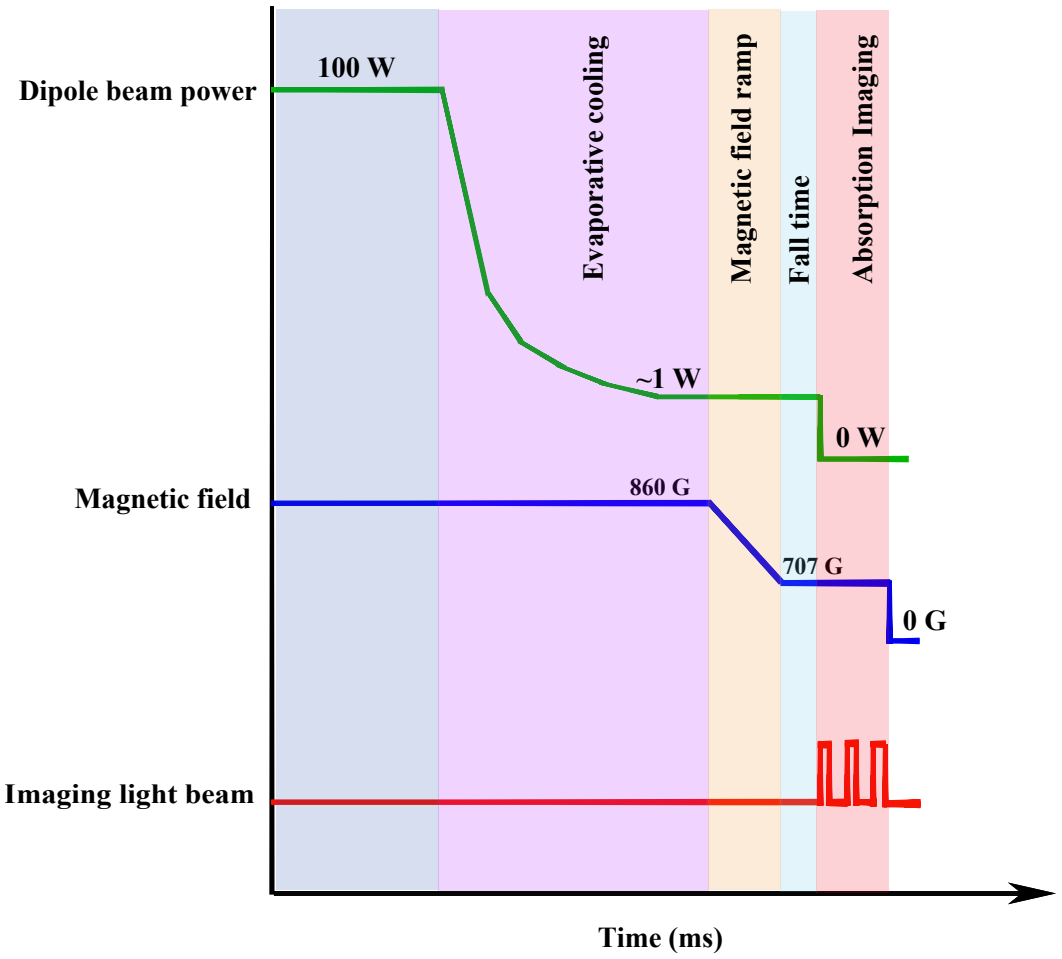

Figure 5.2: Schematic diagram of stages of creation of molecules via magnetic field ramp. The red line represents the camera trigger for absorption imaging and the blue line stands for magnetic field level during the process. The green line represents the dipole beam power variation in each stage. All three line are voltage levels corresponding to each variable.

The experiment was conducted at different magnetic field ramp times varying from 50 ms to 700 ms. The association of atoms into molecules has also been studied by sweeping the magnetic field across the broad Feshbach resonance with different initial cloud temperatures varying from 3.2 μK to 130 nK with radial trapping frequencies ranging from 750 Hz to 622 Hz respectively. Correspondingly the axial trapping frequencies varied from 90 Hz to 74 Hz. The fraction of molecules is determined from the fraction of remnant atoms imaged at 707 G

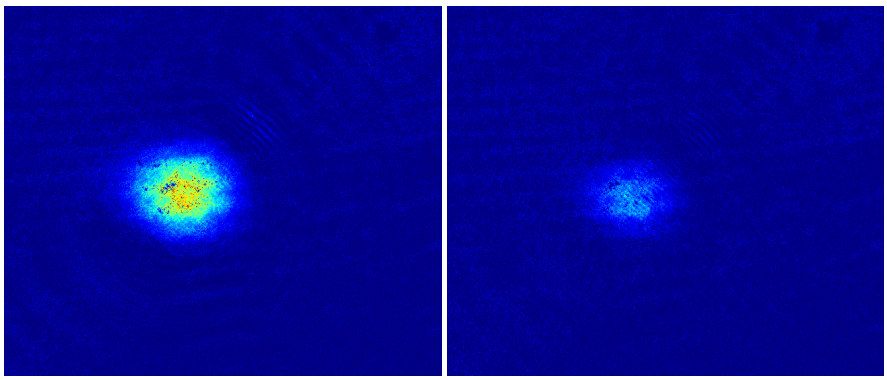

(a) **(b)**

Figure 5.3: Absorption images of atoms before and after the creation of Feshbach molecules. Initial atoms at T=1.5 μK (a) and atoms remaining after the magnetic field ramp (inverse ramp rate = 4 ms/G)(b). Both images are taken after a 1.5 ms fall time.

after 1.5 ms fall time after the magnetic field ramp (see figure5.2). The remnant fraction of atoms is calculated by taking the difference between the atoms measured before and after the magnetic field ramp. It was also verified that molecules can be converted into atoms again by reversing the magnetic field ramp, which confirms that most of the atoms are transformed into molecules and three body losses are very small during the process. The resulting of ^{6}Li molecules as a function of inverse ramp rate is presented and discussed in section 5.4.

5.4 Experimental results and Discussion

The experiment was performed with an equal mixture of spin half states of ^{6}Li atoms in the dipole trap. The two component atomic mixture is prepared in the lowest energy states at a magnetic field of 860.6 G on the BCS side of the Feshbach resonance, employing methods of laser cooling and trapping and subsequent evaporative cooling. Atoms with temperatures ranges from microkelvin to nanokelvin can be produced by evaporative cooling methods described in section

4.2. Depending on the final AOM value at the end of AOM evaporation stage, the final laser power varies; hence the temperature of the atomic cloud can be set in the experiment. During the whole evaporation process, the magnetic field is kept at 860.6 G. In order to create ^{6}Li diatomic molecules, the magnetic field is linearly ramped from 860.6 G to 707 G at the end of AOM evaporative cooling process. The experiment was conducted at different ramp times varying from 50 ms to 700 ms and the association of atoms into molecules has been studied by sweeping the magnetic field across the Feshbach resonance with different initial atomic cloud temperatures. The estimated Feshbach resonance position in ^{6}Li is at 834 G, and the absorption images are taken far below the Feshbach resonance. Since this process is reversible, molecules can be converted back into atoms by reversing the linear field ramp, which is from 707 G to 860.6 G. During the reverse linear magnetic field ramp, the loss of atoms is measured to be less than 10%. The system can be consider as a standard Landau-Zener type and the conversion efficiency as a function of the sweeping rate takes the form [55, 56],

$$n_m = 1 - exp\left(\frac{-2\pi g^2}{\Delta\mu\alpha}\right) \tag{5.11}$$

where $\Delta\mu = 2\mu_B$ is the difference of magnetic moment of the two states and α is the sweep rate. The experimental result of fraction of remaining atoms by varying ramp time with the initial cloud temperature $T/T_F = 1.73$ is shown in the figure 5.4.

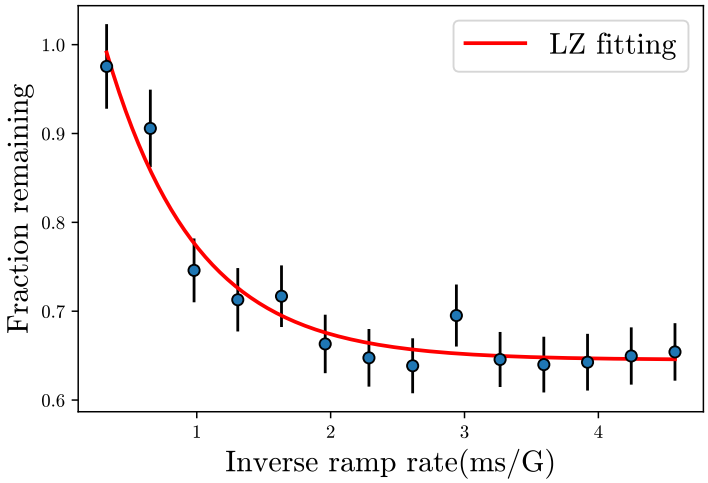

Figure 5.4: Fraction remaining vs inverse ramp rate graph. This graph shows the fraction of atoms remaining after the magnetic field ramp as function of inverse ramp rate. The experiment was conducted with initial atomic cloud temperature, $T = 3.2\,\mu$K ($T/T_{\mathrm{F}} = 1.73$) at 860.6 G. The maximum molecular conversion efficiency calculated by fitting a LZ model is $35.5 \pm 0.5\,\%$. The error bars are the standard error of five measurements.

5.4.1 Landau-Zener model and Power law comparison

The molecular conversion as a function of the inverse ramp rate of the magnetic field strength was measured in our experiment. The molecular conversion efficiency is determined from the decrease in atom number after the magnetic field ramp. In order to compare the different models, we plot the data in linear log plot and fit a LZ model with equation 5.4 and power law with an equation 5.10 given in section 5.2. The comparison between LZ model and Power law approach for the measurements taken at different temperature varies from $\frac{T}{T_F} = 1.73$ to $\frac{T}{T_F} = 0.112$ is shown in figure 5.5.

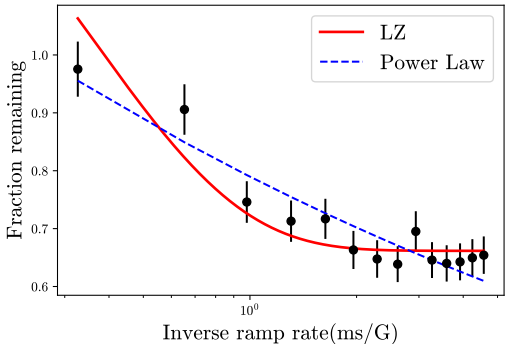

(a) $T/T_F = 1.73$

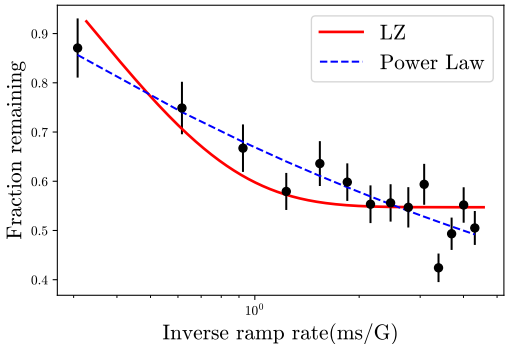

(b) $T/T_F = 1.22$

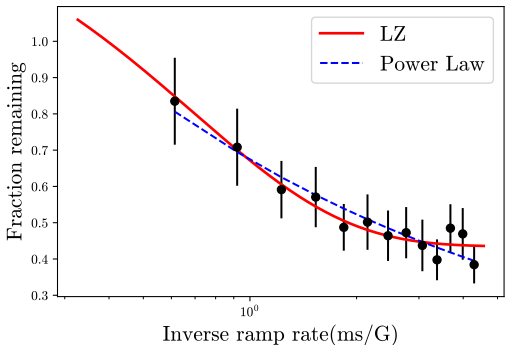

(c) $T/T_F = 0.857$

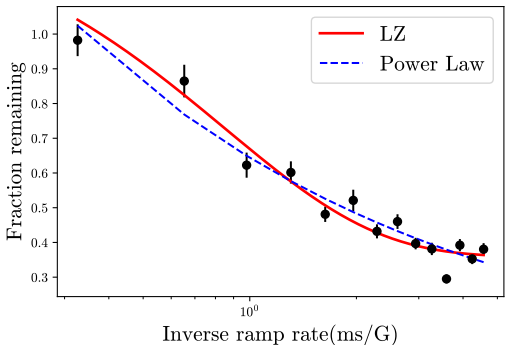

(d) $T/T_F = 0.61$

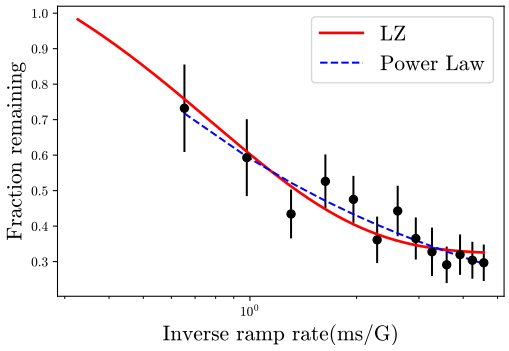

(e) $T/T_F = 0.493$

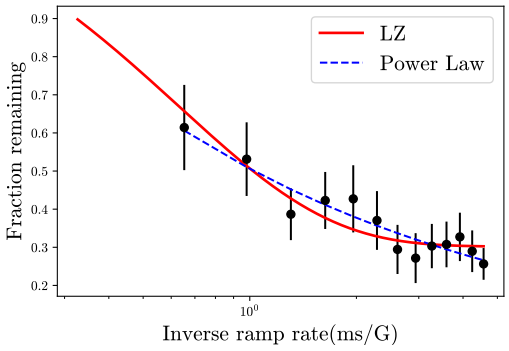

(f) $T/T_F = 0.433$

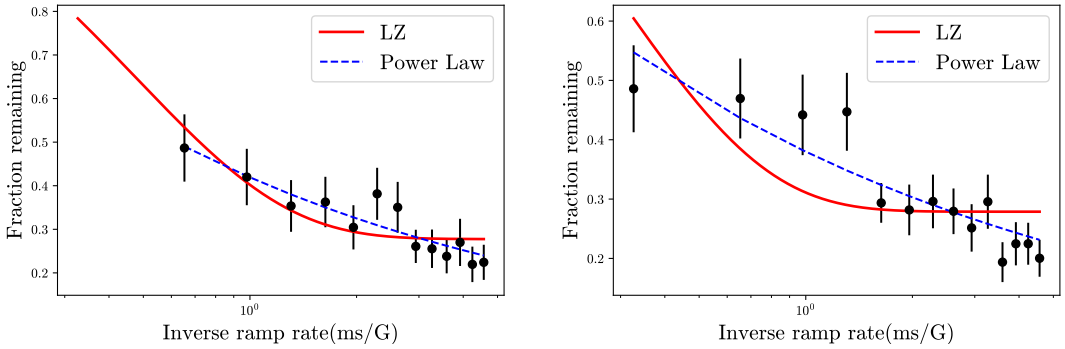

(g) T/T$_F$ = 0.195 **(h)** T/T$_F$ = 0.112

Figure 5.5: Landau-Zener model and Power law fitting with experimental data. Experimental data is taken at different initial cloud temperatures, T/T_{F} = 1.73, 1.22, 0.857, 0.61, 0.493, 0.433, 0.195, 0.112. The x-axis of each graph is in logarithmic scale. The error bars are the standard error of 5 measurements.

The value of coupling coefficient g obtained from the LZ model fitting for different initial cloud temperatures are given in the table below 5.1. The fitting parameters from the power law equation are given in the table 5.2. The power law index values obtained from the fitting curves for the temperatures $T/T_{\mathrm{F}} = 0.857, 0.195, 0.112$ are approximately equal to 1/3, which shows that $\Gamma \propto \dot{B}^{1/3}$ as given in [70]. For temperatures $T/T_{\mathrm{F}} = 0.433$, 0.493 and 0.61 , the power law index values are close to 1/2 and for $T/T_{\mathrm{F}} = 1.22$ and 1.73 (for higher atom numbers) the values are close to 1/5 and 1/6 respectively.

Table 5.1: The fitted coupling coefficients for different temperatures obtained from LZ model fitting. The experimental data is fitted with the LZ model equation given by $n_m = 1 - exp\left(\frac{-2\pi g^2}{\Delta\mu\alpha}\right)$.

Temperature T/T_F	Fitted g g_{LZ} ($\hbar \times$ kHz)
0.112	31.84
0.195	24.80
0.433	21.63
0.493	19.38
0.606	18.59
0.857	20.61
1.220	29.67
1.730	28.71

Table 5.2: The power law function fitting parameters. The experimental data is fitted with the power law function, $\Gamma_A = C\dot{B}^b$. The proportionality constant C and power law index values b for atomic cloud with different temperatures are given in the table.

Temperature, T/T_F	C	b
0.112	0.37	0.326
0.195	0.41	0.367
0.433	0.506	0.423
0.493	0.59	0.458
0.606	0.64	0.414
0.857	0.67	0.366
1.220	0.66	0.21
1.730	0.78	0.17

For both models, a chi-squared (χ_r^2) statistical test is performed on Landau-Zener model fitting and power law fitting. The chi-squared test provides an insight into which model is the better approach to the behaviour of the data set, which is shown in the figure 5.6. As it is also clear from the figure 5.5(g and h)that the Landau-Zener model does not fit well with data with temperature T/T_F=0.195, 0.112(i.e., temperature below Fermi temperature), even though χ_r^2 values are lower and comparable to each other in this case. The performed χ_r^2 test values

for these two models show that both models are comparable within the quality of our data and neither model can be ruled out. The figure 5.6 summarises χ_r^2 values for the fits shown in figure5.5. The relatively large χ_r^2 values show that neither of the models describes the data particularly well. However the LZ model has a slightly lower χ_r^2 value than the linear model.

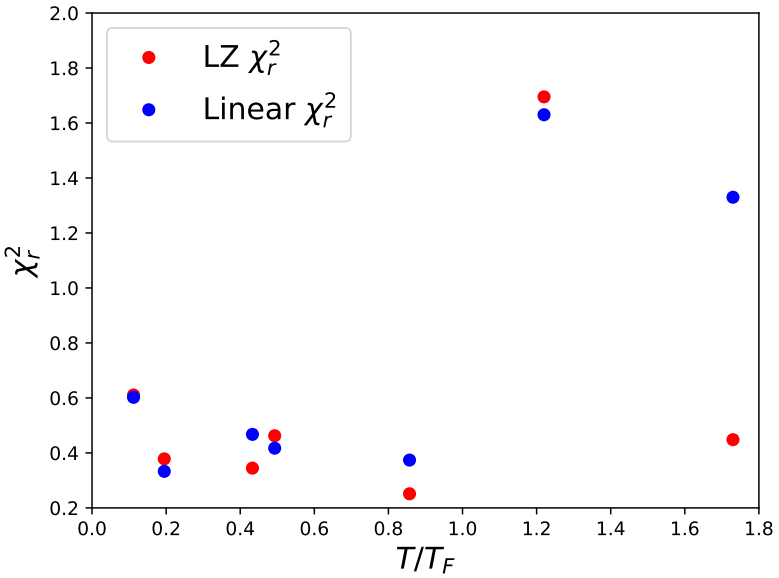

Figure 5.6: A comparison test for LZ model and Power law approach. The graph shows the chi-squared values of Landau-Zener model and power law fitting. It is inferred from the graph that one cannot rule out the power law approach for molecular formation via magnetic field ramp method.

A modified Landau-Zener model is used to fit with our experimental data and a comparison of measured atom-molecule coupling coefficient with the calculated coupling coefficient is given in the section 6.2 in chapter 6.

5.4.2 Temperature dependence of molecule conversion

The Feshbach molecule formation via a magnetic field ramp at different temperature is studied and detailed in this section. As from the experimental studies

conducted with varying ramp time, it is observed that fermionic ^{6}Li atoms are converted into bosonic $^6Li_2$ molecules and most of the atoms are converted into molecules at higher inverse ramp rate as depicted in the figure 5.7. A modified Landau-Zener model is used to fit the data and the saturation value at the plateau region is used to calculate the maximum molecular conversion efficiency during the process.

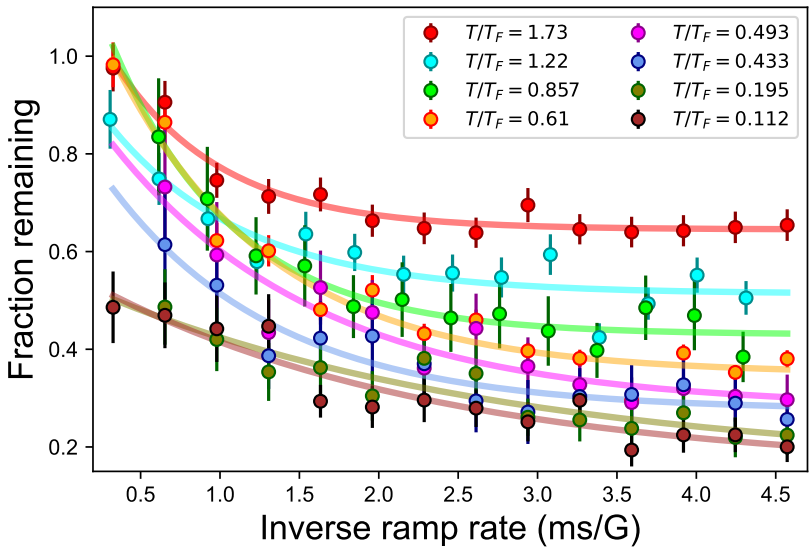

Figure 5.7: Conversion of molecules from fermionic atoms with different initial temperature. The graph shows the fraction of remnant atoms after molecular conversion as a function of inverse ramp rate. The error bars are the standard error of five measurements.

The modified equation for the the Landau-Zener model is given by,

$$n_a = n_0 + (1 - n_0)\exp\left(\frac{-2\pi g_{eff}^2}{\dot{\delta}}\right) \tag{5.12}$$

where n_0 is the remaining atom fraction in the adiabatic limit. The effective atom-molecule coupling coefficient is given by g_{eff} and the inverse ramp rate is represented by $\dot{\delta}$. From the figure 5.7, the molecular conversion efficiencies are found between 35 % to 85 % for initial temperatures between 3.2 μK to 130 nK,

which is shown in figure 5.8. The effective coupling coefficient g_{eff} can be measured from the fit of each experimental curve. The dependence of the effective coupling coefficient on temperature of the atomic sample is studied and discussed in chapter 6.

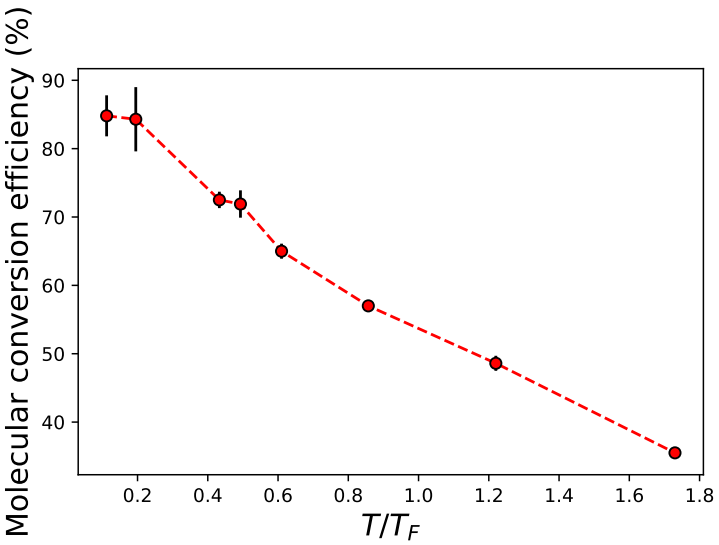

Figure 5.8: Temperature dependence of molecular conversion efficiency. The molecular conversion efficiency is calculated by fitting the experimental data with the LZ model, and the maximum efficiency was determined from the plateau region at the end of the each plot in 5.7 where the inverse ramp rate is high. The error bar corresponds to the error from the fit of the LZ model.

5.4.3 Ramp rate dependence of molecule conversion

In the experiment, the Feshbach molecules are created by sweeping the magnetic field from 860.6 G to 707 G by changing the duration of ramp from 50 ms to 700 ms. As can be depicted in figure 5.9, higher number of atoms are converted into molecules (around 80 %) during a slow ramp when $\mathrm{T/T}_F = 0.112$. When the ramp is fast, the molecular conversion efficiency is 60 % at $\mathrm{T/T}_F = 0.112$.

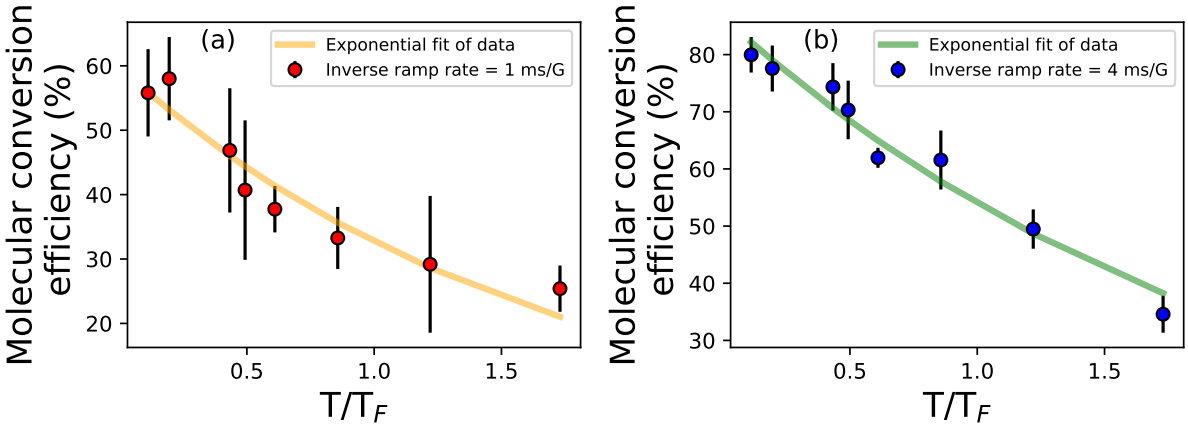

Figure 5.9: Ramp rate dependence of molecular conversion efficiency at different ramp rate. The efficiency of molecular conversion is measured from each experimental data at inverse ramp rate 1 ms/G and 4 ms/G.

The figure 5.9 compares the conversion efficiency for fast (1 ms/G) and slow ramp (4 ms/G) magnetic field ramp for all studied temperatures. It can be seen that for all temperatures the slow rate leads to a 20-30 % higher conversion rate. In both cases, the overall conversion efficiency is larger when the temperature of atoms is lower than the Fermi temperature.

5.4.4 Trap depth dependence of molecule conversion

The initial temperature of the atomic cloud depends on the final value of the AOM in the evaporative cooling process, which is corresponding to the power of the trapping beam in the final stage of atom cloud preparation. This can be represented by the trap depth (U), which is related to the power of the trapping beam (P) by $U = cP$, where c is a proportionality constant. The schematic of the experimental method used to study the trap depth dependence of molecule conversion is illustrated in figure 5.10. The dependence of trap depth on molecule conversion is studied by varying the trap depth at the final stage of evaporative

cooling. The experimental result is shown in figure 5.11, which depicts that the molecular fraction decreases as the trap depth increases.

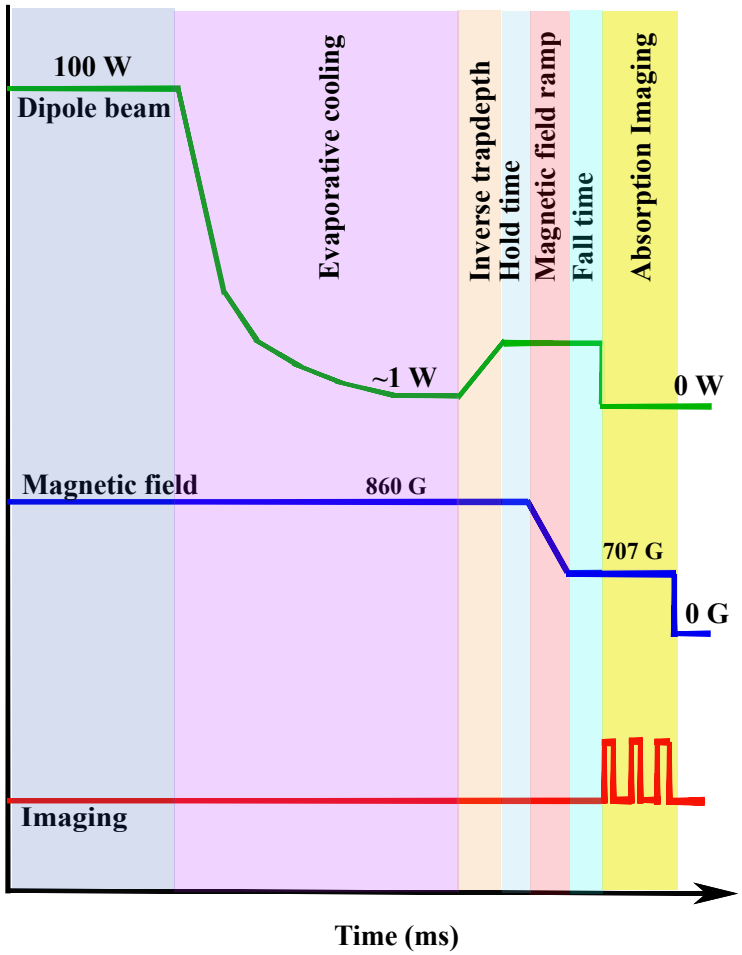

Figure 5.10: The schematic of trap depth dependence of molecular conversion. The plot illustrates the method or steps involve for the study on molecule conversion as a function of trap depth. The x-axis represents the time in ms whereas y-axis represents for the voltage levels applied to the analog or digital channel for controlling experimental sequence.

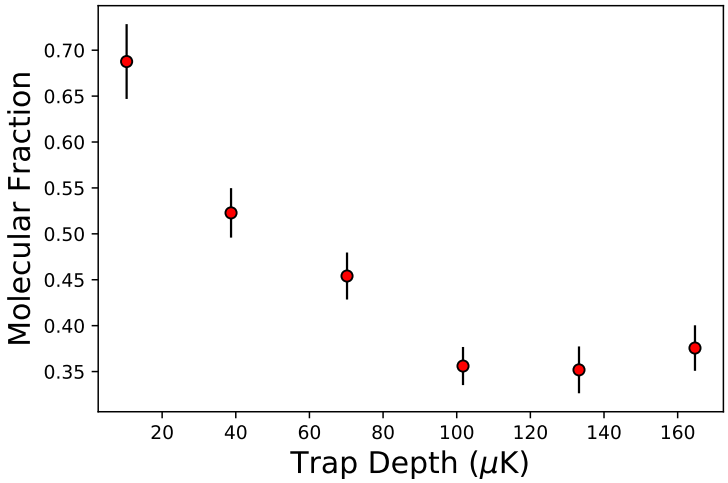

Figure 5.11: The dependence of molecular fraction with trap depth. The graph shows the dependence of atom loss during the magnetic field ramp across Feshbach resonance from 860 G to 697 G by varying the trap depth from 10.36 μK to 164 μK. The inverse ramp rate, (3.68 ms/G) is fixed during the measurements. The error bars are the standard errors of three measurements.

All clouds are prepared at a temperature of 1.5 μK by ramping the dipole trap to a trap depth of 10.36 μK. Then the trap depth is reincreased and the molecular conversion rate is measured. The measurement is conducted at a fixed inverse ramp rate of 3.68 ms/G. One can seen in figure 5.11 that for trap depth higher than 100 μK the molecular fraction is more or less constant, while for a trap depth below 100 μK the conversion rate increases almost linearly with lower trap depth.

5.4.5 Mean density dependence of molecule conversion

The density dependence of the efficiency of molecular conversion when the magnetic field is swept across the Feshbach resonance in ^{6}Li fermionic atoms is investigated in this section. The atomic system is studied by considering it as a two level Landau-Zener model and it was shown that the molecular conversion efficiency

is related to the initial phase space density of the atomic cloud for both bosonic and fermionic systems [72]. The molecular conversion efficiency as a function of magnetic field sweep rate can be fitted with a Landau-Zener equation, which is given by [28],

$$N_{\mathrm{mol}} = N_{\mathrm{max}} \left(1 - e^{-\delta_{\mathrm{LZ}}}\right). \tag{5.13}$$

Here N_{max} represents the asymptotic number of molecules during the very slow magnetic field ramp. The molecular fraction as a function of inverse ramp rate is shown in figure 5.12. The relation between the Landau-Zener parameter δ_{LZ} to the mean density and ramp rate can be expressed as [72],

$$\delta_{\mathrm{LZ}} = \alpha n \Delta a_{\mathrm{bg}} / \dot{B}, \tag{5.14}$$

where α is a constant. The ratio of mean density to the $1/e$ of the ramp rate $(n/\dot{B}_{1/e})$ should be a constant for a true Landau-Zener behaviour, which was investigated and shown in figure 5.13.

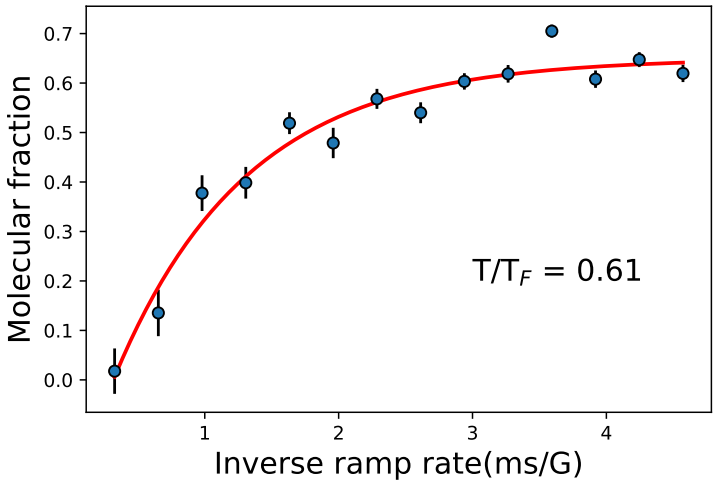

Figure 5.12: Molecular conversion as a function of inverse ramp rate. The measured value of maximum molecular conversion at $T/T_{\mathrm{F}} = 0.61$ is 65.0± 1.1 %. The error bars are the standard errors of five measurements.

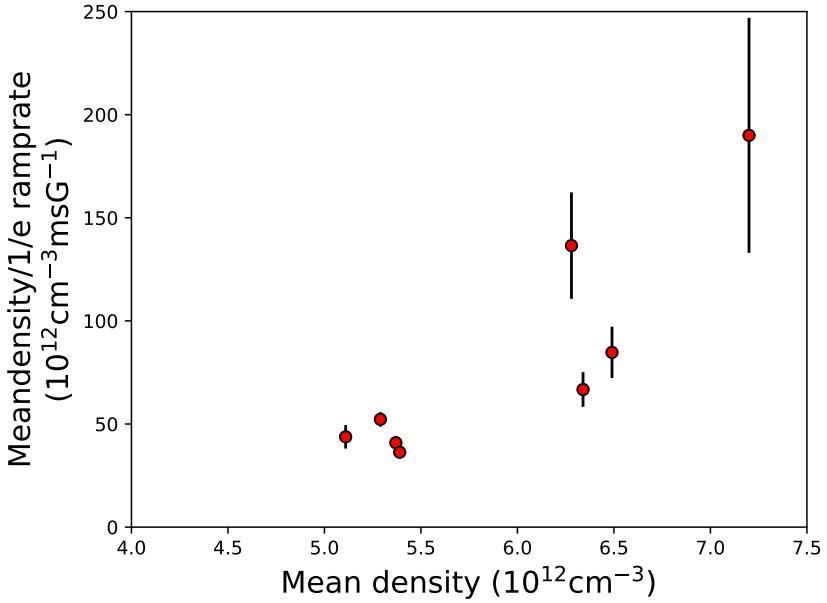

Figure 5.13: Initial mean density divided by $1/e$ of the ramp rate as a function of initial mean density. The error bars are the combined error from the initial mean density and the uncertainty in the $\dot{B}_{1/e}$ by fitting the data with equation 5.13. The atomic cloud experiences significant heating during magnetic field ramping across Feshbach resonance at higher initial densities, hence the error bars are large compared to the lower mean density data. A similar behaviour of the graph was observed in [72] for ^{85}Rb.

One can clearly see that the ratio of mean density to the $1/e$ of the ramp rate is not a constant in the case of higher mean density data. The measured value of $n/\dot{B}_{1/e}$for the highest density is three times larger than the Landau- Zener prediction. A similar behaviour was observed in [72], where a deviation of the Landau-Zener parameter was observed.

5.4.6 The dependence of the molecular fraction on the magnetic field

In addition to all above measurements, we want to investigate how the molecule conversion efficiency changes with final magnetic field during the molecule conversion process. In order to take the measurements we kept the magnetic field

ramp rate constant while changing the magnetic field value at the end of magnetic field ramp. The motivation to the specific measurement was to observe the coherent oscillations between the molecular state and the unbound state. The study of molecular conversion of atoms by differing final magnetic field at a constant ramp rate is studied in this section. The schematic diagram of the experimental method to study the magnetic field dependence of molecular conversion is shown in figure 5.14. As can be seen in the figure, the magnetic field is ramped from the same initial magnetic field (860 G) to different final magnetic field with a constant ramp rate. The experimental results are shown in the figure 5.15.

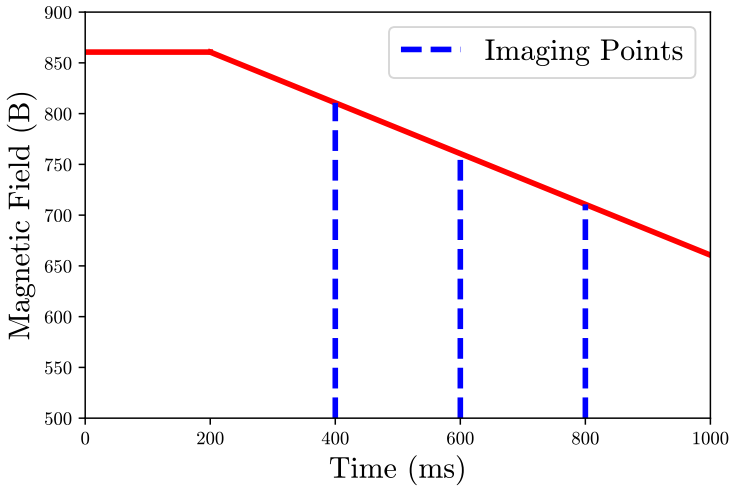

Figure 5.14: The schematic of magnetic field dependence of molecule conversion. The magnetic field is ramped with a constant initial magnetic field to the different final magnetic field.

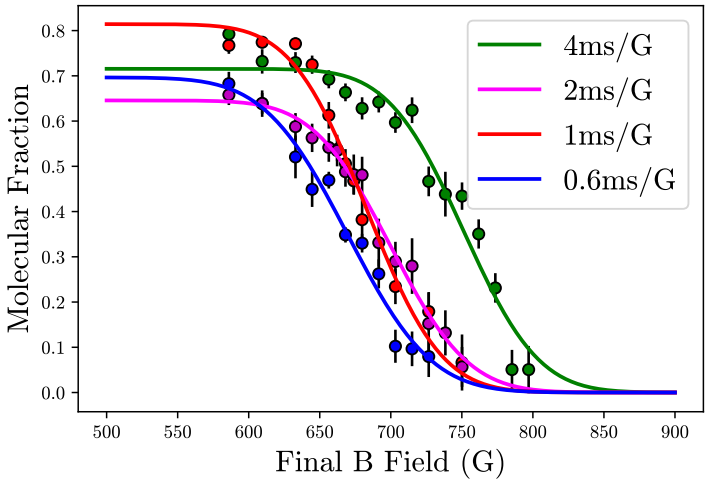

Figure 5.15: Dependence of molecular fraction on final magnetic field. The magnetic field is swept down from 860 G to different final magnetic fields on the BEC side of the Feshbach resonance during the molecule conversion process. The solid circles represent the average of 10 measurements and the error bars are the standard errors calculated from these measurements. The experiment was conducted with an atomic cloud of temperature=1.5 μK.

A theoretical study on Feshbach molecules during the magnetic field ramp is given by [69], which shows that molecular fraction during an adiabatic ramp of magnetic field is given as, $\chi \equiv 2N_M/N_{\rm tot}$, which increases to a maximum value χ_B, where $N_{\rm tot}$ and $N_{\rm M}$ represents the total and molecular population. Here $N_{\rm M}$ depends on the temperature and peak atomic phase space density at $\epsilon_{\rm res}$=0,where $\epsilon_{\rm res}$ is the energy of the resonant closed-channel state. This behaviour is represented by an error function, which is represented by,

$$\chi_{erf}(B) = \chi_B \left\{1 - erf\left[\sqrt{2}(B - B_{cen})/\delta_B\right]\right\}/2. \tag{5.15}$$

In the research paper [69], it is predicted that the dependence of the molecular fraction on the magnetic field resembles this function whose width and centroid are related to the temperature. Our experimental results are fitted with this error function and it is observed that the centroid of the error function is also shifted

from the resonance position as the ramp rate changes from 4 ms/G to 0.6 ms/G as can be seen in figure 5.15. The dependence of molecular formation on the magnetic field by sweeping the magnetic field has been studied on narrow Feshbach resonance region in ^{6}Li [73], and the centroid of the fitting curve coincides with the Feshbach resonance since the shift is on the order of resonance width. Following the research paper [69], the centroid of the error function should occur where $\epsilon_{\text{res}} \approx k_B T_F$ and the shift from the resonance position can be calculated from the expression, $B_{cen} - B_0 \approx \Delta B a_{bg} \sqrt{m k_B T_F}/\hbar$. From figure 5.15, we can read off the difference between B_{cen} and B_0. The measured values of $B_{cen} - B_0$ for a ramp rate 0.6 ms, 1 ms, 2 ms, and 4 ms at a temperature of 1.5 μK are -164.244 G, -151.2281 G, -134.006 G, -82.8538 G respectively. The magnetic field dependence of molecular conversion at a fixed ramp rate with different initial temperature is also studied in this section. The atoms are prepared at a finite temperature as described in the section 4.2. Then the molecule formation is studied by changing the final magnetic field during the magnetic field ramp at a constant ramp rate. The experiment was conducted with an atomic cloud of temperature at 556 nK and 1.5 μK. The experimental result is shown in figure 5.16.

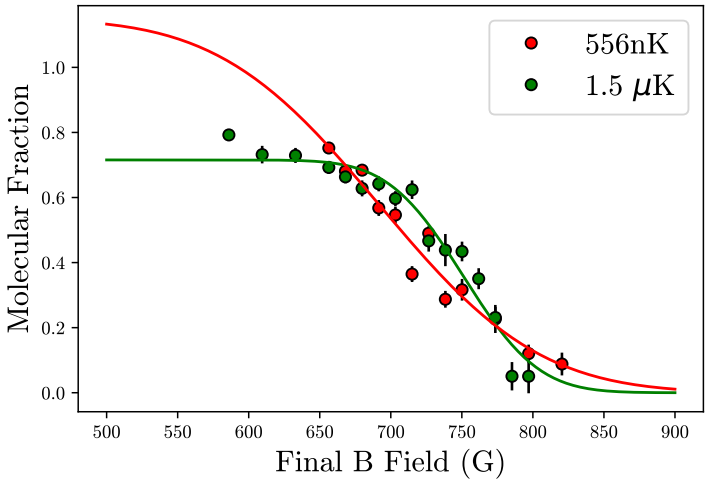

Figure 5.16: Conversion of molecules from fermionic atoms with different initial temperature with a ramprate = 4ms. For these measurements, the magnetic field is swept from 860 G to different values of final magnetic field below Feshbach resonance whilst keeping the ramp rate constant for all data points. The measurements are taken for two initial atomic cloud temperatures, 556 nK and 1.5 μK. The shift in the centroid of the error function from the Feshbach resonance, $B_{cen} - B_0$ for 556 nK and 1.5 μK at a ramp rate 4 ms are -141.6499 G and -82.8538 G respectively. The data points represent the average of 10 measurements and the error bars are the standard errors of these measurements.

As seen in figure 5.16, the red and green lines are the fitted curve with the error function 5.4.6 for 556 nK and 1.5μK respectively. In both cases the centroid of the error function has shifted from the Feshbach resonance. It is evident from the plot that the shift and the width of the error function are larger when the temperature of the atoms are low.

5.4.7 Lifetime measurement of ^{6}Li Feshbach molecules

The molecules produced from fermionic atoms are remarkably stable against inelastic decay. Long lived molecules can be created via magnetic field ramp across Feshbach resonance. The long lifetime observed for these molecules is a consequence of the Pauli principle, which suppresses three-body collisions and hence vibrational quenching. The lifetime of $^6Li_2$ molecules created from fermionic

atoms via magnetic field sweep is determined at 707 G. The magnetic field is linearly ramped from 860 G to 707 G within 50 ms ramp time and then it is ramped up again after holding the molecules in the dipole trap, such that molecules are converted into atoms to the attractive side of the Feshbach resonance. The method used to measure molecule lifetime is illustrated in the figure 5.17. The decay of the $^6Li_2$ molecules at a magnetic field of 707 G is measured by plotting the number of unassociated atoms imaged at 860 G to the hold time after the magnetic field ramp from 860 G to 707 G. By imaging unassociated atoms on the BCS side of the resonance, one can determine how many molecules were lost to inelastic collisions during the hold time. The exponential fit to the measurements gives the $1/e$ of the curve which yields the lifetime of the molecules τ_{mol}. The lifetime of the molecules at 707 G is found to be 1.965 $\pm$0.354 s, as can be seen in figure 5.18.

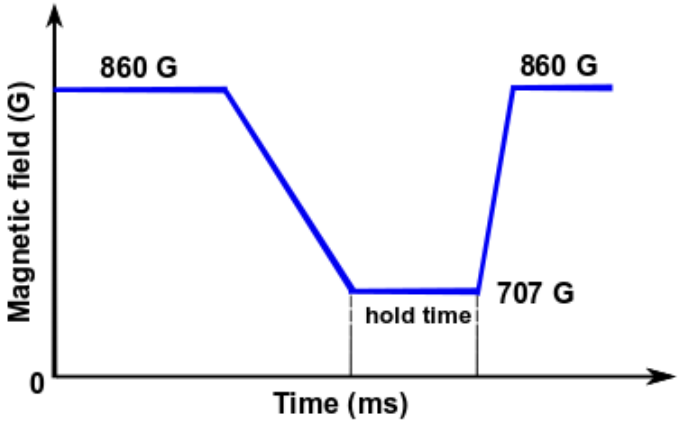

Figure 5.17: Schematic of ^{6}Li molecule lifetime measurements. The plot shows the method involved in the molecule lifetime measurements.

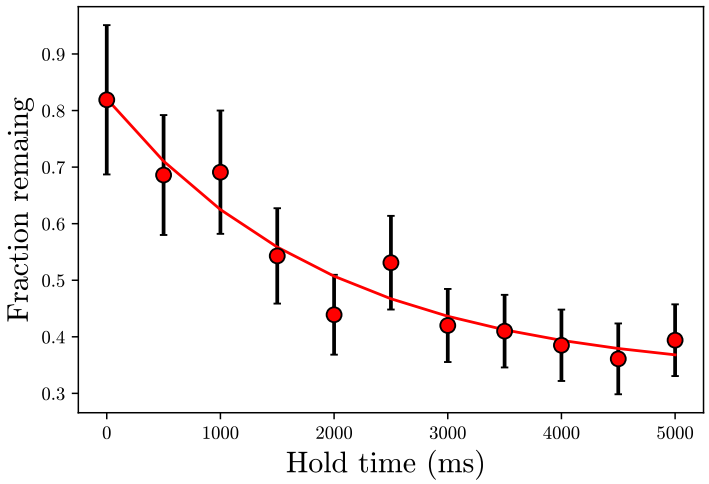

Figure 5.18: Molecular Lifetime of $^6Li_2$ dimer. The graph shows the measurement of the molecular lifetime calculated at 707 G. The magnetic field is ramped from 860 G to 707 G through the Feshbach resonance and back to the starting field. The hold time is the time interval between the traversing the magnetic field on the downward sweep and again on the upward sweep. The error bars are the standard error of three measurements. The lifetime of molecule calculated at 707 G is 1.965 $\pm$0.354 s.

Chapter 6

Dynamics of Feshbach molecule formation

This chapter describes a new theoretical approach to explain the dynamics of molecular formation via magnetic field ramp across a Feshbach resonance in ultracold ^{6}Li atoms close to quantum degeneracy. This was developed by a theory group (W.Li and Y.Zhou) at the University of Nottingham. This theoretical approach is based on a Landau-Zener model, where the coupling constant is not a constant but is allowed to vary with density. A deviation from the theoretically calculated value of the coupling constant was observed in Rb, but a detailed experimental study has not been carried out so far. The dynamics of magnetoassociation is described by Landau-Zener approach for ultracold atoms above Fermi temperature, whereas many-body coherence describes the enhancement of atom-molecule coupling strength close to quantum degeneracy. The comparison of experimental data with theoretical model is also presented in this chapter.

6.1 Landau-Zener transition

The theoretical approaches for describing Feshbach molecule formation are based on Landau-Zener transition. The Feshbach molecule formation from fermionic atoms via magnetic field sweep can be considered as a two atom model [66], which can be described by Landau-Zener transition in which two atoms form a molecule. The dynamics of the molecule formation can be governed by the Hamiltonian given by,

$$H = \begin{pmatrix} 0 & g \\ g & \delta(t) \end{pmatrix}, \tag{6.1}$$

where $\delta(t)$ slowly varies from $-\infty$ to $+\infty$ at a constant rate $\dot{\delta}$. This can be described by a two state problem, where atom pair and molecule are considered as two states in a system. The transition probability of converting atoms into molecules by assuming the system initially in the atomic state can be expressed as,

$$P = \exp\left(-2\pi g^2/\dot{\delta}\right). \tag{6.2}$$

Here g is the atom-molecule coupling strength and $\delta(t) = \Delta\mu(B(t) - B_r)$, where $\Delta\mu$ is the difference of magnetic moment of two states, B_r is the resonant magnetic field strength. Near a Feshbach resonance $\delta(t) = -\alpha t$, where α is the sweeping rate. The time dependent Schrödinger equation can be solved analytically and the molecular conversion rate can be obtained as,

$$\Gamma_m = 1 - \exp\left[-2\pi g^2/\Delta\mu\alpha\right]; \text{in the limit} t \to \infty. \tag{6.3}$$

The atom-molecule coupling strength g can be expressed using a two-channel model, which is given by, $g = \hbar\sqrt{2\pi a_{bg}\Delta_0\Delta\mu/m\mathcal{V}}$ for bosons. For fermions, the atom-molecule coupling strength g [69,75–77] is equal to $g = \hbar\sqrt{4\pi a_{bg}\Delta_0\Delta\mu/m\mathcal{V}}$, where $\mathcal{V}$ represents the mode volume. For ^{6}Li at $B_r = 834.1$ G, $\Delta\mu = 2\mu_B$, the resonance width $\Delta_0 = -300$ G and background scattering length $a_{bg} = -1405$ a_0. The calculation of mode volume is tricky for ^{6}Li atomic cloud, the mode volume

for Fermi gas can be expressed as $\mathcal{V} = \frac{4\pi}{3}\mathrm{R}_x\mathrm{R}_y\mathrm{R}_z$ by considering three radii of the cloud in harmonic trap under Thomas-Fermi approximation. For a non-interacting gas, the radii of the atomic cloud on i axis is represented by,

$$R_i = \mathrm{a_{ho}}\frac{\omega_{\mathrm{ho}}}{\omega_i}(24N)^{1/6}. \tag{6.4}$$

In the case of total number of fermions (N) in a harmonic trap potential, the mean harmonic frequency and mean harmonic length are referred by $\omega_{\mathrm{ho}} = (\omega_x\omega_y\omega_z)^{1/3}$ and $\mathrm{a_{ho}} = \sqrt{\hbar/m\omega_{\mathrm{ho}}}$ respectively. Then the mode volume for a non-interacting gas can be represented by,

$$\mathcal{V} = \frac{4\pi}{3}\mathrm{a}_{\mathrm{ho}}^3\sqrt{24N}. \tag{6.5}$$

For an interacting gas, the shape and the density of the atoms in the trap changes, such that the radii of the dipole trap can be expressed by the equation,

$$R_i = \xi_B^{1/4}a_{ho}\frac{\omega_{ho}}{\omega_i}(24N)^{1/6}. \tag{6.6}$$

The parameter ξ_B is called Bertsch parameter, which is introduced by Papenbrock and Bertsch [78]. This modifies the chemical potential scaled by the Fermi energy of non-interacting gas, which is equal to $\mu = \xi_B E_F^0$ and the trapping frequency is scaled by $\sqrt{\xi_B}\omega_i$. Then the mode volume can be calculated by the equation,

$$\mathcal{V} = \frac{4\pi}{3}a_{ho}^3\xi_B^{3/4}\sqrt{24N}. \tag{6.7}$$

The parameter ξ_B can be calculated with Monte-Carlo method [79] in the BCS regime. Depending on the trapping profile and particle density, ξ_B converges to ≈ 0.37 in dilute limit, which is used in the calculation.

6.2 Comparison of experimental results to the theoretical model

In the experiment, the conversion of molecules is studied by varying the ramp rate at different temperatures varies from 3.2 μK to 130 nK. The molecular conversion is studied by obtaining atom-molecule coupling strength. The atom-molecule

coupling coefficient (g) is a parameter, which depends on the atomic properties such as a_{bg}, $\Delta\mu$ and the volume of the atomic cloud. To extract g_{eff} from the experimental results, the fraction of remnant atoms are measured at different magnetic field ramp rate and fit with an equation based on Landau-Zener model, which is given by,

$$n_a = n_0 + (1 - n_0) \exp\left(-\frac{2\pi g_{\mathrm{eff}}^2}{\dot{\delta}}\right). \tag{6.8}$$

The value of g_{eff} obtained from experimental data (see figure 5.7)is then compared with the theoretically calculated value g_{cal} from the equation,

$$g_{\mathrm{cal}} = \hbar\sqrt{4\pi a_{bg}\Delta_0\Delta\mu/m\mathcal{V}}. \tag{6.9}$$

where the volume is calculated from the equation 6.7 using the atom number N, which is obtained from the experimental data. The fitting curve with different g value with an experimental data is shown in figure 6.1, which depicts that higher the atom-molecule coupling coefficient faster the conversion of molecules.

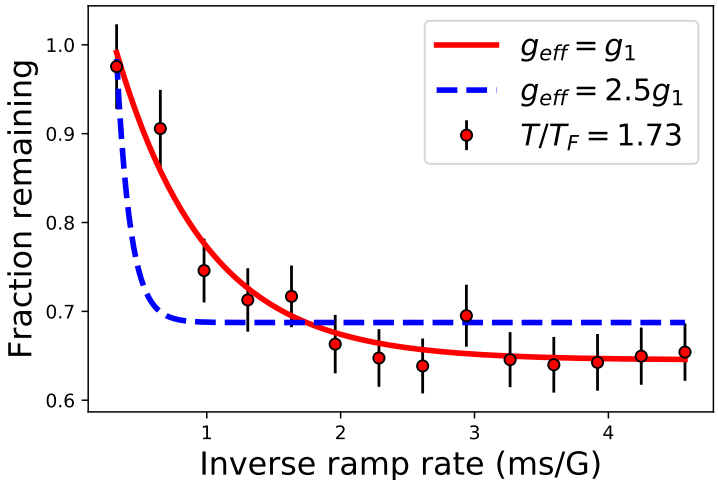

Figure 6.1: LZ model fitting with different g values. The plot shows how the trend of the curve changes with different g values.

The experimental results shows that molecule fraction increases as when the temperature of the atomic cloud decreases. The figure 6.2 shows the ratio of $g_{\mathrm{eff}}^2/g_{\mathrm{cal}}^2$ as

a function of T/T_{F}. Here the g_{eff} is obtained from the experimental data by varying the temperature of the gas. As can be seen in figure 6.2, the fitted coupling coefficient g_{eff} depends on the temperature. The calculated coupling coefficient g_{cal} is obtained from the equation 6.9. For $T \geq T_{\mathrm{F}}$, $g_{\mathrm{eff}}/g_{\mathrm{cal}}$ is around 1 and for $T < T_{\mathrm{F}}$ the fitted atom-molecule coupling strength g_{eff} increases gradually and the value is twice that of g_{cal} when $T/T_{\mathrm{F}} = 0.112$. We find that an enhancement of the coupling coefficient when the temperature of the atomic cloud is less than the Fermi temperature T_{F}, which is an indication of many-body coherence at ultra-low temperature. Here the coupling coefficient is amplified to be $g_T = \sqrt{N_T}g$, where $\mathrm{N}_T = \rho\mathcal{V}_{\mathrm{T}}$, which is the number of molecules in a thermal volume $\mathcal{V}_T$ and ρ is the density. The geometric ratio factor in the enhancement of coupling coefficient with temperature can be figured out by assuming molecules and atoms have the same temperature. The de Broglie wavelength at temperature T is given as, $\lambda_T = \hbar\sqrt{2\pi/Mk_BT}$. Here M is the mass of ^{6}Li molecule and the thermal volume is equal to $\mathcal{V}_T = \lambda_T^3$. At Fermi temperature, the coupling coefficient is given by $g_F = \sqrt{N_F}g$, where $\mathrm{N}_F = \rho\mathcal{V}_F$ and $\mathcal{V}_F = 3\pi^2\hbar^3\sqrt{(2mk_BT_F)^{-3}}$, which is the Fermi volume at Fermi temperature. So that the ratio of squares of coupling coefficient at temperature T to the coupling coefficient at Fermi temperature is given by a geometric ratio,

$$\frac{g_T^2}{g_F^2} = \frac{\mathcal{V}_T}{\mathcal{V}_F} = \frac{2\sqrt{2}}{3\sqrt{\pi}}\left(\frac{T_F}{T}\right)^{3/2}. \tag{6.10}$$

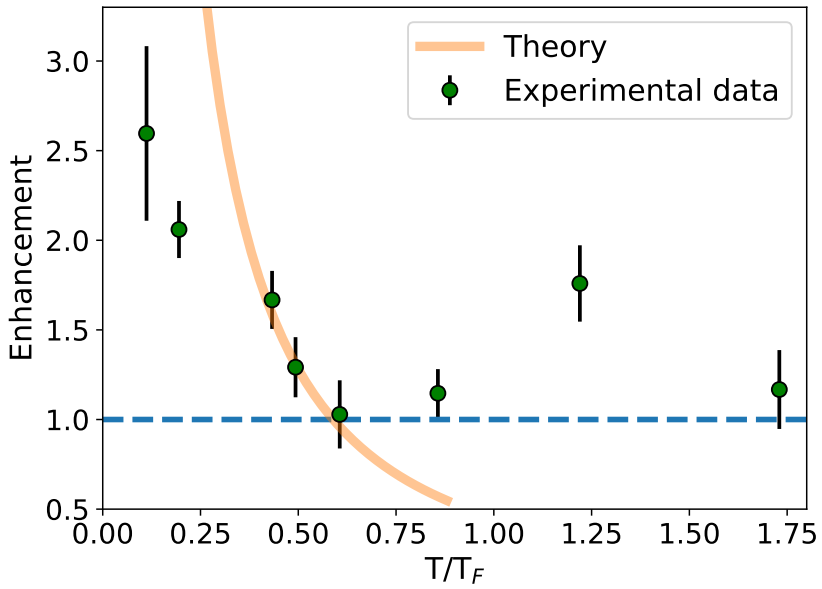

Figure 6.2: The temperature dependence of the coupling coefficient. The plot shows the enhancement factor as a function of T/T_{F}.

From equation 6.10, we can infer that the geometric ratio factor K is proportional to $\mathrm{T}^{-3/2}$. The calculated and fitted values of coupling coefficients are given in the table 6.1.

Table 6.1: The calculated and fitted coupling coefficients and the resulting enhancement factor for the respective temperature.

Temperature T/T_F	Calculated g g_{cal} $(\hbar \times \mathrm{kHz})$	Fitted g g_{eff} $(\hbar \times \mathrm{kHz})$	Enhancement $g^2_{\mathrm{eff}}/g^2_{\mathrm{cal}}$
0.112	47.07	75.4	2.60
0.195	45.40	64.8	2.06
0.433	43.97	56.4	1.67
0.493	42.27	47.7	1.29
0.606	42.23	42.6	1.02
0.857	41.12	43.8	1.15
1.220	46.10	60.8	1.76
1.730	46.44	49.9	1.17

The temperature dependence of molecule formation can be explained as follows.

For atoms with temperature higher than Fermi temperature ($T > T_F$), dynamics of molecular formation is based on Landau-Zener transition. In this case, less number of atoms are being converted into molecules and the thermal wavelength of the molecule is comparable to their size. The atom-molecule coupling takes place at the two-body level at higher temperature. Around Fermi temperature, the thermal wavelength is larger than the molecule size and the molecular gas is partially coherent. For temperature below the Fermi temperature ($T < T_F$), large number of atoms are being converted into molecules. A macroscopic coherence is established during the process and molecules form a Bose-Einstein Condensate. This result indicates that thermal wavelength of the molecules are significantly larger than the scattering length and it leads to collective coupling. This description is depicted in figure 6.3.

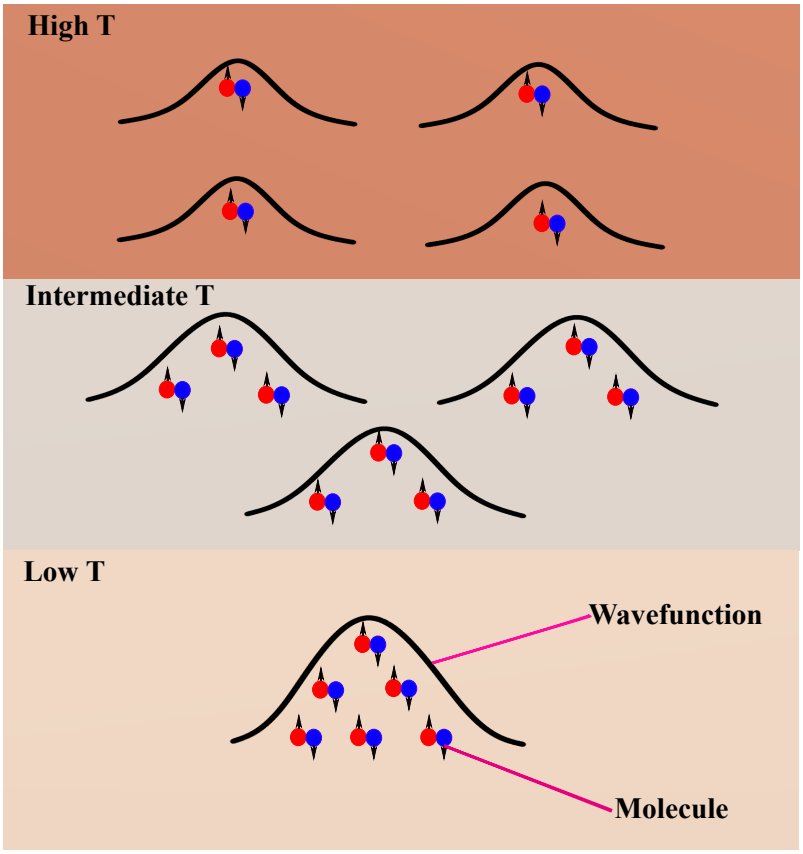

Figure 6.3: The temperature dependence of molecular conversion. The plot shows an illustration of molecule formation at different temperature regions. At $T > T_F$, less number of atoms are converted into molecules. At intermediate T i.e, the temperature of the atomic cloud is around the Fermi temperature, the molecules are partially coherent. At lower temperature i.e, $T < T_F$ a macroscopic coherence exists and molecules form a Bose-Einstein Condensate.

Chapter 7

Conclusion and Future work

7.1 Summary of the results

The dynamics of Feshbach molecule formation in fermionic ^{6}Li atoms is studied during my PhD work. The experimental system is modified to capture 2×10^8 ^{6}Li atoms in the MOT and 2×10^6 atoms in the crossed dipole beam trap created by 100 W IPG laser. At the end of evaporative cooling stage, on the order of 10^5 atoms with a lifetime of 19 s can be held in the dipole trap. The Feshbach molecules were created by sweeping the magnetic field from 806.6 G (BCS region) to 707 G (BEC region) linearly through the Feshbach resonance at 834.1 G. The fraction of molecules created was measured by imaging unassociated atoms after the magnetic field ramp. The experiment was performed with 1-3 $\times10^5$ atoms in each spin state with temperature varies from 3.2 μK to 130 nK. Depending on the trap depth at the final stage of evaporative cooling, the trapping frequencies are varying from 622 - 750 Hz (radially) and 74 - 90 Hz (longitudinally).

The fraction of atoms converted into molecules was studied by varying the rate at which the magnetic field is ramped across a Feshbach resonance in ^{6}Li. The bosonic molecules created from fermionic ultracold ^{6}Li atoms close to degeneracy

were produced and studied by this method. The maximum molecular conversion efficiency of 85 % was produced experimentally in this work. The lifetime of molecules created via magnetic field ramp is measured and found to be 2 s. The study shows that the fraction of atoms that associate into molecules is depending on the temperature of the atomic gas. The molecular conversion efficiency varies from 35 % to 85 % as the initial atomic cloud temperature changes from 3.2 μK to 130 nK. The dependence of mean density and final magnetic field is also studied in the same experimental system. The dependence of magnetic field at which the ramp ends shows a shift in the centroid of the error function, which is used to fit the experimental data. The shift in the centroid is also measured by varying the magnetic field ramp rate at fixed initial atomic cloud temperature. The characterisation of the final magnetic field dependence on molecule conversion is also studied by changing the atomic cloud temperature at a constant ramp rate.

A theoretical model is developed by the theory group in the cold atom group, University of Nottingham to study the dynamics of the Feshbach molecules creation in the fermionic atomic system. It is based on the original Landau-Zener model from which one can determine the atom-molecule coupling constant. The first experimental measurement of atom-molecule coupling constant in a degenerate system is reported by varying the atomic cloud temperature. The coupling constant increases at lower temperature than the Fermi temperature, due to the increased spatial coherence of the atomic gas. The many-body coherence is noticeable by the enhancement of the coupling coefficient as the atom cloud temperature close to degeneracy. The enhancement of coupling constant at temperature below the Fermi temperature leads to the many-body coherence. The atom-molecule coupling coefficient obtained from the experimental data is qualitatively agrees with the theoretically calculated atom-molecule coupling strength.

7.2 Perspective

The Feshbach molecules of lithium-6 can be created in the experimental setup. Since it has greater demand in quantum simulation, quantum information and fundamental physics, higher efficiency molecular conversion is still challenging in the research field. The ultracold diatomic molecules of ^{6}Li by sweeping the magnetic field is created and studied in this thesis. Here is a proposal for non-adiabatic scheme for the formation of Feshbach molecules in ultracold systems which leads to the higher and faster molecular conversion. Designing and developing high fidelity magnetic field generating and optimal timing sequences to enable efficient molecular formation. Molecules of homo-nuclear and hetero-nuclear atoms for e.g. Li_2 and LiCs, near a magnetic Feshbach resonance can be prepared by using the same experimental setup. This rapid and efficient scheme for the production of ultracold diatomic molecules will explore non-equilibrium many-body dynamics, ultracold chemistry, and enables to study fundamental physics. On the other hand, a theoretical study on dependence of final magnetic field to the molecular conversion and shift from the Feshbach resonance will be undertaking in the near future.

The experimental system can be used to produce Bose-Einstein condensate and it can be used to study acoustic analogues to the dynamical Casimir effect by modulating the trap depth at the end of evaporative cooling stage. A sinusoidal modulation can be applied to trap depth while holding the atoms in the dipole beam. The experimental sequence is modified to do the sinusoidal modulation. More background study is needed to perform these experimental measurements.

Appendix A

D1 line cooling

In our experiment in addition to widely used D2 line cooling we are planning to implement D1 line cooling to increase the initial phase space density and to optimise the loading of atoms in the dipole trap. The ^{6}Li D1 gray molasses is based on existence of bright and dark states which leads to the Sisyphus cooling. The D1 line atomic hyperfine structure is given below A.1.

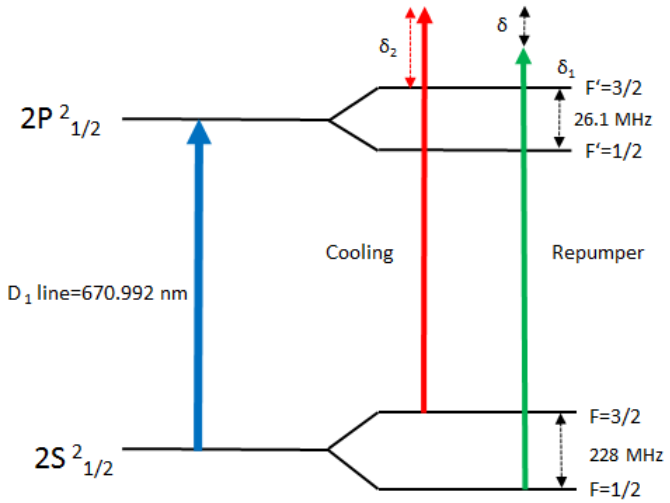

Figure A.1: The atomic energy level diagram of ^{6}Li. The ^{6}Li D1 line transition is shown in the figure.

The optical coupling between cooling and re-pumper can be consider as three

level lambda system in which two ground states are optically coupled to the same excited level.

A.1 Three Level Lambda (Λ) System

A three level Lambda (Λ) configuration in which two lower levels $|b\rangle$ and $|c\rangle$ are coupled to a single upper level $|a\rangle$. Consider a Λ scheme that consists of the energy states $|a\rangle, |b\rangle$ and $|c\rangle$ coupled by two near resonance laser fields of strength obtained in terms of the Rabi frequency Ω_1 (at frequency ω_1) and Ω_2 (at frequency ω_2). The figure A.2 illustrates a three level lambda system. The dipole interaction between the two lower energy levels is forbidden. Then the Hamiltonian of the system is given by,

$$H = H_0 + V_1 + V_2. \tag{A.1}$$

Where, $H_0 = \hbar\omega_a |a\rangle \langle a| + \hbar\omega_b |b\rangle \langle b| + \hbar\omega_c |c\rangle \langle c|$

$V_1 = \hbar\Omega_1 exp\frac{-i\omega_1 t}{2} |b\rangle \langle a| + \hbar\Omega_1 exp\frac{i\omega_1 t}{2} |a\rangle \langle b|$

$V_2 = \hbar\Omega_2 exp\frac{-i\omega_2 t}{2} |c\rangle \langle a| + \hbar\Omega_2 exp\frac{i\omega_1 t}{2} |a\rangle \langle c|$

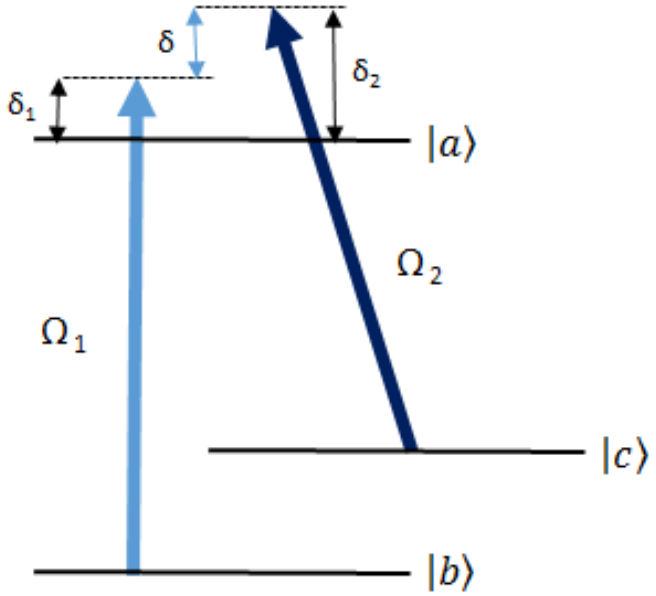

Figure A.2: Three level lambda system

Consider a situation, when the two fields are in resonance, i.e. $\omega_1 = \omega_a - \omega_b$ and $\omega_2 = \omega_a - \omega_c$. Then the three eigenstates of H are:

$$|C_1\rangle = \frac{1}{\sqrt{2}}[-|a\rangle + \frac{\Omega_1}{\sqrt{\Omega_1^2+\Omega_2^2}}|b\rangle + \frac{\Omega_2}{\sqrt{\Omega_1^2+\Omega_2^2}}|c\rangle] \tag{A.2}$$

$$|C_2\rangle = \frac{1}{\sqrt{2}}[|a\rangle + \frac{\Omega_1}{\sqrt{\Omega_1^2+\Omega_2^2}}|b\rangle + \frac{\Omega_2}{\sqrt{\Omega_1^2+\Omega_2^2}}|c\rangle] \tag{A.3}$$

$$|NC\rangle = \frac{\Omega_2}{\sqrt{\Omega_1^2+\Omega_2^2}}|b\rangle - \frac{\Omega_1}{\sqrt{\Omega_1^2+\Omega_2^2}}|c\rangle\,. \tag{A.4}$$

The state $|NC\rangle$ contains no component of $|a\rangle$ and hence there is no coupling between $|NC\rangle$ and $|a\rangle$. Thus any population in $|NC\rangle$ is trapped in that state, which is called as dark state. Over a period of time, dependent upon the rate of spontaneous emission from the excited state, all of the population of the system will build up in $|NC\rangle$. Hence all of the population becomes coherently trapped in a dark state. When $\Omega_1 \ll \Omega_2$, the coupling and non coupling states become,

$$|C\rangle = \frac{1}{\sqrt{2}}|C_1\rangle + \frac{1}{\sqrt{2}}|C_2\rangle \tag{A.5}$$

$$|C\rangle = \frac{\Omega_2}{\sqrt{\Omega_1^2 + \Omega_2^2}}|c\rangle \tag{A.6}$$

$$|C\rangle \approx |c\rangle \tag{A.7}$$

$$|NC\rangle = \frac{\Omega_2}{\sqrt{\Omega_1^2 + \Omega_2^2}}|b\rangle \tag{A.8}$$

$$|NC\rangle \approx |b\rangle\,. \tag{A.9}$$

As per the equation A.9, ground state itself becomes the dark state. The population is trapped in the lower states and there is no absorption even in the presence of the field. This is because of the reason that after being pumped into the dark state, the atoms cannot be excited by either laser field.

A.1.1 Laser design and Spectroscopy setup

External cavity diode lasers (ECDL) are widely used in many experiments since it has simple design and all elements are easily available. ECDLs consist of a laser diode, a collimation lens, a grating on a mirror mount, a piezoelectric transducer, and electronics for current and temperature controller as shown in the photograph of ECDL laser A.3. Since the experimental system is based on ^{6}Li, laser needs to be locked at wavelength 670.992 nm for D1 line cooling. There is no high power laser available operating at the same wavelength so that we designed and developed an External Cavity Diode Laser. A laser diode operating at 660 nm with a nominal output power of (60 mW) have been used and pull the wavelength to the specified value by tuning the grating and increasing the operating temperature to 70 °C. The laser housing design consists of two metal boxes called inner box and outer box which improve laser thermal stability by minimizing air circulation.

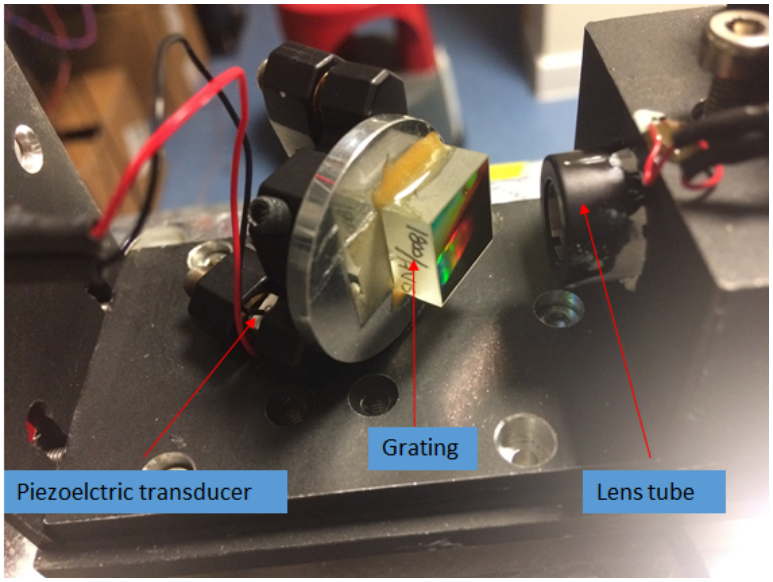

Figure A.3: Home built ECDL. The laser diode is inserted into a lens tube and a grating is attached to a mirror mount, where one can adjust the grating angle. A piezoelectric transducer is used for the fine tuning of the wavelength of the laser.

The inner box is designed such that it can occupy the laser diode and the lens tube for collimation and also has some space for positioning the grating on the mirror mount. The diode ($HL6545MG$) is a H type which can be operated at maximum temperature of 75 °C. It is a cathode grounded laser diode without a photodiode. It is mounted on a lens tube which needs to be rotated such that collimated output beam should be obtained. Our laser design is based on a Littrow type configuration in which the grating is aligned such that first order diffracted beam is coupled to the zeroth order beam to achieve optical feedback for the laser performance. Thus a precise wavelength can be obtained by changing the Littrow angle. The grating ($GH13-18V$) is glued on a circular platform fixed on a mirror mount. The holographic reflective grating has to be positioned such that the first order diffracted beam goes back to the laser for optical feedback. The angle for the grating can be calculated using the equation,

$$\Theta = sin^{-1}\frac{\lambda}{2d},$$

where, λ (670.992 nm) is wavelength of the light and d is the distance between grating teeth. Fine tuning of the laser wavelength is obtained by piezoelectric transducer which is attached to one of the mirror knobs.

A new temperature controller was developed (standard controller allows only 50 °C) in order to make the laser working at higher temperature. It consists of electronic circuits which are controlled by an Arduino program and they are connected to a thermoelectric cooler (peltier) element placed under the inner box. The hot facet of the peltier element is glued using thermally conducting paste to ensure proper contact with metal box. The temperature can be read out via thermistor, which is attached to the lens tube in the mount and it is also fixed using thermally contacting paste. The feedback circuit works in way that the Arduino program compares the set value with the sensor output value. The main components of circuit are Arduino Uno, low power quad operational amplifier (LM324N), standard power MOSFET and resistors (R_1 =R_2 = 33kΩ, R_3 =R_5= 10kΩ and R_4 = 20kΩ). Calibration is done to find the optimum temperature to operate the laser efficiently. A Circuit diagram for the temperature controller is illustrated in figure A.4.

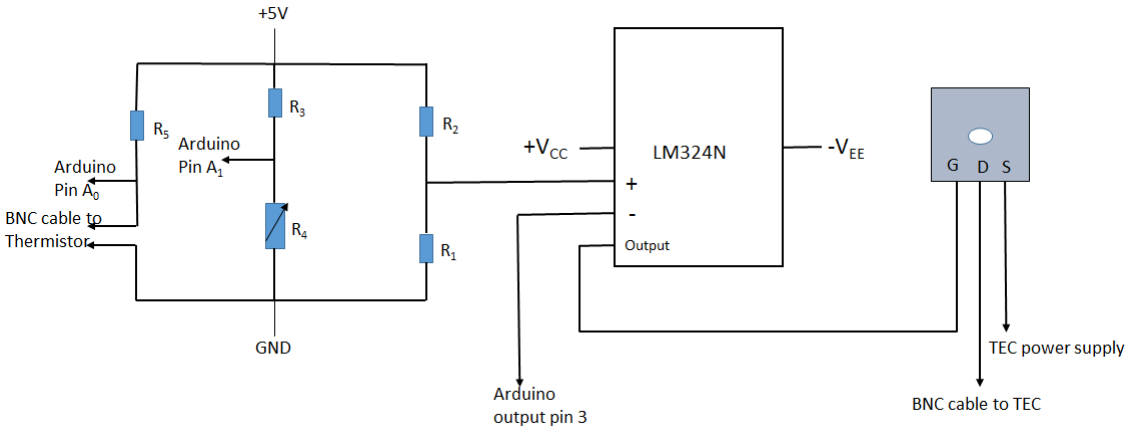

Figure A.4: Circuit diagram of temperature controller.

A.1.2 Saturation absorption spectroscopy

Saturation absorption spectroscopy has been set up in order to lock the laser at a specific transition. The laser has to be optimised by finding the minimum threshold current to operate the laser efficiently and it has to start with lower current. The laser output passes through the prism pairs to modify the beam profile and it reaches the fiber incoupler after passing through the optical isolator and mirrors. The isolator prevents the back reflection of light to the laser diode. The laser beam is then taken to the other table, where the spectroscopy cell (at 370 °C) is placed, by polarisation maintaining fiber. We have introduced a separate path for the new laser beam in the current spectroscopy setup apart from the reference laser beam. A sketch for the saturation absorption spectroscopy set up for the new laser beam is shown in figure A.5.

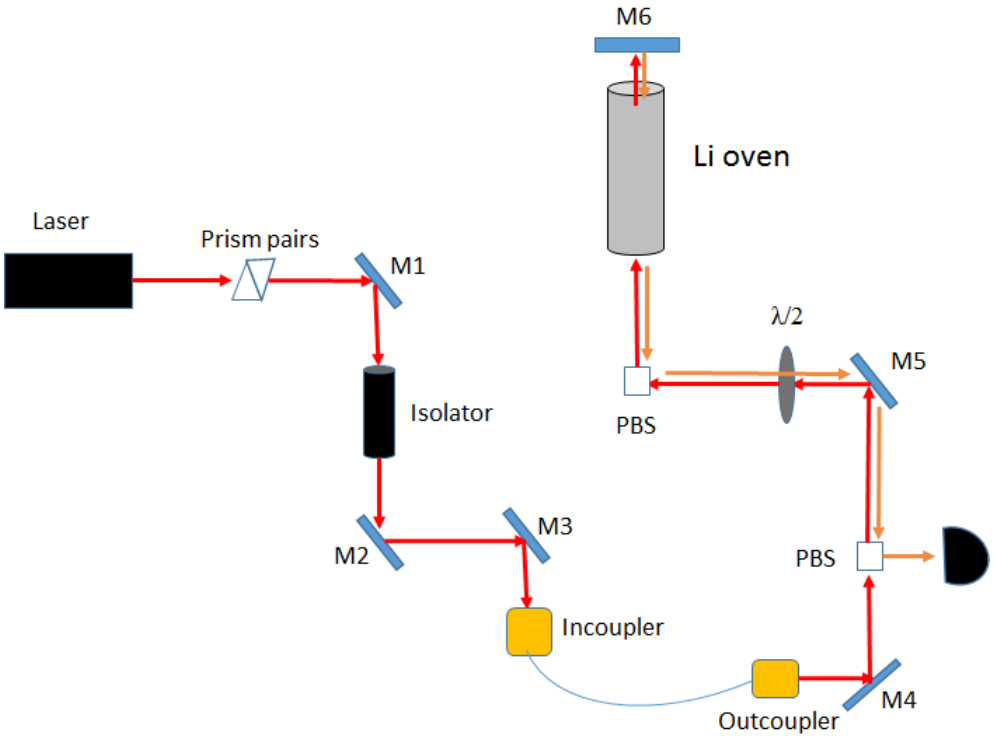

Figure A.5: Saturation Absorption spectroscopy setup.

The laser has to be scanned to observe the Doppler valley and simultaneous tun-

ing the current and piezoelectric transducer gives an absorption signal which is collected by photodetector. This signal can be used as input signal for the locking in amplifier followed by PID card to produce the corresponding error signal.

A.1.3 Design of laser box parts

The design of grating mount and inner box parts developed by a program called SolidWork is shown below A.6, A.7.

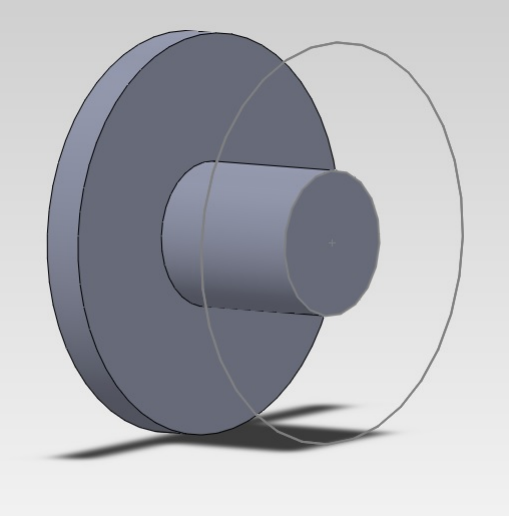

Figure A.6: Design of grating mount. This mount is used to attach to the mirror mount from Thorlab.

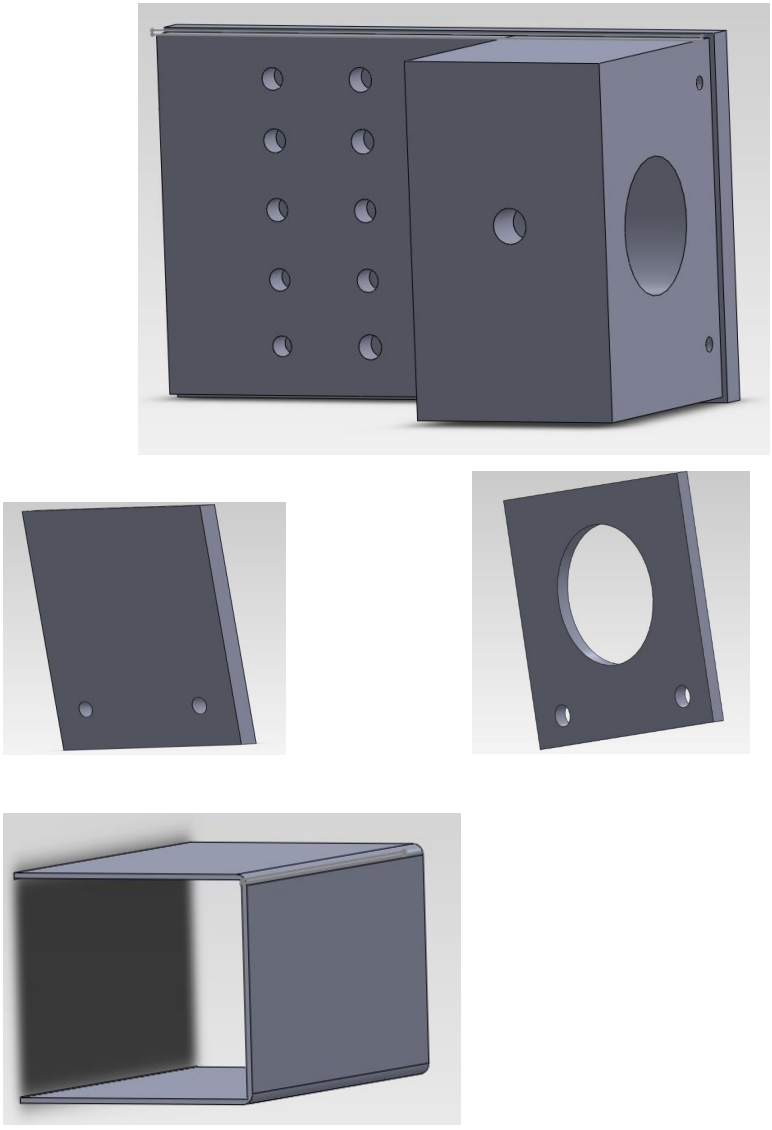

Figure A.7: Design of inner box for laser parts.

Appendix B

The expression for average time between collisions $\tau_{\mathbf{col}}$

This section gives the expression for the average time between collisions during the magnetic field ramp on molecular conversion process. The collisional cross section of the fermionic atoms with scattering length a in the unitary limit is given by,

$$\sigma = \frac{4\pi a^2}{(1 + k^2 a^2)}. \tag{B.1}$$

The scattering cross section close to the Feshbach resonance can be expressed as, $\sigma = 4\pi/k_F^2$, where k_F is the Fermi wave vector. The average time between the collisions can be expressed in terms of atom density n and collisional cross section σ, which is given by,

$$\frac{1}{\tau_{\rm col}} = n\sigma\tilde{v_{\rm rel}}. \tag{B.2}$$

Here average relative velocity $\tilde{v}_{\rm rel} = 4\sqrt{k_B T_F/\pi m}$ and density,

$$n \approx \left(\frac{2mk_B T_F}{\hbar^2}\right)^{3/2} /6\pi^2. \tag{B.3}$$

Then the expression for $\tau_{\rm col}$ can be rewritten as $\tau_{\rm col} \approx \frac{\hbar}{k_B T_F}$.

Appendix C

^{6}Li optics scheme

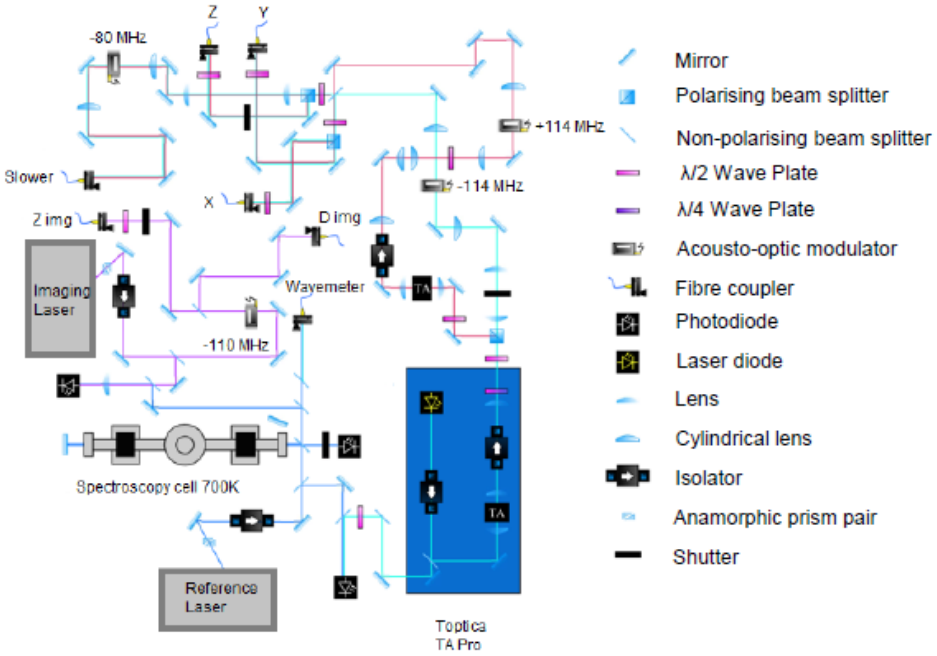

References

[1] T. Köhler, K. Góral, and P. S. Julienne, "Production of cold molecules via magnetically tunable feshbach resonances," *Rev. Mod. Phys.*, vol. 78, pp. 1311–1361, Dec 2006.

[2] J. L. Bohn, A. M. Rey, and J. Ye, "Cold molecules: Progress in quantum engineering of chemistry and quantum matter," *Science*, vol. 357, no. 6355, pp. 1002–1010, 2017.

[3] I. Bloch, J. Dalibard, and S. Nascimbène, "Quantum simulations with ultracold quantum gases," vol. 8, 2012.

[4] W. Ketterle and N. V. Druten, "Evaporative cooling of trapped atoms," vol. 37 of *Advances In Atomic, Molecular, and Optical Physics*, pp. 181–236, Academic Press, 1996.

[5] R. Grimm, M. Weidemüller, and Y. B. Ovchinnikov, "Optical dipole traps for neutral atoms," vol. 42 of *Advances In Atomic, Molecular, and Optical Physics*, pp. 95–170, Academic Press, 2000.

[6] C. A. Regal, C. Ticknor, J. L. Bohn, and D. S. Jin, "Creation of ultracold molecules from a fermi gas of atoms," *Nature*, vol. 424, pp. 47–50, Jul 2003.

[7] M. Greiner, C. Regal, and D. Jin, "Emergence of a molecular bose–einstein condensate from a fermi gas," *Nature*, vol. 426, p. 537–540, Nov 2003.

[8] I. Boettcher, L. Bayha, D. Kedar, P. A. Murthy, M. Neidig, M. G. Ries, A. N. Wenz, G. Zürn, S. Jochim, and T. Enss, "Equation of state of ultracold fermions in the 2d bec-bcs crossover region," *Phys. Rev. Lett.*, vol. 116, p. 045303, Jan 2016.

[9] A. Schirotzek, C.-H. Wu, A. Sommer, and M. W. Zwierlein, "Observation of fermi polarons in a tunable fermi liquid of ultracold atoms," *Phys. Rev. Lett.*, vol. 102, p. 230402, Jun 2009.

[10] Y. J. Lin, K. Jimenez-Garcia, and I. B. Spielman, "Spin–orbit-coupled bose–einstein condensates," *Nature*, vol. 471, p. 83–86, Mar 2011.

[11] K. Günter, T. Stöferle, H. Moritz, M. Köhl, and T. Esslinger, "p-wave interactions in low-dimensional fermionic gases," *Phys. Rev. Lett.*, vol. 95, p. 230401, Nov 2005.

[12] V. V. Flambaum and M. G. Kozlov, "Enhanced sensitivity to the time variation of the fine-structure constant and m_p/m_e in diatomic molecules," *Phys. Rev. Lett.*, vol. 99, p. 150801, Oct 2007.

[13] L. D. Carr, D. DeMille, R. V. Krems, and J. Ye, "Cold and ultracold molecules: science, technology and applications," *New Journal of Physics*, vol. 11, p. 055049, may 2009.

[14] T. A. Collaboration, J. Baron, W. C. Campbell, D. DeMille, J. M. Doyle, G. Gabrielse, Y. V. Gurevich, P. W. Hess, N. R. Hutzler, E. Kirilov, I. Kozyryev, B. R. O'Leary, C. D. Panda, M. F. Parsons, E. S. Petrik, B. Spaun, A. C. Vutha, and A. D. West, "Order of magnitude smaller limit on the electric dipole moment of the electron," vol. 343, no. 6168, pp. 269–272, 2014.

[15] J. J. Hudson, D. M. Kara, I. J. Smallman, B. E. Sauer, M. R. Tarbutt, and E. A. Hinds, "Improved measurement of the shape of the electron," *Nature*, vol. 473, p. 493–496, May 2011.

[16] R. V. Krems, "Cold controlled chemistry," *Phys. Chem. Chem. Phys.*, vol. 10, pp. 4079–4092, 2008.

[17] S. Knoop, F. Ferlaino, M. Berninger, M. Mark, H.-C. Nägerl, R. Grimm, J. P. D'Incao, and B. D. Esry, "Magnetically controlled exchange process in an ultracold atom-dimer mixture," *Phys. Rev. Lett.*, vol. 104, p. 053201, Feb 2010.

[18] S. Ospelkaus, K.-K. Ni, D. Wang, M. H. G. de Miranda, B. Neyenhuis, G. Quéméner, P. S. Julienne, J. L. Bohn, D. S. Jin, and J. Ye, "Quantum-state controlled chemical reactions of ultracold potassium-rubidium molecules," vol. 327, no. 5967, pp. 853–857, 2010.

[19] M. H. G. de Miranda, A. Chotia, B. Neyenhuis, D. Wang, G. Quéméner, S. Ospelkaus, J. L. Bohn, J. Ye, and D. S. Jin, "Controlling the quantum stereodynamics of ultracold bimolecular reactions," vol. 7, no. 6, p. 502–507, 2011.

[20] X. Ye, M. Guo, M. L. González-Martínez, G. Quéméner, and D. Wang, "Collisions of ultracold 23na87rb molecules with controlled chemical reactivities," vol. 4, no. 1, 2018.

[21] A. Micheli, G. K. Brennen, and P. Zoller, "A toolbox for lattice-spin models with polar molecules," vol. 2, p. 341–347, 2006.

[22] A. V. Gorshkov, S. R. Manmana, G. Chen, J. Ye, E. Demler, M. D. Lukin, and A. M. Rey, "Tunable superfluidity and quantum magnetism with ultracold polar molecules," *Phys. Rev. Lett.*, vol. 107, p. 115301, Sep 2011.

[23] W. Lechner and P. Zoller, "From classical to quantum glasses with ultracold polar molecules," *Phys. Rev. Lett.*, vol. 111, p. 185306, Oct 2013.

[24] L. Pollet, J. D. Picon, H. P. Büchler, and M. Troyer, "Supersolid phase with cold polar molecules on a triangular lattice," *Phys. Rev. Lett.*, vol. 104, p. 125302, Mar 2010.

[25] C. A. Regal, M. Greiner, and D. S. Jin, "Observation of resonance condensation of fermionic atom pairs," *Phys. Rev. Lett.*, vol. 92, p. 040403, Jan 2004.

[26] R. Sensarma, M. Randeria, and T.-L. Ho, "Vortices in superfluid fermi gases through the bec to bcs crossover," *Phys. Rev. Lett.*, vol. 96, p. 090403, Mar 2006.

[27] R. Combescot, M. Y. Kagan, and S. Stringari, "Collective mode of homogeneous superfluid fermi gases in the bec-bcs crossover," *Phys. Rev. A*, vol. 74, p. 042717, Oct 2006.

[28] E. Hodby, S. T. Thompson, C. A. Regal, M. Greiner, A. C. Wilson, D. S. Jin, E. A. Cornell, and C. E. Wieman, "Production efficiency of ultracold feshbach molecules in bosonic and fermionic systems," *Phys. Rev. Lett.*, vol. 94, p. 120402, Mar 2005.

[29] G. Zürn, T. Lompe, A. N. Wenz, S. Jochim, P. S. Julienne, and J. M. Hutson, "Precise characterization ofli6feshbach resonances using trap-sideband-resolved rf spectroscopy of weakly bound molecules," *Physical Review Letters*, vol. 110, Mar 2013.

[30] M. Guo, R. Vexiau, B. Zhu, B. Lu, N. Bouloufa-Maafa, O. Dulieu, and D. Wang, "High-resolution molecular spectroscopy for producing ultracold absolute-ground-state na23rb87 molecules," *Physical Review A*, vol. 96, Nov 2017.

[31] D. K. Hoffmann, T. Paintner, W. Limmer, D. S. Petrov, and J. H. Denschlag, "Reaction kinetics of ultracold molecule-molecule collisions," *Nature Communications*, vol. 9, Dec 2018.

[32] T. Volz, N. Syassen, D. M. Bauer, E. Hansis, S. Dürr, and G. Rempe, "Preparation of a quantum state with one molecule at each site of an optical lattice," *Nature Communications*, vol. 2, Oct 2006.

[33] A. Fioretti, D. Comparat, A. Crubellier, O. Dulieu, F. Masnou-Seeuws, and P. Pillet, "Formation of cold cs_2 molecules through photoassociation," *Phys. Rev. Lett.*, vol. 80, pp. 4402–4405, May 1998.

[34] A. N. Nikolov, E. E. Eyler, X. T. Wang, J. Li, H. Wang, W. C. Stwalley, and P. L. Gould, "Observation of ultracold ground-state potassium molecules," *Phys. Rev. Lett.*, vol. 82, pp. 703–706, Jan 1999.

[35] T. Takekoshi, B. M. Patterson, and R. J. Knize, "Observation of cold ground-state cesium molecules produced in a magneto-optical trap," *Phys. Rev. A*, vol. 59, pp. R5–R7, Jan 1999.

[36] E. Timmermans, P. Tommasini, R. Cote, M. Hussein, and A. Kerman, "Inter-condensate tunneling in bose-einstein condensates with feshbach resonances," 1998.

[37] F. H. Mies, E. Tiesinga, and P. S. Julienne, "Manipulation of feshbach resonances in ultracold atomic collisions using time-dependent magnetic fields," *Phys. Rev. A*, vol. 61, p. 022721, Jan 2000.

[38] F. A. van Abeelen and B. J. Verhaar, "Time-dependent feshbach resonance scattering and anomalous decay of a na bose-einstein condensate," *Phys. Rev. Lett.*, vol. 83, pp. 1550–1553, Aug 1999.

[39] T. Bourdel, L. Khaykovich, J. Cubizolles, J. Zhang, F. Chevy, M. Teichmann, L. Tarruell, S. J. J. M. F. Kokkelmans, and C. Salomon, "Experimental study of the bec-bcs crossover region in lithium 6," *Phys. Rev. Lett.*, vol. 93, p. 050401, Jul 2004.

[40] M. Bartenstein, A. Altmeyer, S. Riedl, S. Jochim, C. Chin, J. H. Denschlag, and R. Grimm, "Collective excitations of a degenerate gas at the bec-bcs crossover," *Phys. Rev. Lett.*, vol. 92, p. 203201, May 2004.

[41] S. Musolino, V. E. Colussi, and S. J. J. M. F. Kokkelmans, "Pair formation in quenched unitary bose gases," *Phys. Rev. A*, vol. 100, p. 013612, Jul 2019.

[42] E. Pazy, A. Vardi, and Y. B. Band, "Conversion efficiency of ultracold fermionic atoms to bosonic molecules via feshbach resonance sweep experiments," *Phys. Rev. Lett.*, vol. 93, p. 120409, Sep 2004.

[43] N. Cooper, E. Da Ros, C. Briddon, V. Naniyil, M. T. Greenaway, and L. Hackermueller, "Prospects for strongly coupled atom-photon quantum nodes," *Scientific Reports*, vol. 9, no. 1, p. 7798, 2019.

[44] C. Foot, *Atomic Physics*. New York: Oxford University Press, 1st ed., 2005.

[45] M. E. Gehm, "Properties of 6Li."

[46] A. Ashkin, "Trapping of atoms by resonance radiation pressure," *Phys. Rev. Lett.*, vol. 40, pp. 729–732, Mar 1978.

[47] S. Warriar, *Towards an Ultracold Bose-Fermi Mixture of Cesium and Lithium Atoms*. PhD thesis, University of Nottingham, 2014.

[48] H. J. Metcalf and P. van der Straten, *Laser Cooling and Trapping*. New York: Springer-Verlag, 1999.

[49] A. Paris-Mandoki, *A Single Apparatus for the Production of Ultracold Fermionic Lithium and Cold Bosonic Caesium Gases*. PhD thesis, University of Nottingham, 2015.

[50] K. Xhani, *Production and Observation of Degenerate Quantum Gases of 6Li Fermionic Atoms*. PhD thesis, University of Florence, 2014.

[51] A. J. Moerdijk, B. J. Verhaar, and A. Axelsson, "Resonances in ultracold collisions of ^{6}Li, ^{7}Li, and ^{23}Na," *Phys. Rev. A*, vol. 51, pp. 4852–4861, Jun 1995.

[52] G. Zürn, T. Lompe, A. N. Wenz, S. Jochim, P. S. Julienne, and J. M. Hutson, "Precise characterization of ^{6}Li feshbach resonances using trap-sideband-resolved rf spectroscopy of weakly bound molecules," *Phys. Rev. Lett.*, vol. 110, p. 135301, Mar 2013.

[53] *Bose-Einstein Condensation in Dilute gases*. Cambridge University press, 2002.

[54] S. Jochim, M. Bartenstein, A. Altmeyer, G. Hendl, S. Riedl, C. Chin, J. Hecker Denschlag, and R. Grimm, "Bose-einstein condensation of molecules," *Science*, vol. 302, no. 5653, pp. 2101–2103, 2003.

[55] L. Landau *Phys. Z. Sowjetunion*, vol. 2, no. 46, 1932.

[56] C. Zener *Proc. R. Soc. London*, vol. Ser. A. 137, no. 696, 1932.

[57] G. Sanna and G. Tomassetti, *Introduction to Molecular Beam Gas Dynamics*. Imperial College Press, 2005.

[58] R. Weast, *Handbook of Chemistry and Physics: a ready reference book of Chemical and Physicsal data*. 1969.

[59] G. W. Thomson, "The antoine equation for vapor-pressure data.," *Chemical Reviews*, vol. 38, no. 1, pp. 1–39, 1946. PMID: 21016992.

[60] M. D. Jones, *Preparation of Cold Samples of Caesium-133 and Lithium-6 in a Single Apparatus for Bose-Fermi Mixture Experiments*. PhD thesis, University of Nottingham, 2014.

[61] T. M. Brzozowski, M. Maczynska, M. Zawada, J. Zachorowski, and W. Gawlik, "Time-of-flight measurement of the temperature of cold atoms for short trap-probe beam distances," *Journal of Optics B: Quantum and Semiclassical Optics*, vol. 4, pp. 62–66, jan 2002.

[62] X. Du, L. Luo, B. Clancy, and J. E. Thomas, "Observation of anomalous spin segregation in a trapped fermi gas," *Phys. Rev. Lett.*, vol. 101, p. 150401, Oct 2008.

[63] P. Jouve, *Study of an interactive ^{6}Li molecular Bose Einstein-condensate*. PhD thesis, University of Nottingham, 2018.

[64] C. C. Bradley, C. A. Sackett, J. J. Tollett, and R. G. Hulet, "Evidence of bose-einstein condensation in an atomic gas with attractive interactions," *Phys. Rev. Lett.*, vol. 75, pp. 1687–1690, Aug 1995.

[65] M. W. Zwierlein, C. A. Stan, C. H. Schunck, S. M. F. Raupach, S. Gupta, Z. Hadzibabic, and W. Ketterle, "Observation of bose-einstein condensation of molecules," *Phys. Rev. Lett.*, vol. 91, p. 250401, Dec 2003.

[66] C. Chin, R. Grimm, P. Julienne, and E. Tiesinga, "Feshbach resonances in ultracold gases," *Rev. Mod. Phys.*, vol. 82, pp. 1225–1286, Apr 2010.

[67] K. E. Strecker, G. B. Partridge, and R. G. Hulet, "Conversion of an atomic fermi gas to a long-lived molecular bose gas," *Phys. Rev. Lett.*, vol. 91, p. 080406, Aug 2003.

[68] J. Javanainen, M. Kos˘trun, Y. Zheng, A. Carmichael, U. Shrestha, P. J. Meinel, M. Mackie, O. Dannenberg, and K.-A. Suominen, "Collective molecule formation in a degenerate fermi gas via a feshbach resonance," *Phys. Rev. Lett.*, vol. 92, p. 200402, May 2004.

[69] J. E. Williams, N. Nygaard, and C. W. Clark, "Theory of feshbach molecule formation in a dilute gas during a magnetic field ramp," *New Journal of Physics*, vol. 8, pp. 150–150, aug 2006.

[70] E. Pazy, I. Tikhonenkov, Y. B. Band, M. Fleischhauer, and A. Vardi, "Nonlinear adiabatic passage from fermion atoms to boson molecules," *Phys. Rev. Lett.*, vol. 95, p. 170403, Oct 2005.

[71] J. Chwedeńczuk, K. Góral, T. Köhler, and P. S. Julienne, "Molecular production in two component atomic fermi gases," *Phys. Rev. Lett.*, vol. 93, p. 260403, Dec 2004.

[72] E. Hodby, S. T. Thompson, C. A. Regal, M. Greiner, A. C. Wilson, D. S. Jin, E. A. Cornell, and C. E. Wieman, "Production efficiency of ultracold feshbach molecules in bosonic and fermionic systems," *Phys. Rev. Lett.*, vol. 94, p. 120402, Mar 2005.

[73] K. E. Strecker, G. B. Partridge, and R. G. Hulet, "Conversion of an atomic fermi gas to a long-lived molecular bose gas," *Phys. Rev. Lett.*, vol. 91, p. 080406, Aug 2003.

[74] K. Góral, T. Köhler, S. A. Gardiner, E. Tiesinga, and P. S. Julienne, "Adiabatic association of ultracold molecules via magnetic-field tunable interactions," *Journal of Physics B: Atomic, Molecular and Optical Physics*, vol. 37, p. 3457–3500, Aug 2004.

[75] E. Timmermans, P. Tommasini, M. Hussein, and A. Kerman, "Feshbach resonances in atomic bose–einstein condensates," *Physics Reports*, vol. 315, no. 1, pp. 199–230, 1999.

[76] D. Sun, A. Abanov, and V. L. Pokrovsky, "Molecular production at a broad feshbach resonance in a fermi gas of cooled atoms," *EPL (Europhysics Letters)*, vol. 83, p. 16003, jun 2008.

[77] J. Javanainen and M. Mackie, "Coherent photoassociation of a bose-einstein condensate," *Phys. Rev. A*, vol. 59, pp. R3186–R3189, May 1999.

[78] T. Papenbrock and G. F. Bertsch, "Pairing in low-density fermi gases," *Phys. Rev. C*, vol. 59, pp. 2052–2055, Apr 1999.

[79] J. Carlson, S. Gandolfi, K. E. Schmidt, and S. Zhang, "Auxiliary-field quantum monte carlo method for strongly paired fermions," *Phys. Rev. A*, vol. 84, p. 061602, Dec 2011.

[80] H. Schmaljohann, M. Erhard, J. Kronjäger, M. Kottke, S. van Staa, L. Cacciapuoti, J. J. Arlt, K. Bongs, and K. Sengstock, "Dynamics of $f = 2$ spinor bose-einstein condensates," *Phys. Rev. Lett.*, vol. 92, p. 040402, Jan 2004.

[81] J. Javanainen, M. Kos˘trun, Y. Zheng, A. Carmichael, U. Shrestha, P. J. Meinel, M. Mackie, O. Dannenberg, and K.-A. Suominen, "Collective molecule formation in a degenerate fermi gas via a feshbach resonance," *Phys. Rev. Lett.*, vol. 92, p. 200402, May 2004.

[82] J. Nute, *A Quantum Integrated Light and Matter Interface.* PhD thesis, University of Nottingham, 2017.

[83] W. Demtröder, *Laser Spectroscopy: Vol. 1:Basic Principles.* Springer, 2008.

[84] W. Ketterle, D. S. Durfee, and D. M. Stamper-kurn, "Making, probing and understanding bose-einstein condensates," in *Proceedings of the International School of Physics"ENRICO FERMI" course CXL, Edited by M. Inguscio, S. Strigari and C.E. Wieman (IOS),.*

[85] R. Grimm, M. Weidemüller, and Y. B. Ovchinnikov, "Optical dipole traps for neutral atoms," vol. 42 of *Advances In Atomic, Molecular, and Optical Physics*, pp. 95 – 170, Academic Press, 2000.

[86] G. Kim, *A New Laser Cooling Method For Lithium Atom Interferometry.* PhD thesis, University of California, Berkeley, 2014.

[87] S. Chu, L. Hollberg, J. E. Bjorkholm, A. Cable, and A. Ashkin, "Three-dimensional viscous confinement and cooling of atoms by resonance radiation pressure," *Phys. Rev. Lett.*, vol. 55, pp. 48–51, Jul 1985.

[88] C. A. Leon, *Design and construction of a Lithium vapor oven.* PhD thesis, Western Mishigan University, 1993.

[89] J. Cubizolles, T. Bourdel, S. J. J. M. F. Kokkelmans, G. V. Shlyapnikov, and C. Salomon, "Production of long-lived ultracold li_2 molecules from a fermi gas," *Phys. Rev. Lett.*, vol. 91, p. 240401, Dec 2003.

[90] S. J. J. M. F. Kokkelmans, G. V. Shlyapnikov, and C. Salomon, "Degenerate atom-molecule mixture in a cold fermi gas," *Phys. Rev. A*, vol. 69, p. 031602, Mar 2004.

[91] T. Lompe, *An apparatus for the production of molecular Bose-Einstein condensates.* PhD thesis, Faculty of Physics and Astronomy, University of Heidelberg, 2008.

[92] S. Musolino, V. E. Colussi, and S. J. J. M. F. Kokkelmans, "Pair formation in quenched unitary bose gases," *Phys. Rev. A*, vol. 100, p. 013612, Jul 2019.

[93] J. Cubizolles, T. Bourdel, S. J. J. M. F. Kokkelmans, G. V. Shlyapnikov, and C. Salomon, "Production of long-lived ultracold li_2 molecules from a fermi gas," *Phys. Rev. Lett.*, vol. 91, p. 240401, Dec 2003.

[94] T. Bourdel, L. Khaykovich, J. Cubizolles, J. Zhang, F. Chevy, M. Teichmann, L. Tarruell, S. J. J. M. F. Kokkelmans, and C. Salomon, "Experimental study of the bec-bcs crossover region in lithium 6," *Phys. Rev. Lett.*, vol. 93, p. 050401, Jul 2004.

[95] M. Bartenstein, A. Altmeyer, S. Riedl, S. Jochim, C. Chin, J. H. Denschlag, and R. Grimm, "Collective excitations of a degenerate gas at the bec-bcs crossover," *Phys. Rev. Lett.*, vol. 92, p. 203201, May 2004.

[96] M. Bartenstein, A. Altmeyer, S. Riedl, R. Geursen, S. Jochim, C. Chin, J. H. Denschlag, R. Grimm, A. Simoni, E. Tiesinga, C. J. Williams, and P. S. Julienne, "Precise determination of ^{6}Li cold collision parameters by radio-frequency spectroscopy on weakly bound molecules," *Phys. Rev. Lett.*, vol. 94, p. 103201, Mar 2005.

[97] T. Paintner, D. K. Hoffmann, M. Jäger, W. Limmer, W. Schoch, B. Deissler, M. Pini, P. Pieri, G. Calvanese Strinati, C. Chin, and J. Hecker Denschlag, "Pair fraction in a finite-temperature fermi gas on the bec side of the bcs-bec crossover," *Phys. Rev. A*, vol. 99, p. 053617, May 2019.

[98] G. M. Falco and H. T. C. Stoof, "Atom-molecule theory of broad feshbach resonances," *Phys. Rev. A*, vol. 71, p. 063614, Jun 2005.

Appendix H

Publication: Observation of collectivity enhanced magnetoassociation of ^{6}Li in the quantum degenerate regime

Observation of collectivity enhanced magnetoassociation of ^{6}Li in the quantum degenerate regime

Vineetha Naniyil,[1] Yijia Zhou,[1,2] Guy Simmonds,[1] Nathan Cooper,[1] Weibin Li,[1,2] and Lucia Hackermüller[1]

[1]*School of Physics and Astronomy, University of Nottingham, Nottingham NG7 2RD, United Kingdom*
[2]*Centre for the Mathematics and Theoretical Physics of Quantum Non-equilibrium Systems, University of Nottingham, Nottingham, NG7 2RD, UK*

The association process of Feshbach molecules is well described by a Landau-Zener transition above the Fermi temperature, such that two-body physics dominates the dynamics. However, using ^{6}Li atoms and the associated Feshbach resonance at $B_r = 834.1$G, we observe an enhancement of the atom-molecule coupling as the Fermionic atoms reach degeneracy, demonstrating the importance of many-body coherence not captured by the conventional Landau-Zener model. For this we apply a linear association ramp ranging from adiabatic to non-equilibrium molecule association for various temperatures. We develop a theoretical model that explains the temperature dependence of the atom-molecule coupling. Furthermore, we characterize this dependence experimentally and extract the atom-molecule coupling coefficient as a function of temperature, finding qualitative agreement between our model and experimental results. Accurate measurement of this coupling coefficient is important for both theoretical and experimental studies of molecule associations and many-body collective dynamics.

Introduction.— In the past decades, Feshbach molecules formed via magnetoassociation [1–5] have captured much attention in the study of unitary dynamics [6], collective dynamics [7, 8] and many-body effects [9]. Starting from BCS pairs, deeply bound molecules are created when the magnetic field is tuned across the Feshbach resonance. A simple model that captures the atom-molecule dynamics is a spin-Boson coupled model [10–12], where BCS pairs and molecules are mapped to spin-half and Bosonic particles, respectively. At zero temperature, the spin-Boson model exhibits rich collective, many-body dynamics [13, 14]. Combined with established cooling and trapping techniques [15, 16], this opens up opportunities to explore new fundamental physics [17–21], controlled chemistry [22–26] and the quantum simulation of complex many-body systems [27–30].

A key parameter by which the dynamics of the spin-Boson model is characterized is the atom-molecule coupling coefficient. The coupling coefficient determines the time scale of the Landau-Zener transition [31, 32], and many-body dynamics [10, 11, 33–38] of the atom-molecule system. Many theoretical works have shown that the coupling coefficient depends on the magnetic moment of the atom, background s-wave scattering length and a volume parameter [1, 12]. Here both the magnetic moment and the background s-wave scattering length are constants near the resonance. On the other hand, it has been shown theoretically that the atom-molecule dynamics becomes collective and should depend on N (N to be the number of total atoms in general), i.e. the association is enhanced by many-body coherence [11, 36, 39–42]. This typically requires ultracold temperatures, where the de Broglie wavelength is large, even comparable to the spatial extension of the gas. These experimental and theoretical studies have provided evidence that the atom-molecule dynamics depends on the entire ensemble. An emerging question is to find out how the coupling coefficient depends on the relevant length scales, such as the de Broglie wavelength and the trap dimensions. A systematic experimental investigation of this dependence has yet to be conducted.

In this work, we investigate collectivity enhanced magnetoassociation of ^{6}Li atoms below and above the Fermi temperature [Fig. 1(a)]. The magnetic field is linearly ramped across the broad Feshbach resonance at $B_r = 834.1$ G, from BCS pairs ($B > B_r$) to Feshbach molecules ($B < B_r$) [43], as depicted in Fig. 1(b). The fraction of atoms converted to molecules is measured experimentally, as a function of both the temperature of the atomic gas and the sweep rate of the magnetic field. The atom-molecule coupling coefficient is derived from the experimental data through the Landau-Zener model. We observe that the coupling coefficient increases

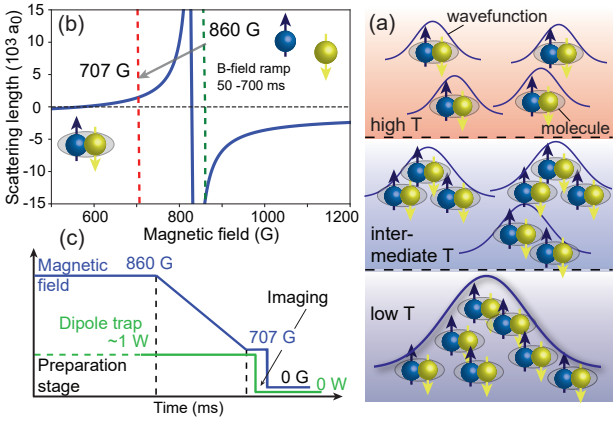

Figure 1. **Temperature dependence of coherence of Feshbach molecules.**(a) Above the Fermi temperature (top), the thermal wavelength of the molecules is comparable to or smaller than their size. Around the Fermi temperature (middle), the thermal wavelength of atoms is larger than the size of BCS pairs, such that the molecules are partially coherent. At very low temperature (bottom), macroscopic coherence in the atomic gas is established and the ^{6}Li molecules form a Bose-Einstein condensate. (b) Broad Feshbach resonance of ^{6}Li at magnetic field $B_r = 834.1$G. By ramping down the magnetic field from 860 G to 707 G, pairs of atoms with opposite spin form Li_2 molecules. (c) Experimental timing. An ensemble of ^{6}Li atoms in $m_f = \pm 1/2$ are prepared with equal populations in a dipole trap. The magnetic field is linearly decreased across the Feshbach resonance to 707 G. We then detect the remaining (unassociated) atoms via absorption imaging.

when the temperature of the atomic gas is lower than the Fermi temperature, due to the increased spatial coherence of the atoms, as illustrated in Fig. 1(a). With the coupling coefficient, we employ an accurate spin-Boson model that takes into account of the effects of many-body coherence and allows simulation of molecular formation dynamics in the regime of quantum degeneracy. This provides insight into the magnetoassociation process at ultracold temperatures and will be important for the development of quantum technologies based on ultracold molecules.

Experiment.— In order to determine the molecular conversion efficiency, we first prepare a cloud of cold ^{6}Li atoms in a crossed optical dipole trap. A balanced spin mixture of two hyperfine states is loaded from a magneto-optical trap and evaporatively cooled under a static magnetic field of $B_i = 860.6\,\mathrm{G}$, thus placing the atoms on the Fermionic side of the Feshbach resonance. With the atoms held in the dipole trap, the magnetic field is then ramped linearly across to the Bosonic side of the resonance according to $B(t) = B_i - \alpha t$, where α is the ramping rate. During this process a certain fraction of the atoms associates into Feshbach molecules. An absorption image of the resulting cloud is taken using light resonant with the D2 line of unassociated atoms of one spin species after a time-of-flight of 1.5 ms. Due to the molecular binding energy, the imaging light is now detuned by many linewidths (178 MHz binding energy vs. natural linewidth of 6 MHz) from the corresponding transition in magneto-associated atoms. As a result, the absorption imaging process detects only the unassociated atoms. The molecular conversion efficiency can then be determined by comparing the number of unassociated atoms remaining after the magnetic field ramp to the number present before. For each experimental setting a calibration procedure is applied by ramping back over the resonance thus dissociating molecules back into atoms — see Appendix B. A range of different ramping speeds are used, such that the total magnetic field ramping time varies from 50 to 700 ms, and by fitting the resulting data to a theoretical prediction [Eq. (3) given later], we obtain the coupling coefficient corresponding to the experimental conditions that have been set. This whole procedure is then repeated at a range of different atom cloud temperatures (trapping frequencies) between 3.2 μK and 130 nK, i.e. both above and below T_F. This allows us to explore the behavior of the coupling coefficient in a broad range of initial temperatures of the system.

We first investigate non-equilibrium and equilibrium molecule formation by varying the magnetic field ramp time over a large range. The experimental results are shown in Fig. 2(a). At a given temperature T, the remnant atom fraction (as determined via absorption imaging) depends on α^{-1} nonlinearly. A general trend is that the remnant atom fraction increases when the magnetic field is changed faster. The fraction of the remnant atoms (molecules) is small (large) when α is small. We find that the remnant atom fraction is non-negligible even in the adiabatic regime. The molecule formation efficiency, i.e. the ratio of the molecules formed to initial atom pairs present, is limited due to, e.g. multiple collisions [44], and many-body effects [45]. In the opposite, diabatic regime when α is large, we find the remnant atom fraction increases significantly after sweeping the magnetic field.

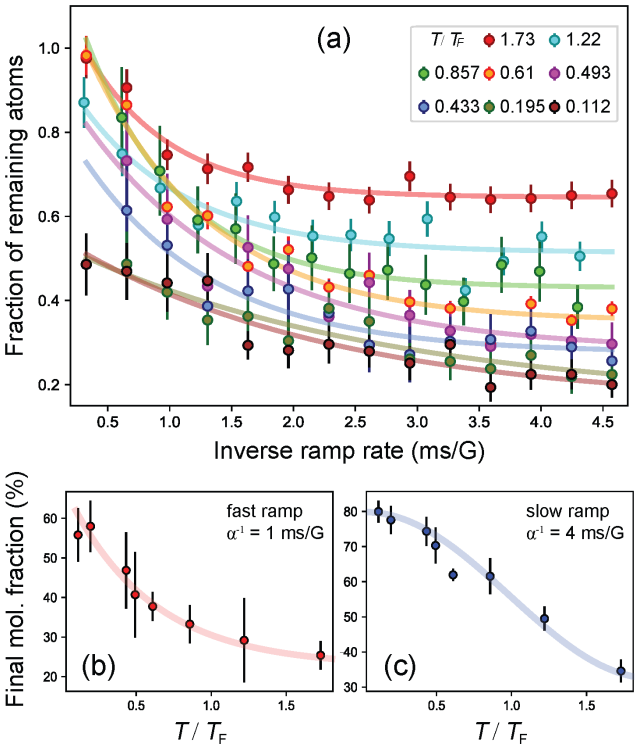

Figure 2. (Color online) **Molecule formation at different temperatures and sweeping rates** (a) Remnant fraction of non-associated atoms after magnetic field ramp. When the inverse ramp rate is low (i.e. fast ramp), the atom fraction is large. Decreasing the ramp speed reduces the remnant atom fraction. In both situations, more atoms are converted to Feshbach molecules when the temperature is reduced. The solid lines are fitting results according to Eq. (3). The error bars are the standard error of 5 measurements. We show the temperature dependence of the molecule fraction for a fast ramp with $\alpha^{-1} = 1$ ms/G in (b) and a slow ramp with $\alpha^{-1} = 4$ ms/G in (c). In both cases, the molecule fraction increases when the temperature is reduced. For the slow ramp, the molecule fractions is around 80 % when $T/T_F \sim 0.1$. In the experiment, the initial and final magnetic field are $B_i = 860.6\,\mathrm{G}$ and $B_f = 707\,\mathrm{G}$ respectively. The ramping rate is varied by changing the duration of the ramp.

We find that the molecule conversion rate changes dramatically at different temperatures. In Fig. 2(b) and (c), the molecule conversion is shown as a function of temperature. When the ramp is fast [Fig. 2(b)], the molecule fraction is low at high temperature and high when the temperature is below the Fermi temperature $T_F = \hbar^2/(2mk_B)(3\pi^2 n)^{2/3}$, with k_B being the Boltzmann constant. The molecule fractions increases monotonically as temperature decreases. Similar dependence is found in the case of a slow ramp [Fig. 2(c)]. However one should note that the overall conversion efficiency is higher in this case. For example, the final molecule fraction (at $T = 130\,\mathrm{nK}$) increases from less than 60 % for $\alpha^{-1} = 1\,\mathrm{ms/G}$ to about $> 80\,\%$ for $\alpha^{-1} = 4\,\mathrm{ms/G}$.

Atom-molecule coupling coefficient.— A key parameter

to describe the molecule formation dynamics is the atom-molecule coupling coefficient. Many theoretical works [1, 12, 36, 46] have shown that the coupling coefficient is given by,

$$g = \hbar\sqrt{\frac{4\pi a_{bg}\Delta_0\Delta\mu}{m\mathcal{V}}} \tag{1}$$

where $\mathcal{V}$, a_{bg}, and Δ_0 are the mode volume, background scattering length, and resonance width, respectively. The coupling coefficient g is a composite parameter and considered as a constant. It connects the microscopic (a_{bg} and $\Delta\mu$) and macroscopic ($\mathcal{V}$ and Δ_0) properties of the system. Although it is an important parameter when modelling the atom-molecule dynamics [10, 11, 33], the value of g has not been widely discussed and a detailed, temperature dependent experimental measurement has not been done so far.

Table I. Overview of the calculated and fitted coupling coefficients and the resulting enhancement factor for the respective temperature.

Fermi Temp. T_F (μK)	Temp. T/T_F	Calculated g g_c ($\hbar\times$kHz)	Fitted g g_f ($\hbar\times$kHz)	Enhancement g_f^2/g_c^2
1.23(1)	0.11(1)	47.07	75.4(7)	2.60(50)
1.30(1)	0.20(1)	45.40	64.8(3)	2.06(20)
1.39(1)	0.43(2)	43.97	56.4(3)	1.67(19)
1.48(1)	0.50(2)	42.27	47.7(4)	1.29(19)
1.53(3)	0.62(1)	42.23	42.6(4)	1.03(21)
1.61(3)	0.86(2)	41.12	43.8(3)	1.15(16)
1.69(2)	1.23(7)	46.10	60.8(4)	1.76(24)
1.86(3)	1.73(4)	46.44	49.9(5)	1.17(24)

To obtain the coupling coefficient, we note that parameters a_{bg} and Δ_0 have been measured in a number of experiments [47]. The mode volume of strongly interacting Fermions in a harmonic trap is $\mathcal{V}_0 = \frac{4\pi}{3}a_{ho}^3\xi_B^{3/4}\sqrt{24N}$, where the oscillator length is $a_{ho} = (\hbar/m\omega)^{1/2}$ with ω the geometric mean of the oscillation frequency. The parameter ξ_B is the Bertsch factor [48] accounting for the atomic interactions. In the dilute limit, $\xi_B \approx 0.37$ is obtained from Monte Carlo simulations [49]. As some atoms do not participate in the formation of molecules, the volume becomes $\mathcal{V} = \sqrt{0.687}\times\mathcal{V}_0$, where 0.687 is the mean molecule fraction. Using the experimentally obtained atom number N (and hence $\mathcal{V}$), we obtain the coupling coefficient g_c. The related parameters and the coupling coefficient are summarized in Table I. The data table shows that the coefficient g_c varies only marginally as we change temperature.

Next, we obtain the coupling coefficient by fitting the experimental data. To this end, the molecule formation is described by a simple, two-level model [47], where two atoms form a molecule through a Landau-Zener (LZ) transition. In this two-state description, the dynamics is governed by the Hamiltonian

$$H = \begin{pmatrix} 0 & g \\ g & \delta(t) \end{pmatrix}, \tag{2}$$

where $\delta(t) = \Delta\mu B(t)$, with $\Delta\mu = 2\mu_B$ being the difference of magnetic moment of the two states. Based on this model, the time-dependent Schrödinger equation can be solved analytically. The molecule occupation probability P is given in the limit $t\to+\infty$ by $P = \exp\left[-2\pi g^2/(\Delta\mu\alpha)\right]$. To take into account the remnant atom fraction even in the adiabatic limit, we fit the atom fraction n_a based on the LZ result with,

$$n_a = n_0 + (1-n_0)\exp\left(-\frac{2\pi g_f^2}{\Delta\mu\alpha}\right), \tag{3}$$

where g_f is the fitted coupling coefficient and n_0 the remaining atom fraction in the adiabatic limit ($\alpha\to 0$). With this equation we accurately fit the experimental data, both at low and high temperature regimes, as shown in Fig. 2(a).

By fitting the experimental data with Eq. (3), we obtained the fitted coupling coefficient g_f, also shown in Table I. The fitted coefficient g_f, however, depends on the temperature. We find that g_f is small at higher temperatures and for $T > T_F$, g_f is nearly identical to g_c. At lower temperatures g_f grows gradually and is almost twice g_c when $T/T_F = 0.11$. The change in the fitted coefficient is seen clearly in Fig. 3, where the ratio $R = g_f^2/g_c^2$ is shown. We note that at $T/T_F = 1.23$, g_f is larger than its neighboring values. It is unclear what causes this discrepancy.

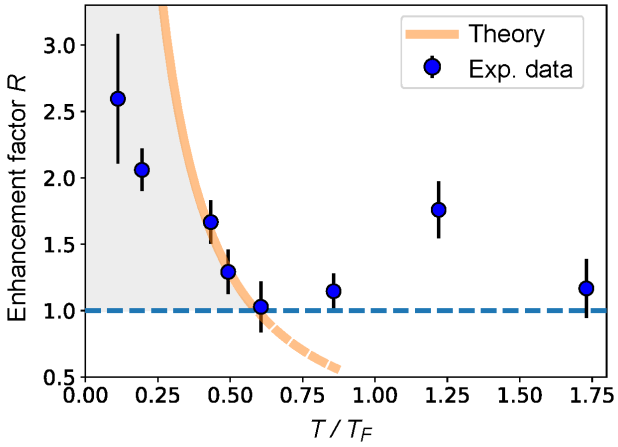

Figure 3. (Color online) **Temperature dependence of the coupling coefficient**. We show the ratio $R = g_f^2/g_c^2$ obtained from the experimental data in figure 2 (see Table I). The orange line represents the geometric ratio factor K as defined in equation (4). The theory estimation is bounded by 1 (blue horizontal line) in the thermal case, and the orange line is dashed where it exceeds this bound.

Coherence enhanced molecule conversion.— We interpret the enhancement of the coupling coefficient due to many-body coherence at ultra-low temperatures, where many molecules are condensed [50]. As a result, the coupling coefficient is amplified to be $g_T = \sqrt{N_T}g$, where $N_t = \rho\mathcal{V}_T$ is the number of molecules in a thermal volume $\mathcal{V}_T$ at density ρ. Assuming that the molecules have the same temperature as the atoms, their de Broglie wavelength at temperature T is given by $\lambda_T = \hbar\sqrt{2\pi/Mk_BT}$, with M being the mass of the Li_2 molecule. Thermal volumes of molecules at temperature T are hereafter $\mathcal{V}_T = \lambda_T^3$. We then compare g_T with the coupling coefficient at the Fermi temperature $g_F = \sqrt{N_F}g$, where

$N_F = \rho \mathcal{V}_F$, with $\mathcal{V}_F = 3\pi^2\hbar^3\sqrt{(2mk_BT_F)^{-3}}$ to be a Fermi volume at the temperature T_F. We characterize the temperature dependence with a geometric ratio factor,

$$K = \frac{g_T^2}{g_F^2} = \frac{\mathcal{V}_T}{\mathcal{V}_F} = \frac{2\sqrt{2}}{3\sqrt{\pi}}\left(\frac{T_F}{T}\right)^{3/2}, \quad (4)$$

which is proportional to $T^{-3/2}$.

This temperature dependence of the geometric ratio factor shows qualitative agreement with the experimentally fitted g_f when the temperature $T < T_F$, as shown in Fig. 3. We thus can interpret the experimental result as follows. When the temperature is high $T > T_F$, the thermal volume is smaller than the Fermi volume, $\mathcal{V}_T < \mathcal{V}_F$. The atom-molecule coupling takes place at the two-body level in this case, for high temperatures. When $T < T_F$, however, the thermal volume is larger than the Fermi volume, which leads to many-body enhanced collective atom-molecule coupling. This means that the molecule conversion efficiency will be high at lower temperatures, which is consistent with the experimental result.

Quantum dynamics of finite systems.— With the coupling coefficient at hand, we study the atom-molecule coupling dynamics. We consider a low temperature regime, $T < T_F$, using a typical value of the coupling coefficient. The Hamiltonian [10, 11, 50] describing the dynamics of molecule formation is given by $H = \sum_j H_j$, where the j-th pair Hamiltonian H_j reads

$$H_j = \delta(t)\hat{b}_j^\dagger\hat{b}_j + \varepsilon_j\left(\hat{c}_{j\uparrow}^\dagger\hat{c}_{j\uparrow} + \hat{c}_{j\downarrow}^\dagger\hat{c}_{j\downarrow}\right) + g\left(\hat{b}_j^\dagger\hat{c}_{j\downarrow}\hat{c}_{j\uparrow} + \text{H.c.}\right).$$

Here $\hat{b}_j$ ($\hat{b}_j^\dagger$) is the Bosonic annihilation (creation) operator of a molecule in the j-th energy level of the harmonic trap, while $\hat{c}_{j\sigma}$ ($\hat{c}_{j\sigma}^\dagger$) denotes the annihilation (creation) operator of a Fermionic atom with spin σ ($\sigma = \uparrow, \downarrow$) . The parameter $\delta(t) = \Delta\mu(\alpha t + B_0)$ gives the molecular energy, where B_0 is the initial magnetic field, and ε_j is the kinetic and trap energy of the atom pair. It is a good approximation to neglect this term when the temperature is low [11]. The atom-molecule coupling coefficient, g, is given by equation (1). At low temperatures, molecules condense into the ground state, such that we can neglect their index, i.e. $\hat{b}_j \to \hat{b}$ ($\hat{b}_j^\dagger \to \hat{b}^\dagger$).

We have solved the Hamiltonian H for different numbers of atoms numerically, as shown in Fig. 4. For this, we have set the magnetic field $B > B_r$ ($B < B_r$) when $t < 0$ ($t > 0$) to mimic the Feshbach molecule formation dynamics. With only one pair of atoms, the molecule fraction is negligible when the magnetic field is larger than B_r (i.e. $t < 0$). Close to the resonance ($t \to 0$) the molecule fraction increases rapidly. Above the resonance ($t > 0$), the molecule fraction oscillates rapidly around a saturation value, and the amplitude of the oscillation decays gradually at later times.

Increasing the number of initial atom pairs, the dynamics of the molecule fraction has a similar dependence on time. However, the molecule fraction when $t > 0$ is increased, due to the quantum coherence (collectivity) enhanced coupling $\sim \sqrt{N}g$, see Fig. 4. We have carried out calculations for up to ten pairs of atoms, where fast oscillations are seen in the molecule fraction when $t > 0$. We then take the average value of these individual realizations, assuming they are equally weighted. This procedure averages out the large amplitude oscillations, where the molecule fraction quickly reaches a steady value when $t > 0$. We note that such dephasing can also be obtained when a thermal average is performed [50]. The simulation shows also that molecules form during a short period $\propto 1/g$ where the magnetic field changes about $g/\Delta\mu$ in the vicinity of the resonance. This time scale is different from what is observed in the experiment and worth careful investigation in the future.

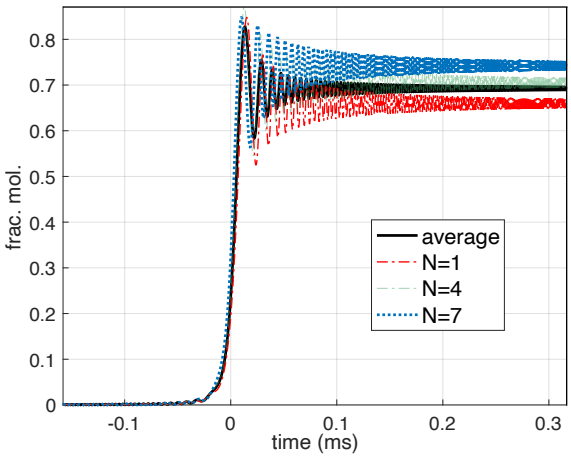

Figure 4. (Color online) **Quantum dynamics of Feshbach molecule formation**. When the total number of atom pairs is small, the molecule fraction is low. For a fixed number of atom pairs, the molecule fraction oscillates rapidly. Due to strong dephasing, the average molecule fraction quickly reaches a steady value. In the simulation, we have used $g = 50$ kHz, which is in the range of the experimental data. Other parameters are $\alpha = 1$ G/ms and B is tuned from $B_r - 0.158$ G to $B_r + 0.316$ G.

Conclusion.—Our experiment shows that the fraction of atoms associated into molecules increases when both the temperature of the atomic gas and the sweeping rate of the magnetic field are decreased. We have measured the atom-molecule coupling coefficient, which increases at lower temperatures and in the adiabatic regime, as a result of many-body coherence. The qualitative trends predicted by our theory agree with our experimental findings, and quantitative agreement appears strong at temperatures only slightly below the Fermi temperature. The quantitative differences at even lower temperature indicates that a more sophisticated model is therefore needed to fully describe the experiment. Our study provides an accurate experimental measurement of the atom-molecule coupling coefficient. Exploitation of these enhanced coupling coefficient might lead to a path for more efficient molecule creation.

ACKNOWLEDGMENTS

Daniele Baldolini is thanked for historic contributions to construction of experimental apparatus. This work was supported by the EPSRC grants EP/R024111/1 and EP/M013294/1 and by the European Comission grant

ErBeStA (no. 800942). W. L. acknowledges support from the UKIERI-UGC Thematic Partnership (IND/CONT/G/16-17/73), the Royal Society through the International Exchanges Cost Share award No. IEC\NSFC\181078, and a RPA grant from the University of Nottingham.

Appendix A: technical details of experimental procedure

Generation of the cold atom cloud prior to magnetoassociation begins with a magneto-optical trap (MOT) [51]. The MOT is loaded via a Zeeman slower [52], which slows an atomic beam that is transmitted through a differential pumping stage from a source chamber. Over a 10 second loading cycle, the MOT captures $\sim 2 \times 10^8$ ^{6}Li atoms. An additional cooling step, in which the trapping lasers are tuned to half a natural linewidth below resonance (for optimal Doppler cooling), brings the temperature of this atom cloud down to $\sim 300\ \mu$K.

An optical dipole trap is loaded from this cold cloud. A 100 W fibre laser, operating at 1070 nm, is used to produce a crossed-beam dipole trap, in which each beam is focused to a waist of 80 μm. The crossing angle is 14 degrees. This captures up to 2×10^6 atoms.

These atoms are then evaporatively cooled to a regime close to quantum degeneracy to temperatures between $0.1 - 2.0$ T/T_F with total atom numbers between 100.000 - 200.000 atoms. After the loading, the dipole trap is first held at constant power for 600 ms, following which the power in the optical dipole trap is ramped down to the range of tens to hundreds of mW. The end point depends on the final trap depth desired and is reached in a series of linear ramps that collectively approximate an exponential decay of the trapping power. The power is lowered through a combination of reducing the laser current and the use of an acousto-optic modulator. A photodiode is used to measure the optical power that passes through the dipole trap, with servo-controlled feedback to the acousto-optic modulator enabling active stabilization of the dipole trap's depth to its set value. This is necessary to reduce unwanted heating effects arising from small variations in trap depth.

At the end of this evaporative cooling cycle, which lasts ~ 10 s, on the order of 10^5 atoms typically remain, at temperatures ranging from tens of nK to several μK. The cloud is then held at constant trap depth corresponding to trapping frequencies between 622 - 750 Hz (radially) and 74 - 90 Hz (longitudinally).

The magnetic field is then ramped linearly from 860.6 G to the BEC side of the Feshbach resonance (707 G). The linear magnetic field ramp is applied through a change in the current in the Feshbach coils as shown exemplary in the Fig.5.

Appendix B: determination of molecule fraction via absorption imaging

To reduce the impact of technical noise sources on the absorption imaging, the atom cloud was released from the dipole trap and allowed to expand for a period of 1 to 2 ms (depending on exact experimental parameters) prior to imaging. The size of the atom cloud after this period was typically some hundreds of micrometers, which greatly exceeds our imaging resolution of 3 μm. Each absorption image is background-subtracted and then normalized to an equivalent image taken 50 ms after the atoms have been dispersed, which greatly reduces the influence of technical noise sources on our data.

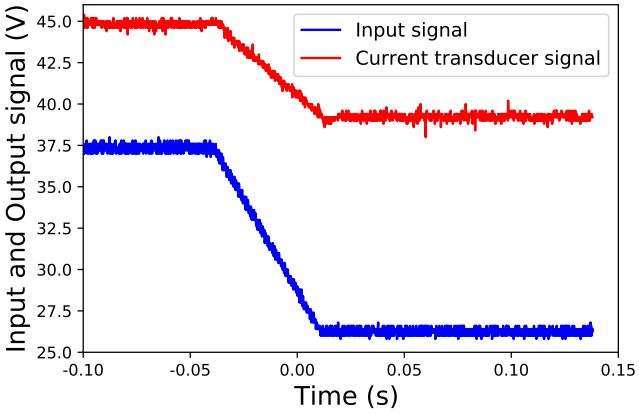

Figure 5. (Color online) **Magnetic field ramp.** Current transducer signal for a 50 ms ramp.

We also carry out additional control experiments to account for the effect of loss of unassociated atoms from the dipole trap during the magnetic field ramp. If not properly accounted for, this could cause overestimation of the molecular fraction after the ramp, since we assume that atoms not seen in the absorption image are associated into molecules. We therefore conduct, for each set of experimental conditions under which we take data, a control experiment in which the magnetic field is ramped across the Feshbach resonance and then back again, thus dissociating any molecules that were previously formed. This process is time-symmetric, taking twice as long as the unidirectional ramp, and we therefore assume that the fraction of the atoms remaining after this process is equal to the square of the total fraction remaining (in both associated and unassociated forms) after a unidirectional ramp. This allows us to estimate the reduction in apparent atom number that results from atom loss during the magnetic field ramp under each set of experimental conditions employed. By dividing the apparent unassociated atom fraction that we measure using absorption imaging by this value, we can thus eliminate the systematic bias resulting from atom loss during the magnetic field ramp.

Appendix C: Landau-Zener Transition of a two-level system

The molecule formation via sweeping magnetic field through the Feshbach resonance can be modeled to be a Landau-Zener (LZ) transition. Using a two-state process pic-

true, LZ describes the transition under the Hamiltonian

$$H = \begin{pmatrix} \varepsilon & g \\ g & \delta(t) \end{pmatrix}, \tag{C1}$$

where $\delta(t)$ slowly increases from $-\infty$ to $+\infty$ at a constant speed $\dot{\delta}$. Analytical solution reveals that the flip, or transition, probability is

$$P = \exp\left(-2\pi g^2/\dot{\delta}\right). \tag{C2}$$

Near Feshbach resonance, $\delta(t) = \Delta\mu(B(t) - B_r)$, where $\Delta\mu$ is the difference of magnetic moment, B_r is the resonant magnetic field strength. g is the atom-molecule coupling strength. For fermions, it is equal to $g = \hbar\sqrt{4\pi a_{bg}\Delta_0\Delta\mu/m}/\sqrt{\mathcal{V}}$ [12]. For ^{6}Li at $B_r = 834.1$ G, $\Delta\mu = 2\mu_B$, the resonance width $\Delta_0 = -300$ G and background scattering length $a_{bg} = -1405$ a$_0$. $\mathcal{V}$ is the mode volume. To obtain the volume, we note that typically two-body interactions will change the shape and density of atoms in the trap. Papenbrock and Bertsch [48] introduced a parameter ξ_B such that the chemical potential is scaled by the Fermi energy of the non-interacting case $\mu = \xi_B E_F^0$. The trapping frequency is then scaled by $\sqrt{\xi_B}\omega_i$ accounting for the change of effective trapping frequency. Then the radii of the atomic cloud read

$$R_i = \xi_B^{1/4} a_{ho} \frac{\omega_{ho}}{\omega_i} (24N)^{1/6}, \tag{C3}$$

yielding the volume of a spherical gas,

$$\mathcal{V} = \frac{4\pi}{3} a_{ho}^3 \xi_B^{3/4} \sqrt{24N}. \tag{C4}$$

In the BCS regime, ξ_B is calculated by the Monte Carlo method [49]. Though depending on trapping profile and particle density, ξ_B converges to ≈ 0.37 in dilute limit, which is used in the calculation.

Appendix D: Many-body Model of the atom-molecule coupling

The formation of bosonic molecules from pairs of fermionic atoms is modelled by a spin-boson coupled system [10, 11, 50]. The Hamiltonian consists of different molecular states, such that $H = \sum_i H_i$, where Hamiltonian H_j reads

$$H_j = \delta(t)\hat{b}_j^\dagger \hat{b}_j + \varepsilon_j\left(\hat{c}_{j\uparrow}^\dagger \hat{c}_{j\uparrow} + \hat{c}_{j\downarrow}^\dagger \hat{c}_{j\downarrow}\right) + g\left(\hat{b}_j^\dagger \hat{c}_{j\downarrow}\hat{c}_{j\uparrow} + \text{H.c.}\right).$$

Here $\delta(t) = \Delta\mu(\alpha t + B_0)$ gives the molecular energy, where α and B_0 are the ramping rate and the initial value of the magnetic field. ε_j is the kinetic and trap energy of the atom pair. Here ε_j denotes the energy of a pair of . Typically, it can be the harmonic levels $\varepsilon_j = \hbar\omega(j + 1/2)$, or free space by replacing j by $\mathbf{k}$, $\varepsilon_\mathbf{k} = k^2/2m$. $\delta(t)$ is the molecular energy. If all molecules are in the ground state, i.e., forming a molecular BEC, then we can neglect the index j, as all molecules have identical one.

When sweeping the magnetic field from 860 G to 707 G, the molecule energy changes from $\delta(t_0)/\hbar = -457$ MHz to $\delta(t_f)/\hbar = 2232$ MHz. The maximum value of ε_j (Fermi level) is roughly $\varepsilon_F = \hbar^2/(2m)(3\pi^2 n)^{2/3} \approx \hbar \times 50.5$ kHz for density $n = 10^{12}$ cm^{-3}. If we take the full range of magnetic field, the numerical cost in the simulation will be very expensive. To simplify the calculation, we have chosen initial value of magnetic field relatively close to the resonance, which captures the LZ transition dynamics.

Anderson Pseudospin representation

When the molecules are condensed to the ground, this allows us to further simplify the model using the Anderson pseudospin. The Andreson pseudospin connects the spin operator via

$$\begin{aligned} \hat{S}_i^+ &= \hat{c}_{i\downarrow}^\dagger \hat{c}_{i\uparrow}^\dagger \\ \hat{S}_i^- &= \hat{c}_{i\uparrow}\hat{c}_{i\downarrow} \\ \hat{S}_i^z &= \hat{c}_{i\uparrow}^\dagger \hat{c}_{i\uparrow} + \hat{c}_{i\downarrow}^\dagger \hat{c}_{i\downarrow} - 1 \end{aligned}$$

which are spin operators for a spin-half particle with correlations $S_j^x = (S_j^+ + S_j^-)/2$ and $S_j^y = -i(S_j^+ - S_j^-)/2$. The commutation relations are $[S_j^+, S_j^-] = 2S_j^z$, $[S_j^+, S_j^z] = -S_j^+$ and $[S_j^-, S_j^z] = S_j^-$. The total number $2N$ of particles are conserved, $2N_b + \sum_j^N (2S_j^z + 1) = 2N$, which can be seen from the commutation relation $[H, N] = 0$.

The Hamiltonian can be simplified to a Tavis-Cummings model (or Dicke model without counter-rotating terms)

$$H = \delta(t)\hat{b}^\dagger\hat{b} + \sum_i \varepsilon_i \hat{S}_i^z + g\sum_i \left(\hat{b}^\dagger \hat{S}_i^- + \hat{S}_i^+ \hat{b}\right). \tag{D1}$$

A c-number part $\sum_i \varepsilon_i$ is discarded, i.e. neglecting the kinetic energy of atom pairs. This is a good approximation when the temperature is low. The Heisenberg equation of the operator can be obtained,

$$i\frac{\partial}{\partial t}\hat{b} = \delta(t)\hat{b} + g\sum_i \hat{S}_i^- \tag{D2a}$$

$$i\frac{\partial}{\partial t}\hat{S}_i^- = 2\varepsilon_i \hat{S}_i^- - g\hat{S}_i^z \hat{b} \tag{D2b}$$

$$i\frac{\partial}{\partial t}\hat{S}_i^+ = -2\varepsilon_i \hat{S}_i^+ + g\hat{b}^\dagger \hat{S}_i^z \tag{D2c}$$

$$i\frac{\partial}{\partial t}\hat{S}_i^z = 2g\left(-\hat{b}^\dagger \hat{S}_i^- + \hat{S}_i^+ \hat{b}\right) \tag{D2d}$$

As the total number of atoms is conserved, one can solve the dynamics numerically when N in the order of a few hundred to thousand with a normal desktop PC. For numbers close to the experimental situations (hundreds of thousands of atoms), one many use the mean field theory, i.e. decoupling mean value of operator products as $\langle AB\rangle \approx \langle A\rangle\langle B\rangle$ to solve the coupled equation.

[1] E. Timmermans, P. Tommasini, M. Hussein, and A. Kerman, Phys. Rep. **315**, 199 (1999).
[2] E. Hodby, S. T. Thompson, C. A. Regal, M. Greiner, A. C. Wilson, D. S. Jin, E. A. Cornell, and C. E. Wieman, Phys. Rev. Lett. **94**, 120402 (2005).
[3] F. A. van Abeelen and B. J. Verhaar, Phys. Rev. Lett. **83**, 1550 (1999).
[4] F. H. Mies, E. Tiesinga, and P. S. Julienne, Phys. Rev. A **61**, 022721 (2000).
[5] C. A. Regal, C. Ticknor, J. L. Bohn, and D. S. Jin, Nature **424**, 47 (2003).
[6] T. Bourdel, L. Khaykovich, J. Cubizolles, J. Zhang, F. Chevy, M. Teichmann, L. Tarruell, S. J. J. M. F. Kokkelmans, and C. Salomon, Phys. Rev. Lett. **93**, 050401 (2004).
[7] M. Bartenstein, A. Altmeyer, S. Riedl, S. Jochim, C. Chin, J. H. Denschlag, and R. Grimm, Phys. Rev. Lett. **92**, 203201 (2004).
[8] D. Wellnitz, S. Schütz, S. Whitlock, J. Schachenmayer, and G. Pupillo, Phys. Rev. Lett. **125**, 193201 (2020).
[9] S. Musolino, V. E. Colussi, and S. J. J. M. F. Kokkelmans, Phys. Rev. A **100**, 013612 (2019).
[10] E. Pazy, A. Vardi, and Y. B. Band, Phys. Rev. Lett. **93**, 120409 (2004).
[11] E. Pazy, I. Tikhonenkov, Y. B. Band, M. Fleischhauer, and A. Vardi, Phys. Rev. Lett. **95**, 170403 (2005).
[12] R. A. Duine and H. T. C. Stoof, Phys. Rep. **396**, 115 (2004).
[13] C. Sun and N. A. Sinitsyn, Phys. Rev. A **94**, 033808 (2016).
[14] C. Sun, V. Y. Chernyak, A. Piryatinski, and N. A. Sinitsyn, Phys. Rev. Lett. **123**, 123605 (2019).
[15] W. Ketterle and N. Van Druten, Adv. At. Mol. Opt. Phys. **37**, 181 (1996).
[16] R. Grimm, M. Weidemüller, and Y. Ovchinnikov, Adv. At. Mol. Opt. Phys. **42**, 95 (2000).
[17] T. Köhler, K. Góral, and P. S. Julienne, Rev. Mod. Phys. **78**, 1311 (2006).
[18] V. V. Flambaum and M. G. Kozlov, Phys. Rev. Lett. **99**, 150801 (2007).
[19] L. D. Carr, D. DeMille, R. V. Krems, and J. Ye, New J. Phys. **11**, 055049.
[20] T. A. Collaboration, J. Baron, W. C. Campbell, D. DeMille, J. M. Doyle, G. Gabrielse, Y. V. Gurevich, P. W. Hess, N. R. Hutzler, E. Kirilov, I. Kozyryev, B. R. O'Leary, C. D. Panda, M. F. Parsons, E. S. Petrik, B. Spaun, A. C. Vutha, and A. D. West, Science **343**, 269 (2014).
[21] J. J. Hudson, D. M. Kara, I. J. Smallman, B. E. Sauer, M. R. Tarbutt, and E. A. Hinds, Nature **473**, 493 (2011).
[22] R. V. Krems, Phys. Chem. Chem. Phys. **10**, 4079 (2008).
[23] S. Knoop, F. Ferlaino, M. Berninger, M. Mark, H.-C. Nägerl, R. Grimm, J. P. D'Incao, and B. D. Esry, Phys. Rev. Lett. **104**, 053201 (2010).
[24] S. Ospelkaus, K.-K. Ni, D. Wang, M. H. G. de Miranda, B. Neyenhuis, G. Quéméner, P. S. Julienne, J. L. Bohn, D. S. Jin, and J. Ye, Science **327**, 853 (2010).
[25] M. H. G. de Miranda, A. Chotia, B. Neyenhuis, D. Wang, G. Quéméner, S. Ospelkaus, J. L. Bohn, J. Ye, and D. S. Jin, Nat. Phys. **7**, 502 (2011).
[26] X. Ye, M. Guo, M. L. González-Martínez, G. Quéméner, and D. Wang, Sci. Adv. **4**, eaaq0083 (2018).
[27] A. Micheli, G. K. Brennen, and P. Zoller, Nat. Phys. **2**, 341 (2006).
[28] A. V. Gorshkov, S. R. Manmana, G. Chen, J. Ye, E. Demler, M. D. Lukin, and A. M. Rey, Phys. Rev. Lett. **107**, 115301 (2011).
[29] L. Pollet, J. D. Picon, H. P. Büchler, and M. Troyer, Phys. Rev. Lett. **104**, 125302 (2010).
[30] W. Lechner and P. Zoller, Phys. Rev. Lett. **111**, 185306 (2013).
[31] K. Góral, T. Köhler, S. A. Gardiner, E. Tiesinga, and P. S. Julienne, J. Phys. B: At. Mol. Opt. Phys. **37**, 3457 (2004).
[32] F. H. Mies, E. Tiesinga, and P. S. Julienne, Phys. Rev. A **61**, 022721 (2000).
[33] M. Holland, S. J. J. M. F. Kokkelmans, M. L. Chiofalo, and R. Walser, Phys. Rev. Lett. **87**, 120406 (2001).
[34] K. E. Strecker, G. B. Partridge, and R. G. Hulet, Phys. Rev. Lett. **91**, 080406 (2003).
[35] M. H. Szymańska, K. Góral, T. Köhler, and K. Burnett, Phys. Rev. A **72**, 013610 (2005).
[36] D. Sun, A. Abanov, and V. L. Pokrovsky, EPL **83**, 16003 (2008).
[37] A. Altland, V. Gurarie, T. Kriecherbauer, and A. Polkovnikov, Phys. Rev. A **79**, 042703 (2009).
[38] S. Yi and S. W. Kim, Phys. Rev. A **93**, 013616 (2016).
[39] I. Tikhonenkov, E. Pazy, Y. B. Band, M. Fleischhauer, and A. Vardi, Phys. Rev. A **73**, 043605 (2006).
[40] Y. B. Band, I. Tikhonenkov, and A. Vardi, Mol. Phys. **106**, 349 (2008).
[41] J. Liu, L.-B. Fu, B. Liu, and B. Wu, New J. Phys. **10**, 123018 (2008).
[42] J. Liu, B. Liu, and L.-B. Fu, Phys. Rev. A **78**, 013618 (2008).
[43] J. Cubizolles, T. Bourdel, S. J. J. M. F. Kokkelmans, G. V. Shlyapnikov, and C. Salomon, Phys. Rev. Lett. **91**, 240401 (2003).
[44] J. E. Williams, N. Nygaard, and C. W. Clark, New J. Phys. **8**, 150 (2006).
[45] P. A. Murthy, M. Neidig, R. Klemt, L. Bayha, I. Boettcher, T. Enss, M. Holten, G. Zürn, P. M. Preiss, and S. Jochim, Science **359**, 452 (2018).
[46] J. Javanainen and M. Mackie, Phys. Rev. A **59**, R3186(R) (1999).
[47] C. Chin, R. Grimm, P. Julienne, and E. Tiesinga, Rev. Mod. Phys. **82**, 1225 (2010).
[48] T. Papenbrock and G. F. Bertsch, Phys. Rev. C **59**, 2052 (1999).
[49] J. Carlson, S. Gandolfi, K. E. Schmidt, and S. Zhang, Phys. Rev. A **84**, 061602(R) (2011).
[50] J. Javanainen, M. Koštrun, Y. Zheng, A. Carmichael, U. Shrestha, P. J. Meinel, M. Mackie, O. Dannenberg, and K.-A. Suominen, Phys. Rev. Lett. **92**, 200402 (2004).
[51] E. Raab, M. Prentiss, A. Cable, S. Chu, and D. Pritchard, Phys. Rev. Lett. **59**, 2631 (1987).
[52] A. Paris-Mandoki, M. Jones, J. Nute, J. Wu, S. Warriar, and L. Hackermüller, Rev. Sci. Instrum. **85**, 113103 (2014).